

NASA CR-54678

00027

MEASUREMENT OF SPUTTERING YIELDS AND ENERGY TRANSFER EFFICIENCIES OF LIQUID METALS

by

H.L. GARVIN

GPO PRICE \$ _____

CFSTI PRICE(S) \$ _____

Hard copy (HC) 3.00

Microfiche (MF) .65

prepared for

ff 653 July 65

NATIONAL AERONAUTICS AND SPACE ADMINISTRATION

CONTRACT NAS 3-6273

FACILITY FORM 602

N60-18198
(ACCESSION NUMBER)

95
(PAGES)

CI-54678
(NASA CR OR TMX OR AD NUMBER)

(THRU)

(CODE)

23
(CATEGORY)



HUGHES RESEARCH LABORATORIES

A DIVISION OF HUGHES AIRCRAFT COMPANY

3011 MALIBU CANYON ROAD

MALIBU, CALIFORNIA 90265

NOTICE

This report was prepared as an account of Government sponsored work. Neither the United States, nor the National Aeronautics and Space Administration (NASA), nor any person acting on behalf of NASA:

- A.) Makes any warranty or representation, expressed or implied, with respect to the accuracy, completeness, or usefulness of the information contained in this report, or that the use of any information, apparatus, method, or process disclosed in this report may not infringe privately owned rights; or
- B.) Assumes any liabilities with respect to the use of, or for damages resulting from the use of any information, apparatus, method or process disclosed in this report.

As used above, "person acting on behalf of NASA" includes any employee or contractor of NASA, or employee of such contractor, to the extent that such employee or contractor of NASA, or employee of such contractor prepares, disseminates, or provides access to, any information pursuant to his employment or contract with NASA, or his employment with such contractor.

Requests for copies of this report should be referred to

National Aeronautics and Space Administration
Office of Scientific and Technical Information
Attention: AFSS-A
Washington, D.C. 20546

NASA CR-54678

FINAL REPORT

MEASUREMENT OF SPUTTERING YIELDS AND ENERGY
TRANSFER EFFICIENCIES OF LIQUID METALS

by

H. L. Garvin

prepared for

NATIONAL AERONAUTICS AND SPACE ADMINISTRATION

Submitted April 1967
Approved January 1968

CONTRACT NAS 3-6273

Technical Management
NASA Lewis Research Center
Cleveland, Ohio 44135

HUGHES RESEARCH LABORATORIES
A Division of Hughes Aircraft Company
3011 Malibu Canyon Road
Malibu, California 90265

TABLE OF CONTENTS

	LIST OF ILLUSTRATIONS	v
I.	INTRODUCTION	1
II.	EXPERIMENTAL APPARATUS	5
	A. Vacuum System	5
	B. Quadrupole Mass Analyzer	8
	C. Ion Source	13
	D. Target Assembly	15
	E. Deposition Thickness Monitor	17
III.	EXPERIMENTAL RESULTS	21
	A. Mercury Ion Bombardment	21
	B. Cesium Ion Bombardment	48
IV.	INTERPRETATION OF RESULTS	61
V.	CONCLUSIONS	79
	ACKNOWLEDGMENTS	81
	REFERENCES	83

THEORY OF THE EARTH

THEORY OF THE EARTH

THEORY OF THE EARTH

THEORY OF THE EARTH

THEORY OF THE EARTH

THEORY OF THE EARTH

THEORY OF THE EARTH

THEORY OF THE EARTH

THEORY OF THE EARTH

THEORY OF THE EARTH

THEORY OF THE EARTH

THEORY OF THE EARTH

THEORY OF THE EARTH

THEORY OF THE EARTH

THEORY OF THE EARTH

THEORY OF THE EARTH

THEORY OF THE EARTH

THEORY OF THE EARTH

THEORY OF THE EARTH

LIST OF ILLUSTRATIONS

Fig. 1.	Schematic drawing of liquid metal sputtering apparatus	6
Fig. 2.	Photograph of liquid metal sputtering apparatus with associated electronic supplies	7
Fig. 3.	Residual gas spectrum in vacuum chamber with ion pump indicating 3×10^{-8} Torr	9
Fig. 4.	Schematic view of Quadrupole Mass Analyzer and target assemblies	10
Fig. 5.	Components of EAI quadrupole mass analyzer prior to assembly	11
Fig. 6.	Photograph of Quadrupole Mass Analyzer Assembly	12
Fig. 7.	Photograph of electron-bombardment-type ion source	14
Fig. 8.	Photograph of target assemblies with half of aperture shield removed	18
Fig. 9.	Mass spectrum showing mass peaks sputtered from Mg target	22
Fig. 10.	Mass spectrum showing mass peaks sputtered from Mg target (residual background suppressed)	23
Fig. 11.	Mass spectrum with ion beam on but with residual gas spectrum suppressed	24
Fig. 12.	Sputtered ion spectra resulting from mercury ion bombardment of aluminum	25
Fig. 13.	Angular distribution of sputtered versus vaporizing aluminum	26
Fig. 14.	Peak height of sputtered aluminum ions as observed when target temperature is varied from 185°C to 938°C	28
Fig. 15.	Peak height of sputtered aluminum ions versus target temperature	29

Fig. 16.	Relative sputtering yield of Al^{27} as a function of bombardment energy	30
Fig. 17.	Observations of the effect of the retardation potential on the peak height due to sputtered aluminum ions	31
Fig. 18.	Peak height of sputtered aluminum ions as a function of retardation potential for four values of ion bombardment energy	33
Fig. 19.	Peak height of sputtered aluminum ions as a function of retardation potential	34
Fig. 20.	Spectrum of sputtered ions resulting from ion bombardment of liquid gallium target	35
Fig. 21.	Photos of output signal due to bombardment of gallium target biased to +67.5 V	36
Fig. 22.	Peak height due to gallium ions created by bombardment of liquid gallium target biased to +67.5 V	37
Fig. 23.	Peak height of sputtered gallium ions as a function of target temperature	39
Fig. 24.	Sputtering yield of gallium ions as a function of ion bombardment energy	40
Fig. 25.	Peak height of sputtered gallium ions as a function of retardation potential	41
Fig. 26.	Peak height of sputtered indium ions and atoms as a function of target temperature	42
Fig. 27.	Peak height of sputtered indium ions and atoms as a function of bombarding energy	43
Fig. 28.	Peak height of sputtered indium atoms and ions as a function of retardation potential	44
Fig. 29.	Spectra showing sputtered lead atoms in the presence of residual mercury vapor	46
Fig. 30.	Vaporizing spectrum of lead isotopes in the presence of mercury vapor	47
Fig. 31.	Peak height of sputtered lead atoms as a function of mercury ion bombarding energy	49

Fig. 32.	Peak height of sputtered lead atoms as a function of target temperature	50
Fig. 33.	Sputtered spectra due to cesium ion bombardment of indium and lead targets	51
Fig. 34.	Peak height of sputtered indium atoms versus retarding potential at two values of cesium ion bombardment energy	53
Fig. 35.	Spectra showing cesium ions sputtered from lead target under argon ion bombardment	54
Fig. 36.	Sputtered ions produced by cesium ion bombardment of aluminum at 5 keV	56
Fig. 37.	Peak height of sputtered aluminum ions versus retarding potential with bombarding energy as a parameter. $T_{Al} = 60^{\circ}C$	57
Fig. 38.	Peak height of sputtered cesium ions (resulting from bombardment of aluminum target) versus retarding potential. $T_{Al} = 60^{\circ}C$	58
Fig. 39.	Retardation plots of sputtered aluminum and cesium ions resulting from cesium ion bombardment of aluminum target. $T_{Al} = 60^{\circ}C$	59
Fig. 40.	Retardation plots of sputtered aluminum ions under Hg ion bombardment. E_s = characteristic energy of sputtered ions	63
Fig. 41.	Retardation plots of sputtered aluminum ions under Cs ion bombardment. E_s = characteristic energy	64
Fig. 42.	Comparison of characteristics, E_s , of sputtered Al ions under Hg and Cs ion bombardment	65
Fig. 43.	Retardation plot of cesium ions sputtered from aluminum target. E_s = characteristic energy indicated by slope	67
Fig. 44.	Retardation plots for indium ions and atoms under Hg ion bombardment. E_s = characteristic energy	68
Fig. 45.	Retardation plots for Al, Ga, and In ions due to Hg ion bombardment	69

Fig. 46.	Characteristic energies of ionic species as a function of target mass	70
Fig. 47.	Retardation plot for sputtered indium ions under Hg-, Cs-, and Ar-ion bombardment. E_s = characteristic energy indicated by slope of line . . .	71
Fig. 48.	Retardation plots of sputtered indium ions as a function of Cs ion bombardment energy. E_s = characteristic energy	72
Fig. 49.	Dependence of characteristic energies of sputtered Al-ions on bombarding energy. $T_{Al} = 60^\circ C$	74
Fig. 50.	Retardation plots for Al sputtered by Hg ions	75
Fig. 51.	Characteristic energies of sputtered aluminum ions as a function of target temperature	76

I. INTRODUCTION

The effects of ion bombardment of surfaces have been studied with great interest since the early observations of material transfer in electrical discharges. The term "sputtering" has been applied to the mechanism whereby energetic particles incident on a surface give rise to the ejection of atomic or ionic species from the surface. During the past 15 years extensive experimental research has been directed toward observation of the characteristics of sputtering at various ranges of incident particle energy and for many different combinations of bombarding ions and target materials.¹⁻¹⁵ The ions have been generated by glow discharges, low pressure electron bombardment sources, and surface ionization of alkali vapor. Their bombarding energies have varied from the sputtering threshold region of 10 to 100 eV up to the MeV ranges experienced in radiation damage phenomena. A great volume of experimental evidence has been accumulated concerning the dependence of sputtering yield (expressed as the number of surface atoms removed for each incident ion) on the mass, energy, and angle of incidence of the bombarding ion, and on the mass, temperature, and crystalline arrangement of the target atoms. However, the exact theoretical description of the process has been difficult to formulate, and only in recent years have models been successful in depicting the phenomenon.¹⁶⁻¹⁹

The upsurge of interest in the application of electrostatic ion propulsion for deep space missions or for long duration synchronous satellite station-keeping brought forth the recognition that sputtering could be an important factor in determining thruster lifetime.^{11, 20} The propellant ions of mercury, cesium, or other materials are accelerated to the range of 2 to 10 keV to produce the desired high specific impulse of the thruster. Ions created by charge exchange collisions in the primary beam or ions which are improperly focused impinge on the accelerating electrodes and cause damaging erosion; this erosion may ultimately cause the end of the thruster's useful operating life. In addition, in electron-bombardment type thrusters, the performance of the electron emitting cathode will be strongly influenced by the bombardment of ions created in the discharge chamber.

It had been suggested¹⁴ that the sputtering of metals in their liquid state might differ significantly from that in the solid state and that this difference might be employed in extension of the electrode life by using a porous structure through which a liquid metal flows to produce a continuously replaceable surface or in other aspects of thruster design.

Although extensive investigations have been carried out on the sputtering of single-crystal and polycrystalline materials, it was realized that very little was known of the sputtering characteristics of metals in their liquid state. One of the few reports on the sputtering of liquid metals was the early work by Seeliger and Sommermeyer in 1935.²¹ Therefore, this program was initiated to investigate the sputtering yields and transfer efficiencies for aluminum, gallium, indium, cerium, lead, and tin, when operated in their liquid states in the temperature range from 600 to 1000°C under bombardment by mercury and cesium ions.

It was necessary to identify the sputtered species in order to distinguish them from vaporizing target or beam material. In addition, it was considered desirable to observe the energy of these species. Therefore, an experimental system was designed in which a Quadrupole Mass Analyzer (QMA) was used for detection of the sputtered particles. Retardation methods were used to determine their velocity (energy). The QMA was mounted on a rotating arc assembly to permit observation of the ejected species into all angles from the target. In the original concept of the system, the liquid metal was permitted to flow through porous tungsten disks; this technique might be used in an ion engine application where liquid metals would be used for continuous replacement of the surfaces of accelerating electrodes. This concept would have been attractive experimentally since it would permit variation in ion beam incident angle as well as variation in observation angle. Unfortunately, the highly reactive nature of most of the sample metals precluded the possibility of performing this type of experiment. In order to make maximum use of the system, it was decided to perform the observations on target boats in which the metals could be heated and held as a flat pool.

In the course of the program, the sputtering of aluminum, gallium, indium, and lead was observed under bombardment by mercury and cesium ions at 1 to 10 keV energy at target temperatures up to 950°C. The results indicate that the sputtering yield of aluminum, gallium, and indium decrease slightly at elevated temperatures, and, as they go from the solid to liquid state, a decrease in yield of the order of 25% is observed. This magnitude and direction of change is of interest in formulating the theories of sputtering mechanics. However, since there is not a great decrease in yield (at least an order of magnitude), the complexity involved in applying the technique to protect porous electrode structures is scarcely justified.

The observations of the energies of ejected particles confirm earlier measurements that the average energies are well above thermal values. In addition, the profile of energies indicates a Maxwellian distribution with characteristic energies E_s which were observed for their dependence on bombarding energy, target temperature, and target

mass. Characteristic energies of 27.7, 17.3, and 14.2 eV were observed in the ionic species of aluminum, gallium, and indium when bombarded by 6 keV mercury ions at normal incidence. These energies are of interest in formulating the theoretical model of sputtering. In addition, they appear to justify the interest in plasma and ion beam sputtering for the deposition of thin film materials where bonding characteristics and effective mobility in the formation of crystallites are important.

1. The first part of the document is a letter from the President of the United States to the Congress, dated January 3, 1862. It is a very important document, as it contains the President's message to Congress, and is one of the most important documents in the history of the United States.

II. EXPERIMENTAL APPARATUS

A. Vacuum System

A fundamental requirement in the investigation of sputtering phenomena is that the surface of the metallic target be free from contamination. In particular, it is desired that the arrival rate of residual gas atoms be small compared with that of bombarding ions and, if possible, small compared with the vaporizing rate of target atoms. The vacuum chamber developed for the performance of this experiment is a 32-in. diameter bakable dome with an 11-in. flange mounting it to a 500 liter/sec General Electric Triode Ion Pump. A 10-in. flange was used to mount the ion source on the top of the chamber (shown in Fig. 1 (schematic) and Fig. 2 (photograph)). Five bakable flanges located around the mid-line of the chamber were used for mounting the internal assemblies. Of these, two 6-in. flanges at opposite sides of the chamber were used to mount and position the rotating arc structure, holding the QMA detector. One 8-in. flange perpendicular to the axis of rotation of the detector mounting arc provided support and motion to the liquid metal target assemblies, and two 4-in. flanges were used to mount the Deposition Thickness Monitor and a viewing window. A liquid nitrogen cryopanel was installed as a flat canister along one side of the chamber and a copper baffle was attached to it and extended 4 in. above the pumping port. This cooled baffle prevented arcing noise in the ion pump from being picked up at the QMA and also prevented mercury or cesium droplets from directly entering the pump.

The pump and chamber were baked to 350°C for 8 hours prior to installing the internal assemblies, and a pressure of 4×10^{-10} Torr was attained. Care was taken to insure the cleanliness of each component as it was installed. During initial test runs with the QMA, standard coaxial cable (RG88A) with teflon insulation was used to carry in the rf signal and to carry out the output signal. Mass analysis of the residual gases in the chamber indicated that high molecular weight organic vapors were coming from the teflon. When subjected to the operating temperatures of the ion source and the hot targets, the teflon softened and the coaxial leads eventually shorted. Thus, it became necessary to replace these cables with asbestos-insulated, high-temperature coaxial leads. Under these conditions, with prolonged operation at operating temperatures, the pressure improved to an indicated 2×10^{-8} Torr* and the residual spectrum was relatively

* Experience with similar ultrahigh vacuum systems in which flash filament type ion gauges were employed as a check against ion pump current values would indicate that the actual pressure in the system was probably on the order of 1×10^{-9} Torr.

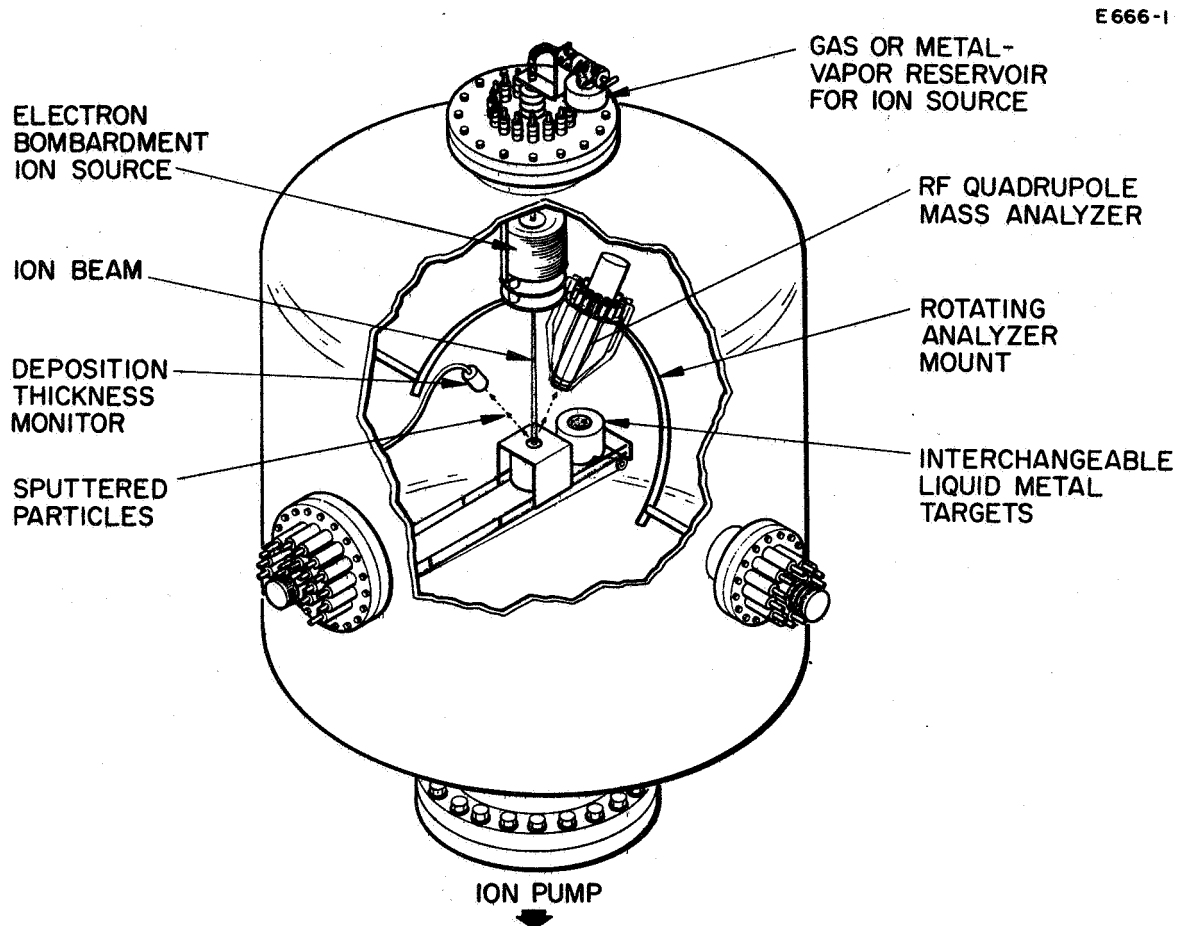


Fig. 1. Schematic drawing of liquid metal sputtering apparatus.

M 5011

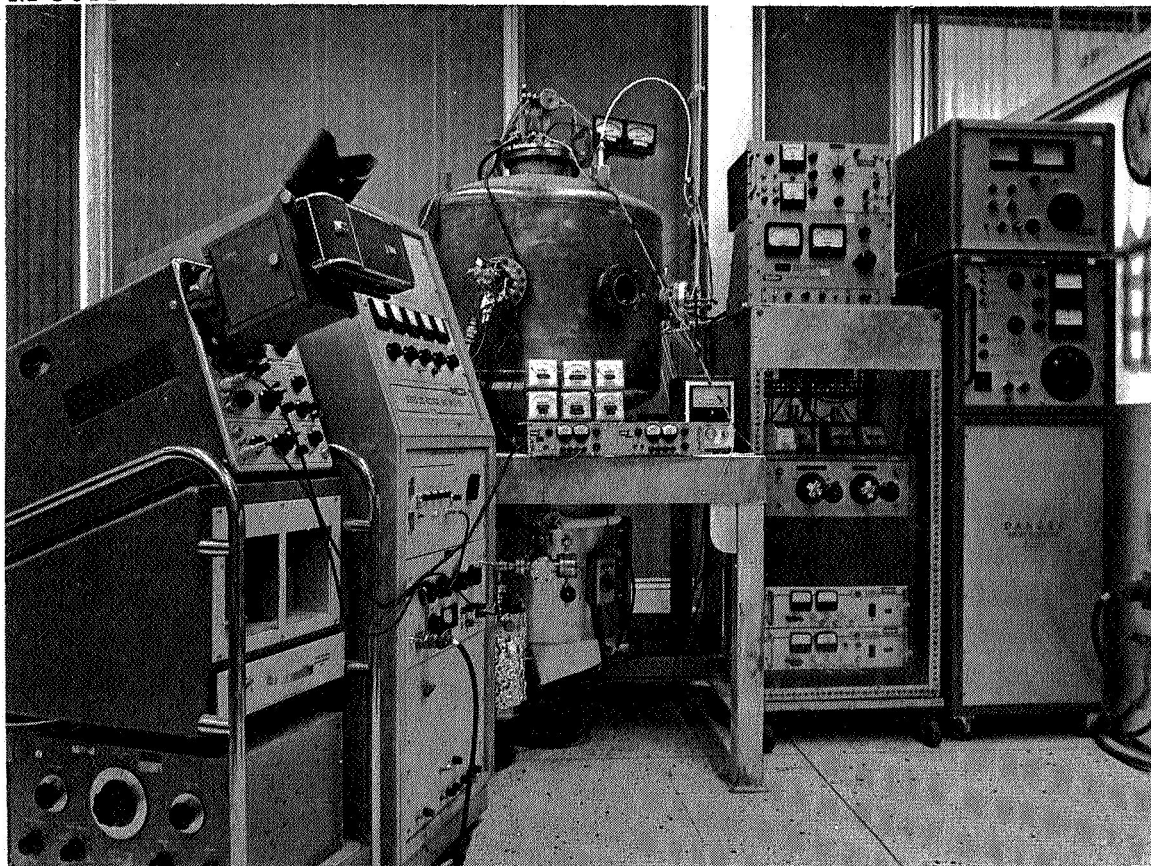


Fig. 2. Photograph of liquid metal sputtering apparatus with associated electronic supplies.

clear of organic vapors (see Fig. 3). When the ion gun was operated with mercury or cesium, these vapors represented the primary contribution to chamber pressure; even then, the pressure only reached an indicated 5×10^{-8} to 2×10^{-7} Torr.

The arrival rate of oxygen, water vapor, or nitrogen is expected to be less than 10^{12} atoms/cm²-sec, whereas typical arrival rates of ion beam materials or of vaporizing target material are expected to be on the order of 10^{13} to 10^{14} atoms/cm²-sec.

B. Quadrupole Mass Analyzer

The heart of this experimental apparatus is the QMA detector which serves both to analyze the mass distribution of the sputtered species and to detect the residual gas species in the chamber. The Paul-type rf spectrometer²² was chosen as the mass analyzer in order to (1) provide flexibility of operating resolution and sensitivity, (2) permit angular rotation of the entire detector within the limited diameter of the vacuum chamber — which would be difficult with magnetic separators, (3) permit mass analysis independent of velocity of the sputtered particles, and (4) permit bakeout of the entire detection unit.

During the initial months of this program no short QMA was available commercially which could be mounted and rotated within the 32 in. diameter vacuum chamber. Thus, a special QMA was designed and fabricated at Hughes Research Laboratories for preliminary observation of the sputtering of the aluminum and gallium liquid metal targets and solid targets of magnesium alloy. When the Ultek QMA Model 200* became available, its engineering provided high mass resolution and good rf shielding in the output, as well as automatic range scanning features which facilitated experimental observations. Therefore, this unit was purchased to perform the measurements necessary in this program.

The QMA was mounted in a protective shroud which contained an entrance chamber $3/4$ in. long with a 0.100 in. aperture for collimation of entrance particles (see schematic drawing, Fig. 4, and Figs. 5 and 6). A transverse electron beam was provided to ionize the neutral particles entering the axially mounted ionizer and QMA. When operating with a resolution capability of 100 (i.e., the ability to clearly separate mass peaks 1 amu apart at mass 100), the sensitivity of the detector is 23 A/Torr of argon using a standard of 1 mA electron bombardment emission

*Ultek Corporation, 920 Commercial St., Palo Alto, California. This unit employed the quadrupole assembly and electronic supplies developed by Electronic Associates, Inc.

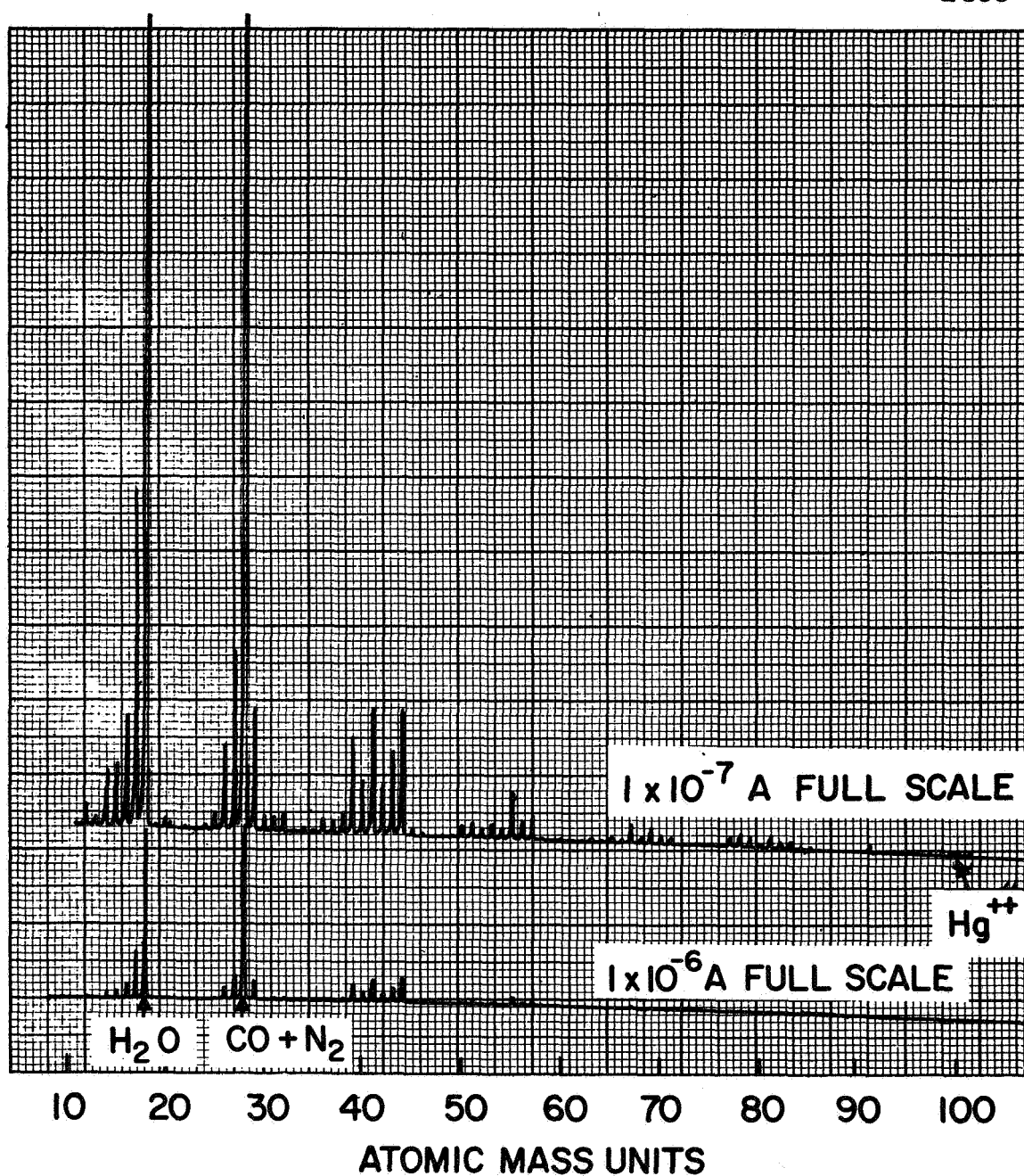


Fig. 3. Residual gas spectrum in vacuum chamber with ion pump indicating 3×10^{-8} Torr.

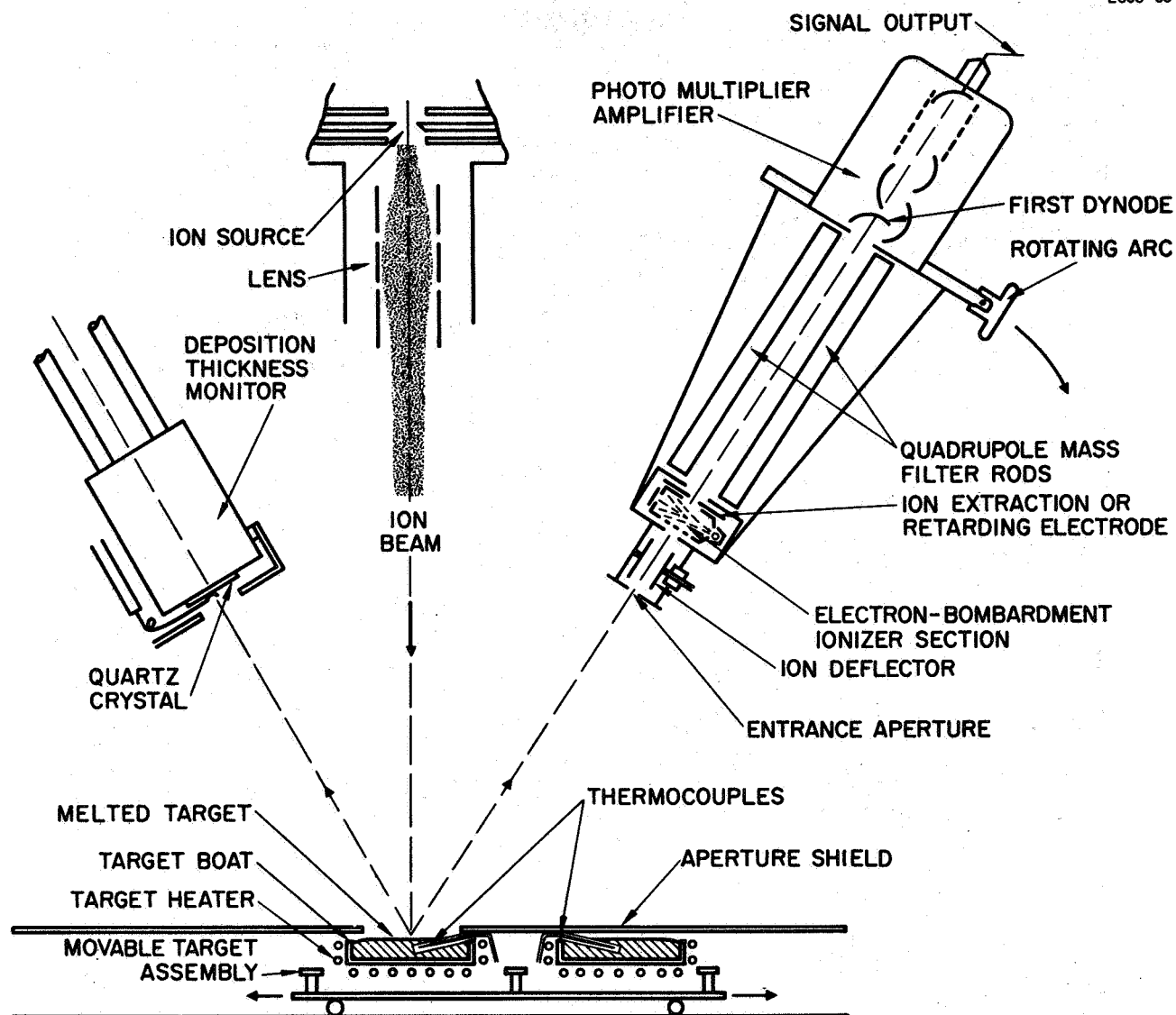


Fig. 4. Schematic view of Quadrupole Mass Analyzer and target assemblies.

M 4875

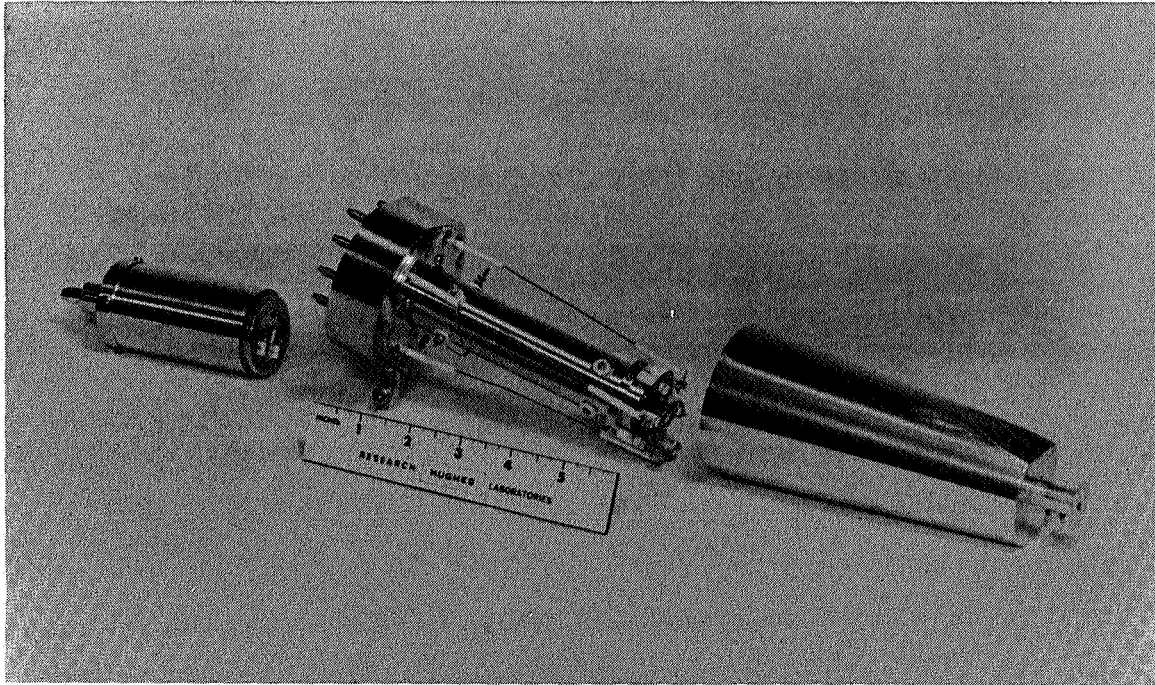


Fig. 5. Components of EAI quadrupole mass analyzer prior to assembly. Photomultiplier is shown at left, the mass filter and axial ionizer structure are in the center and the protective shroud with the collimating apertures and ion deflection chamber are shown at the right in the photo. The flat side of the shroud near its entrance permits sputtering measurements to be made at angles close to the bombarding ion beam.

M 4873

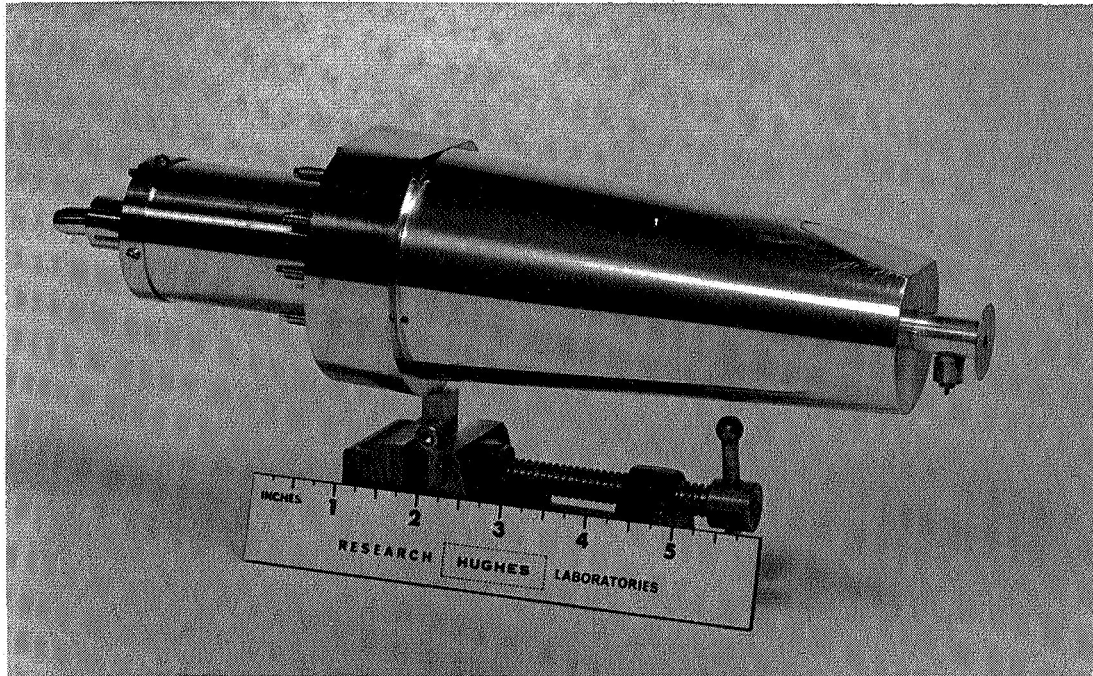


Fig. 6. Photograph of Quadrupole Mass Analyzer Assembly.

current. With this same resolution the detector has approximately 10% of this sensitivity for the detection of vaporizing aluminum vapor streaming into the entrance aperture.

The ionizer structure on the forward end of the rf quadrupole filter is shaped as shown in Fig. 4. When detecting sputtered particles, the bombarding electron stream was turned off to detect the ionic species alone. When a dc voltage up to 120 V is applied to the deflecting plates in the entrance chamber, the ions are deflected from entering the filter. With the ions rejected but with the electron bombardment on, the neutral sputtered species can be observed. By setting the ionization cage and entrance potentials to ground (the target potential), the extraction electrode could be used as a retarding potential and the energy of sputtered neutral species were observed.

The QMA was equipped with a 10-stage electron photomultiplier structure to give an amplification of approximately 10^5 to the output signal. The first beryllium-copper dynode of the photomultiplier is biased to -3000 V and receives the incident ions from the filter. Thus, sputtered positive ions or bombardment-ionized neutral species are detectable in this system and, with a relatively minor change, negative ions can also be identified. The first dynode is in line with the sputtered target, and thus fast neutral particles and x-rays or photons also strike the dynode to contribute to the noise background. In spite of this, the sputtered signal usually was clearly visible above this background signal.

The QMA was mounted on a rotating arc assembly (see Fig. 1) which was ball-bearing supported and moved by a bakable flexible bellows assembly. Although 360° of rotation is available, the usable travel is limited to 20° from the target normal by interference with the incident ion beam and 20° from the target surface plane due to interference with the target shield. Thus, the usable quadrant is 20° to 70° , with the present target and ion source assemblies.

The alignment of the QMA was accomplished by mounting it onto the rotating arc with the photomultiplier assembly removed. Then a light beam was directed through the quadrupole rods and ionizer apertures to project onto the target. The mounting clamp is set in such a way that the axis of the mass analyzer is directed to the center of the metal target at all angles of rotation.

C. Ion Source

The ion source employed was an electron-bombardment type with magnetic confinement and a single extraction aperture (see Fig. 7). Although a contact ionization source could have been used for producing an alkali ion beam, we used the electron bombardment type because

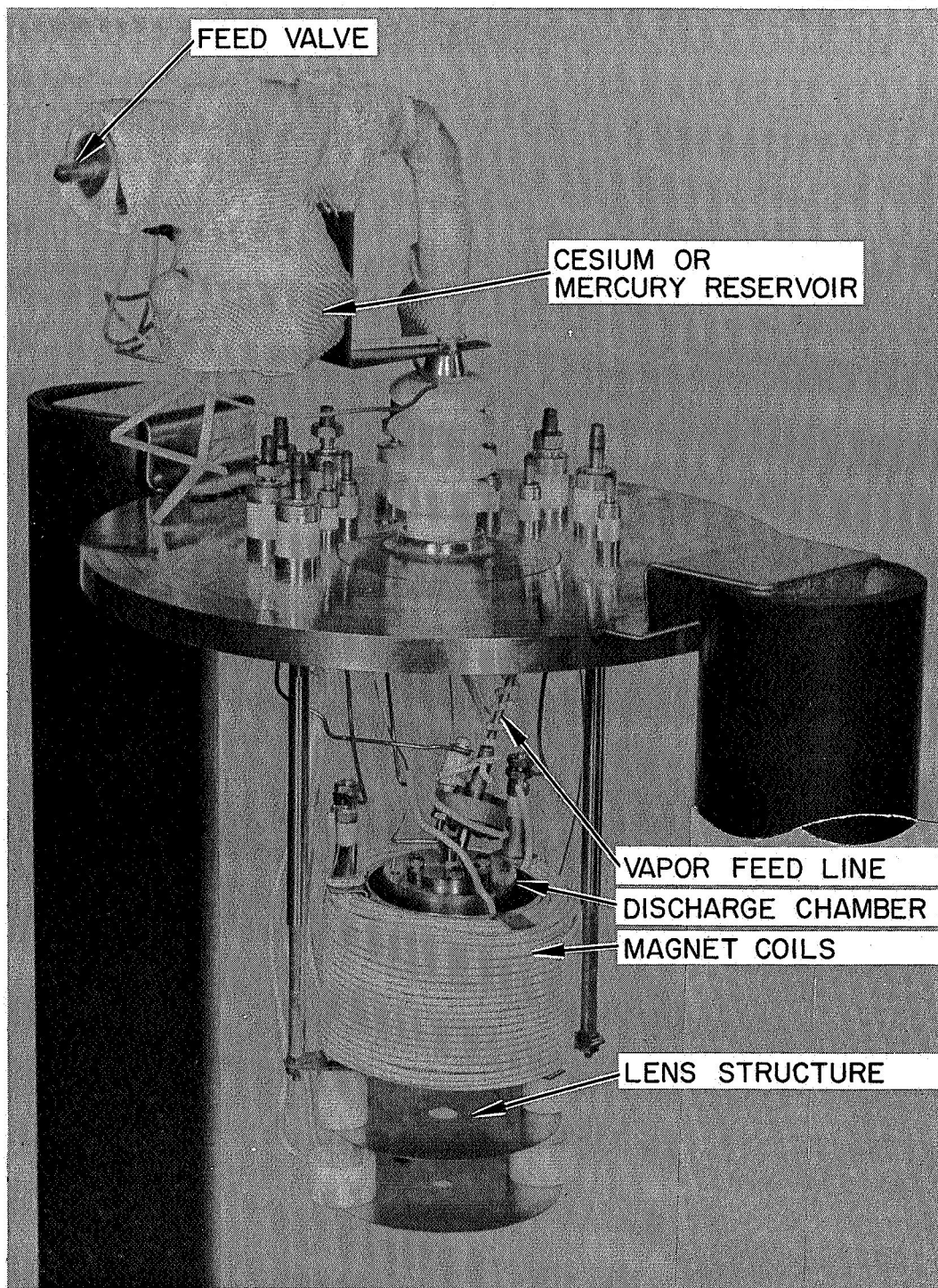


Fig. 7. Photograph of electron-bombardment-type ion source.

it was required for production of ion beams of mercury or the inert gases. It also could be converted easily to a cesium ion source merely by replacing the liquid mercury reservoir with a liquid cesium reservoir.

The accelerating electrode structure of the ion source was developed from ion optical studies made on the electrolytic trajectory tracer-analog computer system. The accel-decel nature of the ion optics permits the gun to produce an ion beam with energies of 1 to 15 keV but the presence of metallic vapors, particularly of cesium, tends to limit the useful upper energy to the range of 10 keV.

A three-element Einzel lens was used to concentrate the ion beam onto the metallic target. Beam current densities employed were in the range 0.1 to 10 mA/cm² at the source, which produced a detectable sputtered signal with 10 to 300 μ A at the 1 in. diameter target. The discharge voltage was maintained at 30 V for a mercury beam and at 10 V for a cesium beam. These energies are sufficiently low to assure²³ that the beam will consist of less than 2% doubly charged ions.

D. Target Assembly

The early attempts to use a porous target assembly through which liquid metal flowed to wet the surface met with considerable difficulty. In cases such as aluminum and gallium, where the liquid would wet the porous structure of tungsten, it also reacted severely with the tungsten and destroys the porous material when operated at 900 to 1000°C. Similar difficulties were encountered with tin and indium through porous tungsten and molybdenum targets; the flow of these metals was impeded by oxide films until a sufficiently high temperature was reached that flow began; the metals then flooded through the porous material and balled up or ran off the outer surface. Even sputter-cleaning of the porous surface did not facilitate the formation of a smooth, uniform, liquid film.

For highly reactive materials such as aluminum, it was considered possible to use a porous structure of high purity Al₂O₃; however, because the liquid aluminum will not wet the structure, capillary action tends to prevent flow and excess pressure then is required to cause flow. The resulting surface on the front of the target will be composed of tiny spherical drops rather than a smooth plane; thus the sputtering results of angular variations of the ion beam incident on these droplets will be extremely difficult to interpret.

The concept of a rotatable target is very attractive from the standpoint of making sputtering measurements at various incident angles, but the physical task is difficult using reactive liquid metals. At this point in the program, it was decided that the most meaningful observations on liquid metals could be made while they were held in a flat boat. Then, if the basic results warranted the effort, porous structures with liquid metal surfaces could be developed.

The restriction to a horizontal liquid target requires motion of the ion source if nonnormal incident ion bombardment is of interest. The exit particle detector then must move in the plane of the incident ion beam and target normal as well as perpendicular to that plane, if integrated yield is to be observed. The latter motion is required because sputtering out of the incident plane may not have a cosine distribution. For first observations, the experiments were performed with the ion source in the perpendicular to the surface, and axial symmetry could be assumed for the exit particle distribution (a safe assumption when single crystal targets are not employed).

The target boats to contain aluminum and gallium samples were made of boron nitride because this material presented the least hazard to high temperature operation. When the aluminum was heated in boats of high purity alumina, the liquid metal did not immediately wet the walls; however, after several heating and cooling cycles over a 10-hour period, the aluminum reacted with the slight impurities in the Al_2O_3 and began to bond to it. The thermal expansion and cooling of the 1-1/4 in. diameter metal pool cracked the boat so that another heat cycle could not be attempted. With the boron nitride boats the aluminum may have reacted slightly with the inner surfaces of the boat, but the surface tended to flake off and avoid straining the boat.

The reactivity was sufficiently low for indium and lead samples that Al_2O_3 boats were used without mishap.

To measure the temperature of the melted target material the thermocouple wires were jointed in the bottom of a thin-walled thimble which was inserted down into the liquid metal. This provided temperature readings which were accurate to within $\pm 15^\circ$ for relatively slow changes of target temperature.

The electrical lead to measure the ion bombardment current was made by inserting a graphite probe into the liquid metal. For aluminum, gallium, indium, and lead, the reaction with the graphite was sufficiently slow that the experiments could be performed.

The cerium and tin targets presented technical difficulties even when operated as a flat pool in a target boat. When the cerium was heated to 900°C to melt it, the graphite probe and its molybdenum mounting wire were lost in the melt. In addition, even though 99.5% pure samples were employed, the cerium and tin showed surface films which required heating to above 1000°C for removal when heated in the vacuum. These films may have been formed by interaction with the boat materials; it was expected that the surface contamination could cause erroneous sputtering observations. It was then decided to proceed with the measurements using bombardment by mercury and cesium ions on the other four materials before experimenting with boat materials for use with liquid cerium and tin. When the contract period was consumed in making extensive measurements on the materials of primary interest, time did not permit further experimentation to overcome the technical difficulties with cerium and tin. A future program aimed at observing the sputtering characteristics of these materials in their solid and liquid phases could be of considerable interest.

The target assembly (shown in Fig. 8) was made to hold two target boats with a magnetic coupling drive to position either one under the ion beam. Each target is separately heated and monitored as to temperature and incident ion beam. A titanium plate covered the target assembly and served as a defining aperture for the bombarding beam. Titanium metal was chosen for its high temperature properties and for its easily identifiable mass (74% abundance at 48 amu), which could be used to indicate when the ion beam or the QMA detector was focused on the shield and not on the target.

E. Deposition Thickness Monitor

A crystal-controlled Deposition Thickness Monitor (DTM)* was used to monitor the sputtering or vaporizing rate in an attempt to calibrate the QMA to obtain absolute sputtering yield values. The DTM was mounted at a measured distance and angle from the target and thus the QMA signal could be checked when it was at this same angle. A defining aperture restricted the entrance direction to the DTM; however, some sputtered material from the shield still fell onto the crystal, complicating the possibility of obtaining an accurate absolute yield number.

An electronic counter (Hewlett-Packard Model 5245L) was used to monitor the frequency of the crystal and a deposition rate as low as 10^{-10} g/cm²-sec was detectable. The quartz piezoelectric crystals with the DTM had a silver contact film vapor deposited onto one side. The unit operated satisfactorily to observe sputtering by an inert gas ion beam; however, when used with the mercury beam, the silver film peeled off of the crystal and the frequency became erratic. The mercury vapor apparently amalgamated with the silver film and caused it to separate from

*Unit employed was Model DTM-2a manufactured by Sloan Instruments, Inc., Santa Barbara, California.

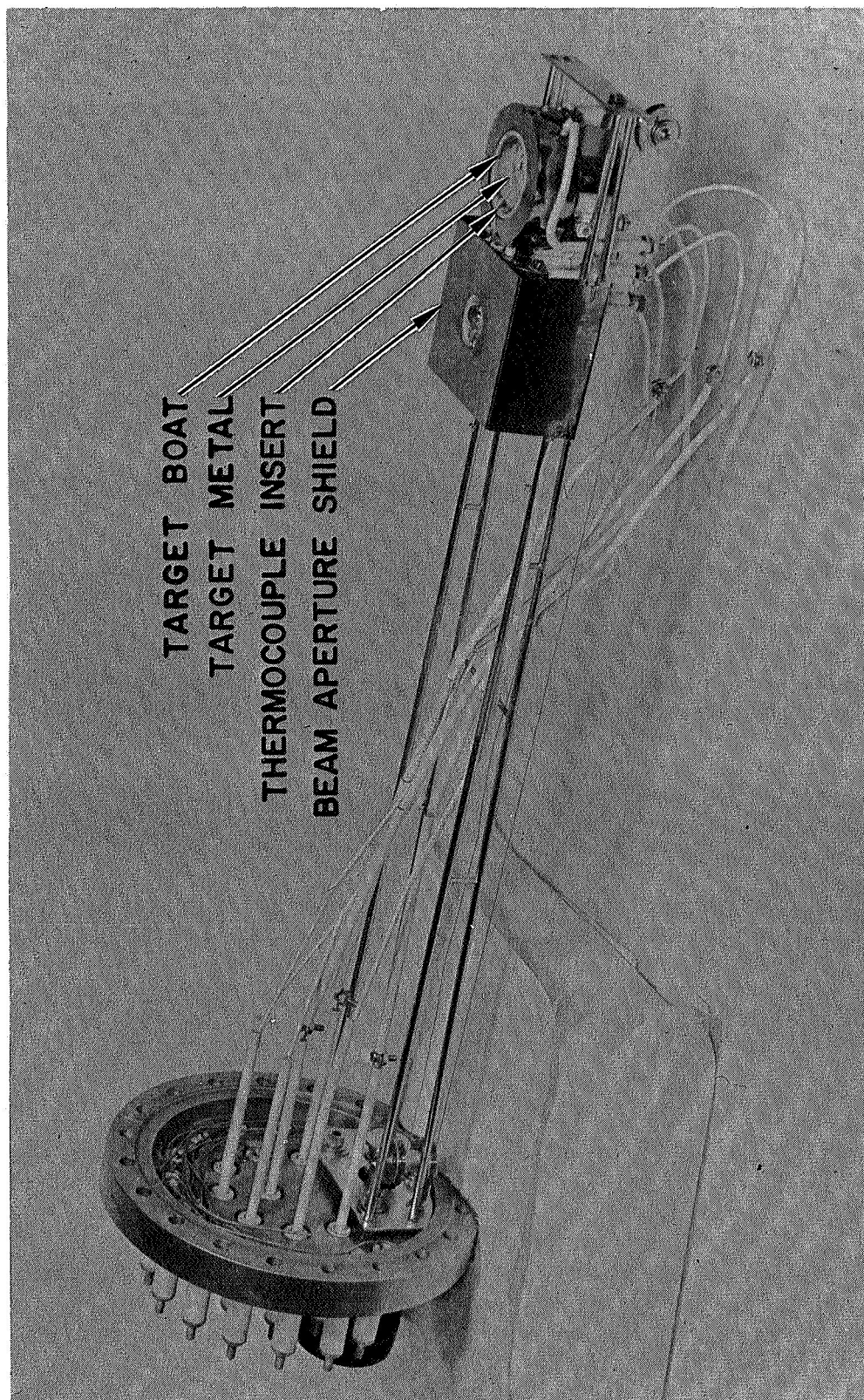


Fig. 8. Photograph of target assemblies with half of aperture shield removed.

the quartz. A thin film of nickel-iron alloy was sputter-deposited onto the crystals and was found to perform very well. The sputtering process gave better adhesion to the quartz and the alloy is less susceptible to mercury attack.

To compare the sensitivities of the DTM and the QMA the units were each set at 40° from the surface normal of the lead target, which was slowly heated to 600°C . When the lead target temperature T_{Pb} reached 470°C (vapor pressure of Pb = 5×10^{-6} Torr), the QMA showed that the vaporizing lead peaks with twice the background level (approximately 5×10^{-9} A). The signal was observed to increase to a 2.25×10^{-7} A signal at the $T_{\text{Pb}} = 565^\circ\text{C}$ (vapor pressure of Pb = 1.9×10^{-4} Torr). At this point the DTM frequency changed at a rate of 256 Hz/min of deposition, indicating an arrival of 1.7×10^{13} atoms/cm²-sec. A frequency change of 2 Hz/min is detectable, which indicates a lower observable limit of approximately 10^{11} atoms/cm²-sec. As mentioned above, the simultaneous arrival of material sputtered from the target and the shield makes the determination of an absolute sputtering rate very difficult.



III. EXPERIMENTAL RESULTS

A. Mercury Ion Bombardment

The first observations made in the program were on the sputtering of aluminum by argon ions. In order to test the feasibility of the detection system, a QMA was installed at a fixed angle to an aluminum target plate in a glass-cross vacuum system. The residual gas spectrum showed a high peak at 28 amu because of the CO and N₂ in the system. Organic radicals at 27 amu were sufficiently large that the 27 amu peak resulting from aluminum was difficult to see. Therefore, a target of magnesium alloyed with 3% aluminum was installed. When this target was bombarded with the ion beam, the peaks at 24, 25, and 26 amu were seen to rise in the residual gas display (see Fig. 9). When the extraction voltage of the QMA ionizer was reduced to zero, the signal resulting from species with thermal velocities were suppressed; however, the sputtered atoms had sufficient velocity directed up the line of the QMA that they were clearly visible in the output signal (see Figs. 10 and 11). The peaks indicate the isotopes of magnesium in their proper ratios (79% amu 24, 10% amu 25, and 11% amu 26). The mass 27 peak is attributable to the aluminum in the alloy. Elimination of the electron bombardment in the QMA ionizer reduced the mass peaks by approximately a factor of two. This indicated that the probability of sputtering ions compared with neutral atoms must be of the same order as the probability of ionizing these sputtered neutral atoms; these were later found to be traveling at considerably greater than thermal velocities.

When the feasibility of performing the experiment was established, the QMA was installed on the rotary arc in the metal vacuum chamber. The mercury ion source and the liquid aluminum and gallium targets were also installed. The aluminum sputtered ion peak appeared as shown in Fig. 12 after the aluminum target was bombarded with 5 keV mercury ions. The sputtered neutral aluminum atoms did not appear to be detectable despite repeated attempts at observation. The sputtered aluminum ion peak height was typically 2×10^{-7} A above the background noise level of 10^{-9} A and thus was easily visible.

In order to establish that the sensitivity of the QMA detector was not affected by its angular position (it might have been caused by being close to the electrostatic and magnetic fields of the ion source), the residual gas spectrum was observed with all the source voltage applied, but with the beam turned off at the valve in the mercury feed line. Using the mass 28 peak height for comparison (see Fig. 13), it can be seen that the sensitivity to neutral particles which are isotropic in distribution is essentially constant. When the aluminum particles (sputtered by 5 keV mercury ions) were detected on the QMA, the amplitude of the mass 27 peak followed a distribution which was slightly peaked toward the surface normal. When the Einzel lens was turned on, its field tended to shift the sputtered ion signal away from the surface normal.

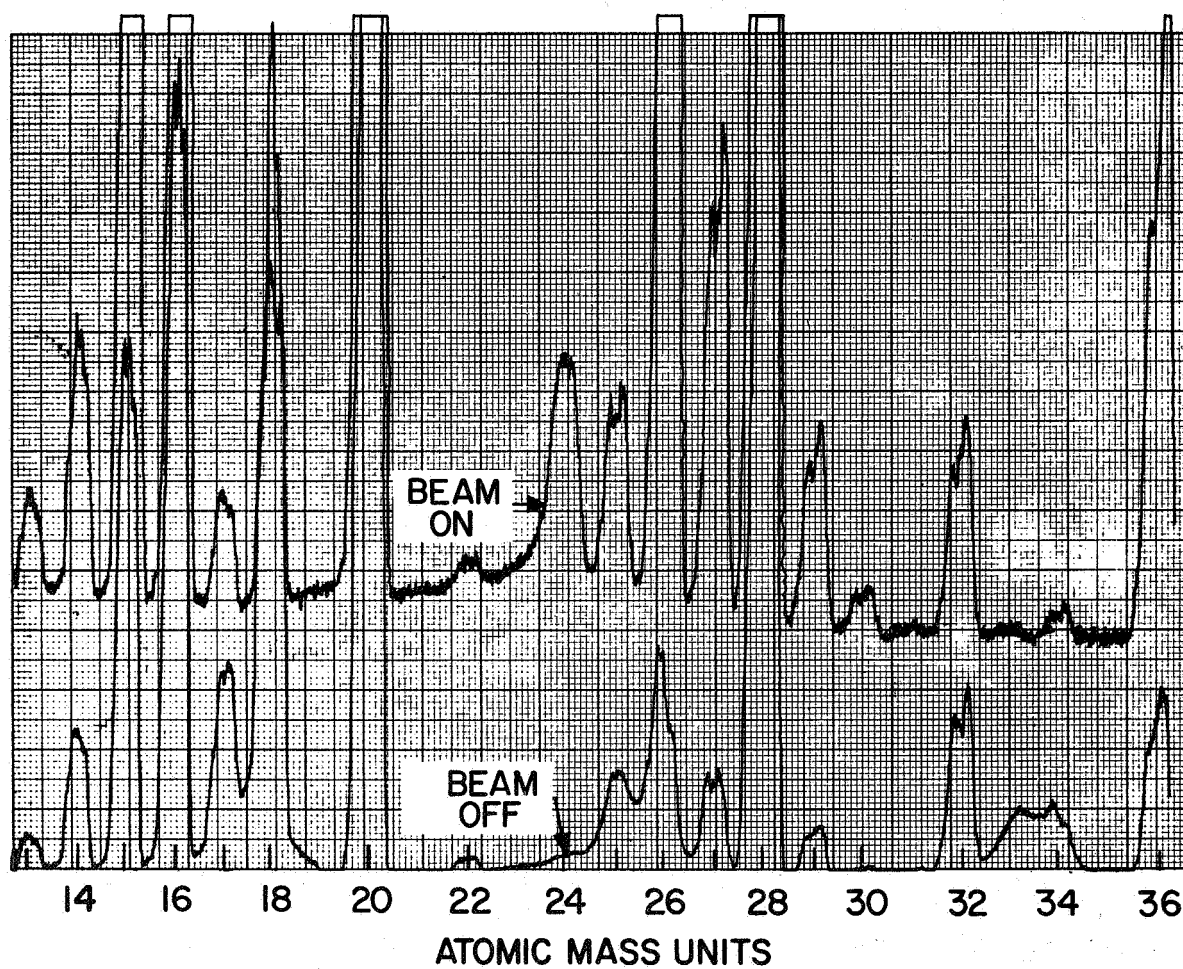


Fig. 9. Mass spectrum showing mass peaks sputtered from Mg target.

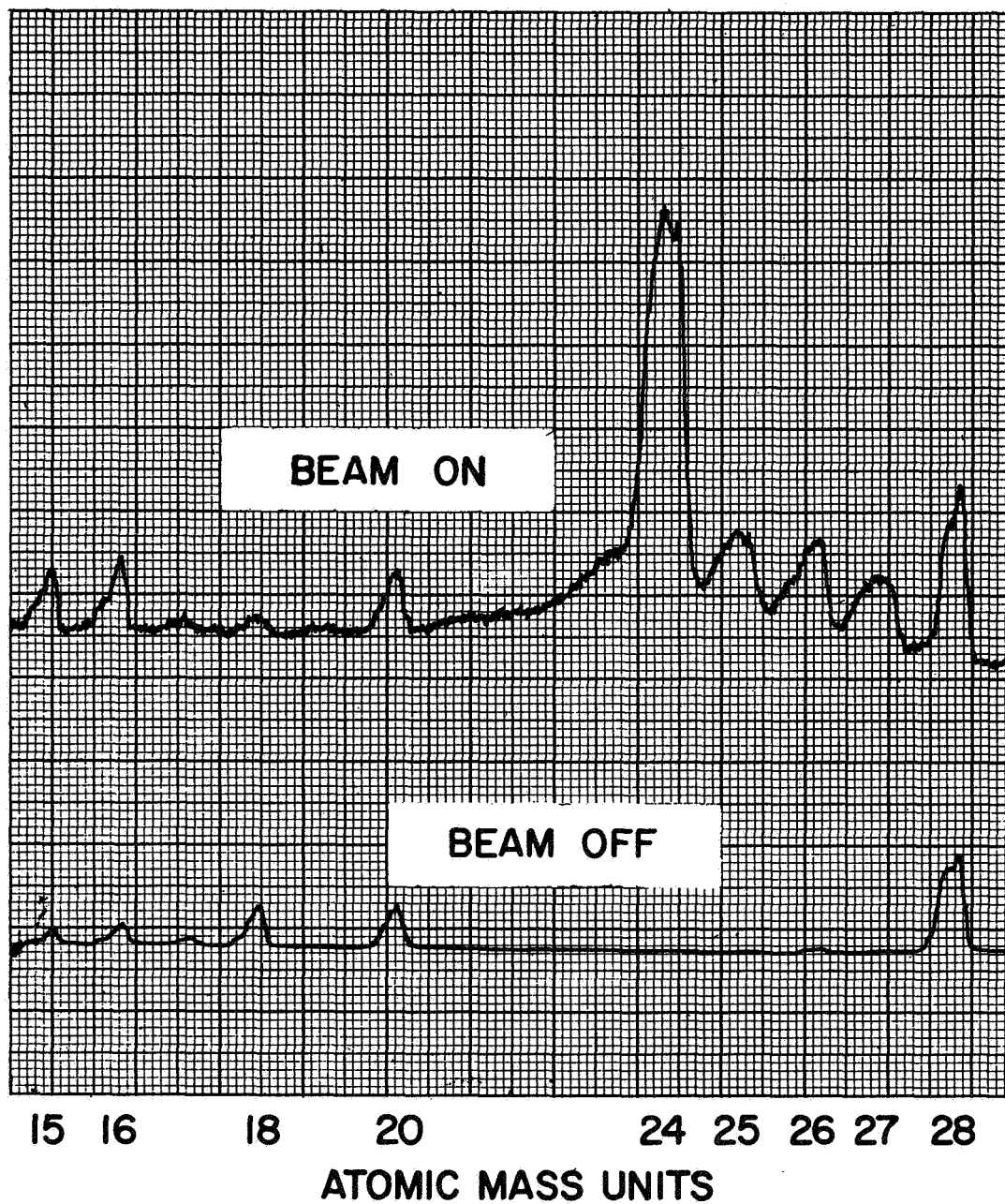


Fig. 10. Mass spectrum showing mass peaks sputtered from Mg target (residual background suppressed).

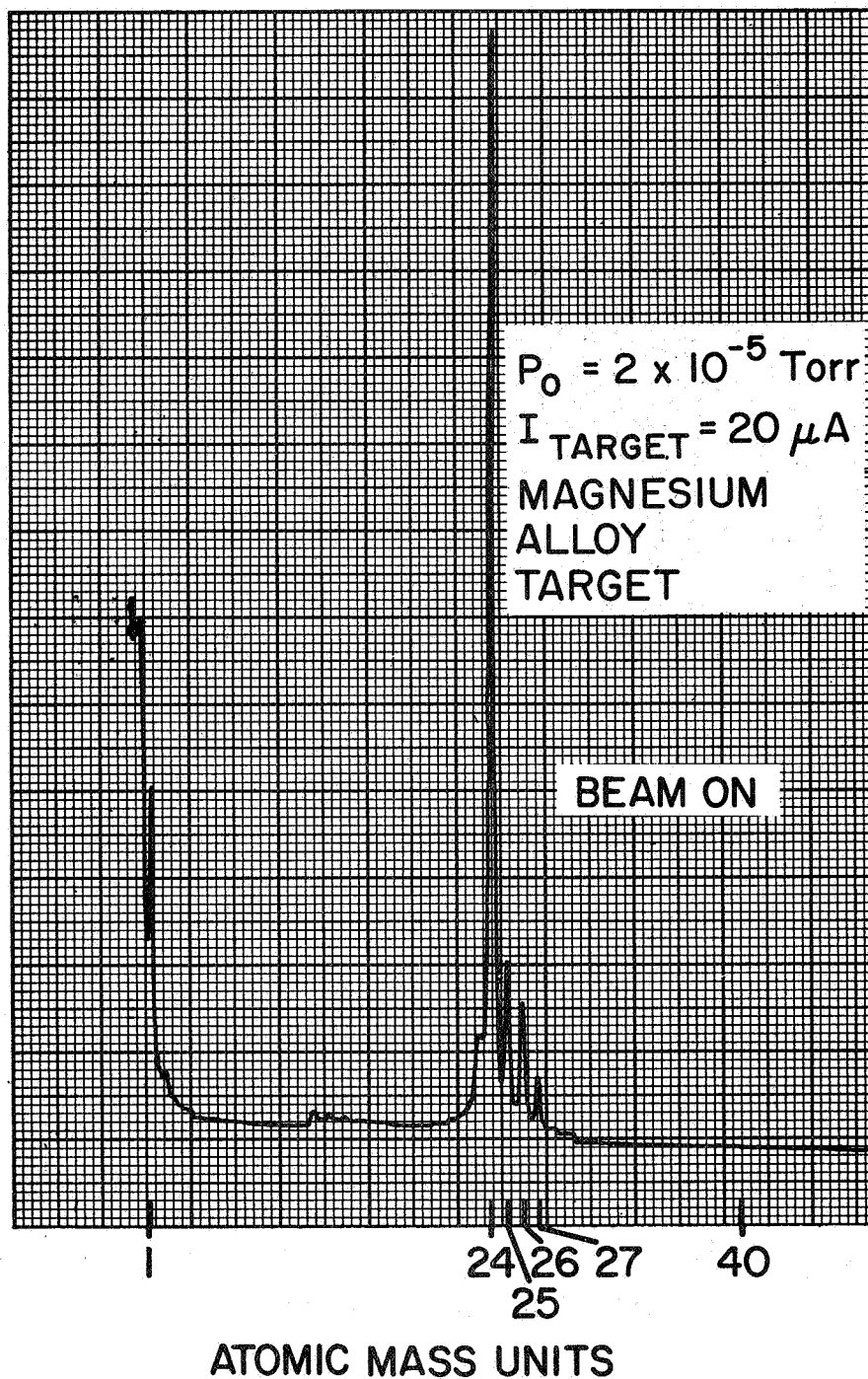


Fig. 11. Mass spectrum with ion beam on but with residual gas spectrum suppressed.

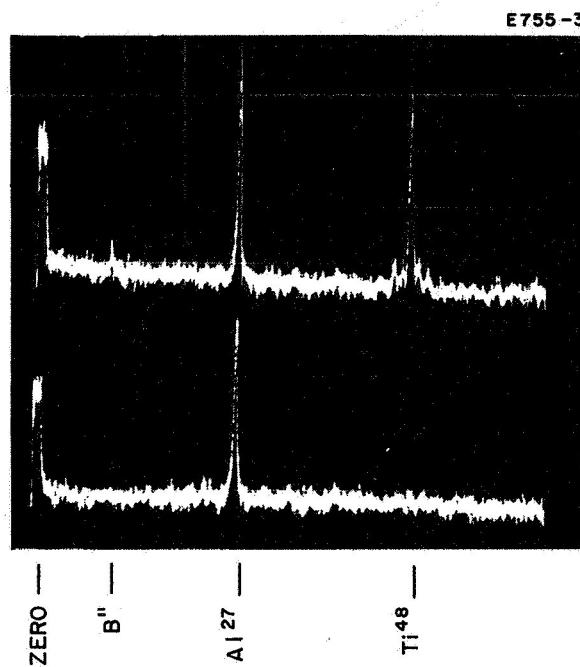


Fig. 12.
Sputtered ion spectra resulting from
mercury ion bombardment of
aluminum.

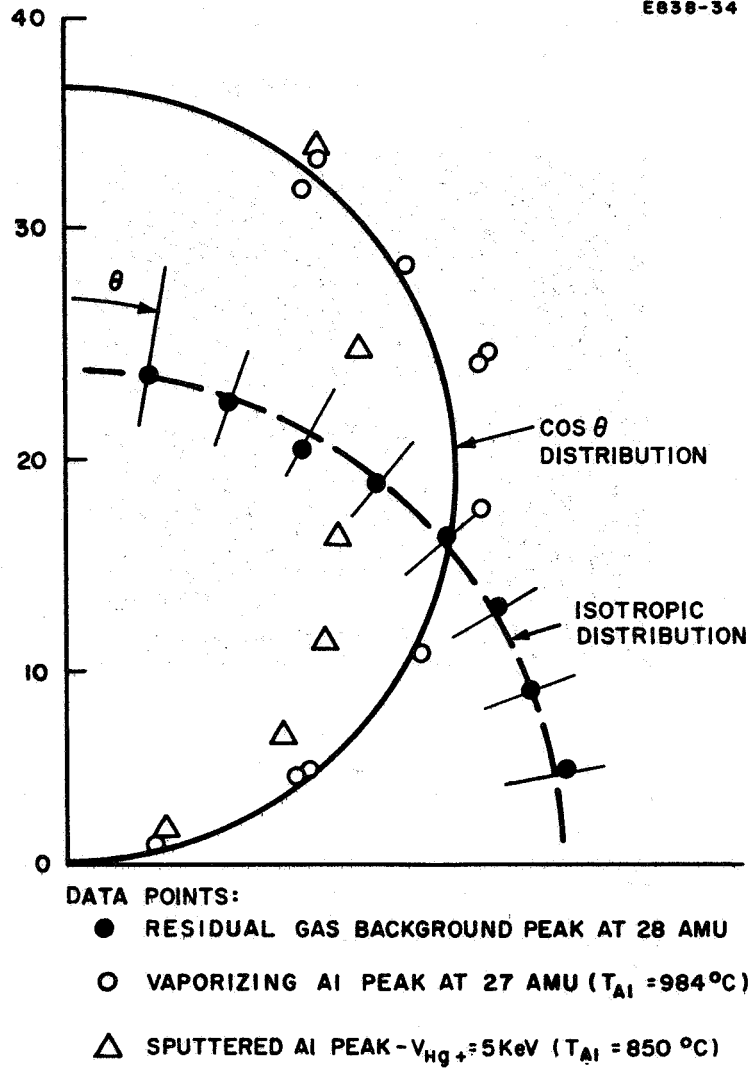


Fig. 13. Angular distribution of sputtered versus vaporizing aluminum.

Next, observation was made of the sputtering peak height as the aluminum target temperature was changed. Figure 14 shows photographs of the sputtered aluminum peak as the temperature went from 100°C up through the melting point (indicated as 650°; the true value is 660°C). A summary of the data is shown in Fig. 15. It is evident that the yield has decreased by approximately 25% in going from the solid to the liquid phase. The observation was repeated several times both with increasing and decreasing temperature; the change in yield was observed in each case. The large variations in yield which occurred at the melting point were too unstable to be observed quantitatively; they were probably related to the sputtering from thin surface films on the molten pool.

The sputtering peak height was observed at various ion bombardment energies at target temperatures above and below the melting point. The results are shown in Fig. 16. The indication is that for bombarding energies less than 8 keV the solid target (at 60 and 528°C) shows a decrease in yield for the same bombarding energy as the temperature increases. These results differ from those reported by Magnuson, *et al.*,¹¹ and by Veksler²⁴ in which the sputtering yields for refractory metals were seen to increase with target temperature. When the target is liquid, the yield is still lower and does not reach as high a maximum value even for the higher bombarding energy.

Attempts were made to observe the time of flight of the sputtered signal in order to determine the energy distribution in the sputtered particles. The ion beam was maintained constant on the target and a 1 to 10 μsec pulse was applied to the extraction aperture of the QMA ionizer in an attempt to gate the flow of ions through the mass filter. The expected time of flight through the 10 cm QMA would be about 15 μsec; thus, the delayed pulse was expected to be spread in time, indicating the velocity spectrum of the particles. Unfortunately, the rf pickup in the output of the QMA was sufficiently high that the microsecond pulse could not be resolved in the background signal. Therefore, we were unable to make a time-of-flight observation of particle velocity. Instead, it was possible to use the ionizer cage and extraction electrode of the QMA (see Fig. 4) to establish a retarding potential and thus determine the energy distribution in the sputtered particles.

For sputtered ions, the target and detection entrance apertures were maintained at a common ground potential and the incident ions were then retarded (see Fig. 17) by applying a positive voltage to the ionization cage or the extraction electrode. Both of these techniques had the same ion retardation effect. Use of the extraction electrode was preferred so that the same effective fields would be applied when observing sputtered ions or neutral particles. In the case of neutral species the electron bombardment ionization took place in the ionization

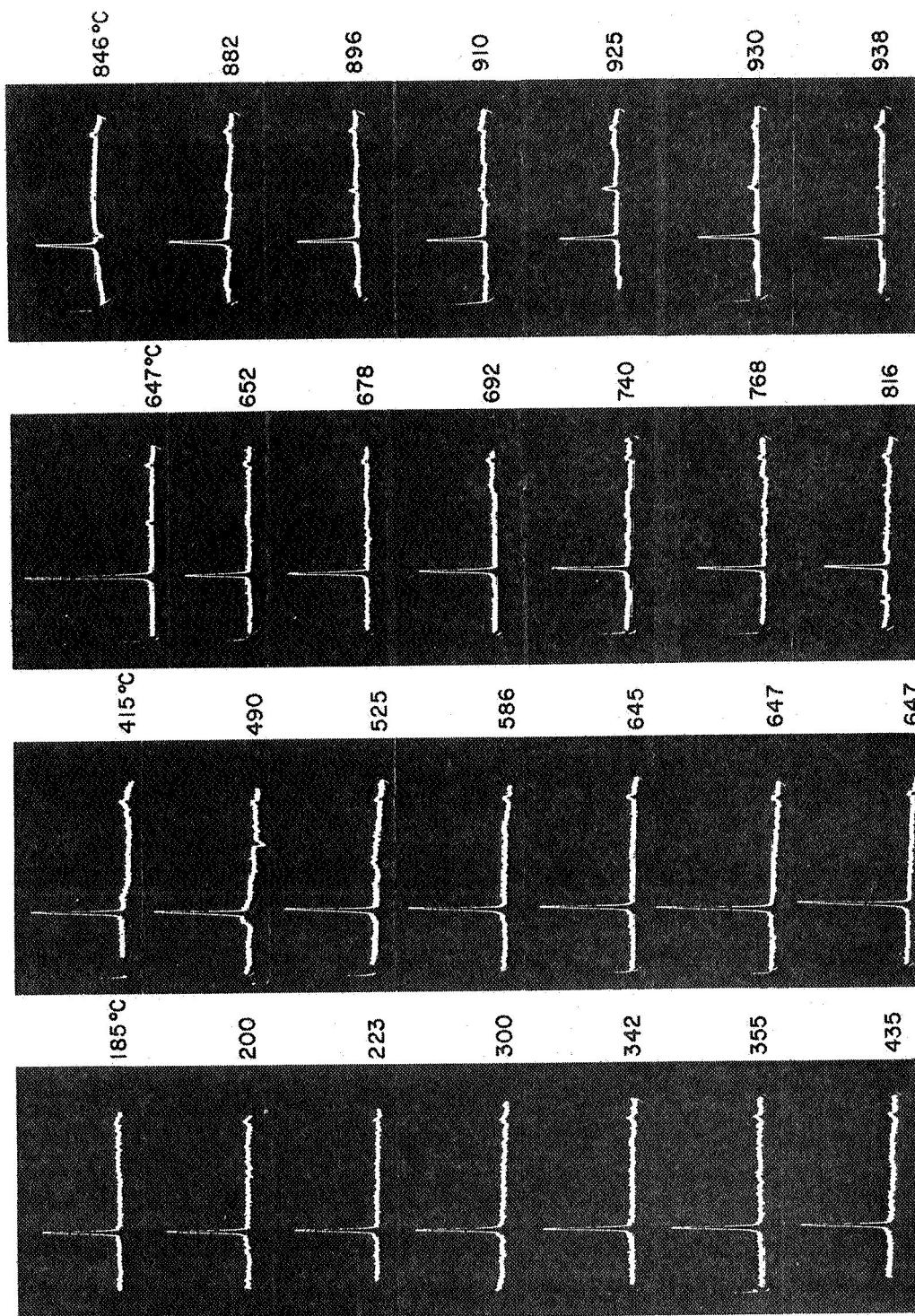


Fig. 14. Peak height of sputtered aluminum ions as observed when target temperature is varied from 185°C to 938°C.

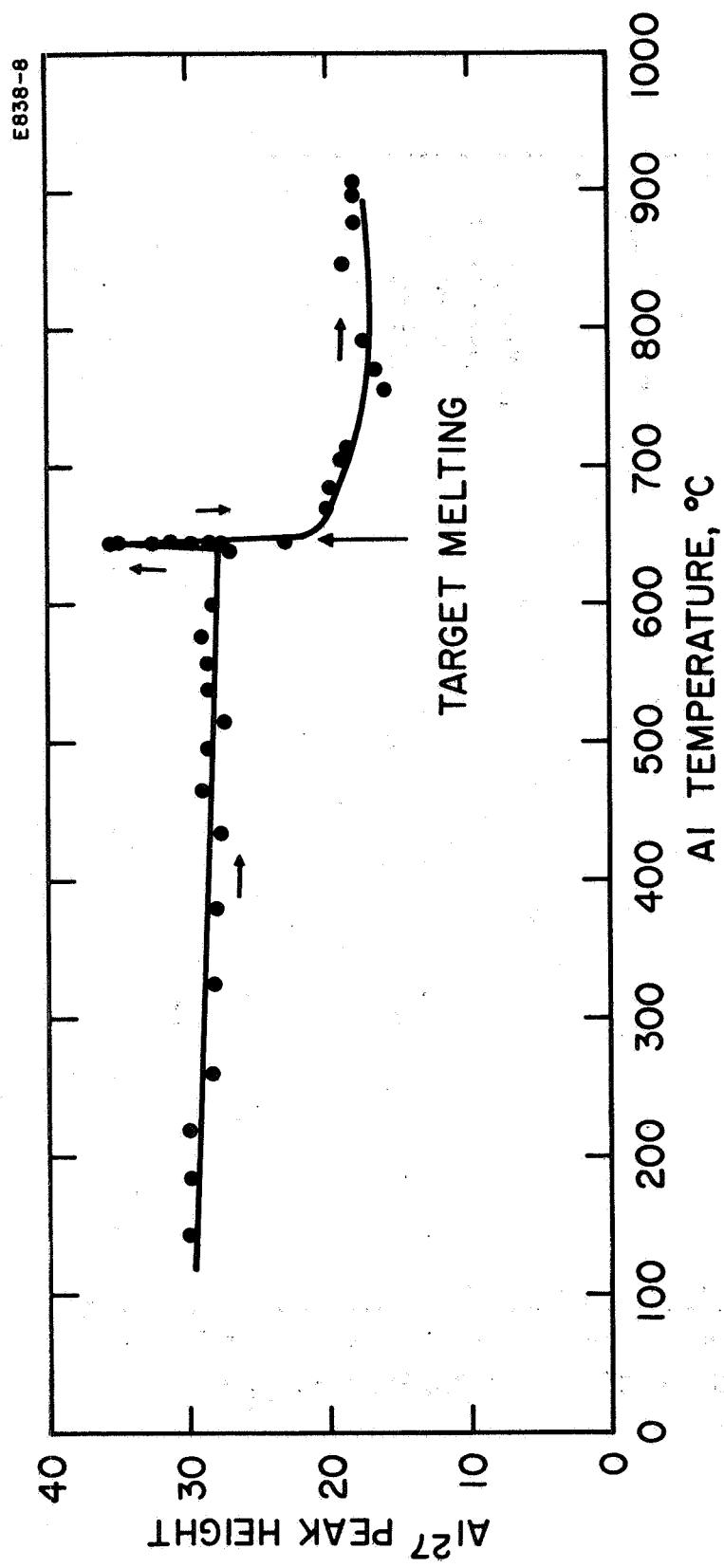


Fig. 15. Peak height of sputtered aluminum ions versus target temperature.

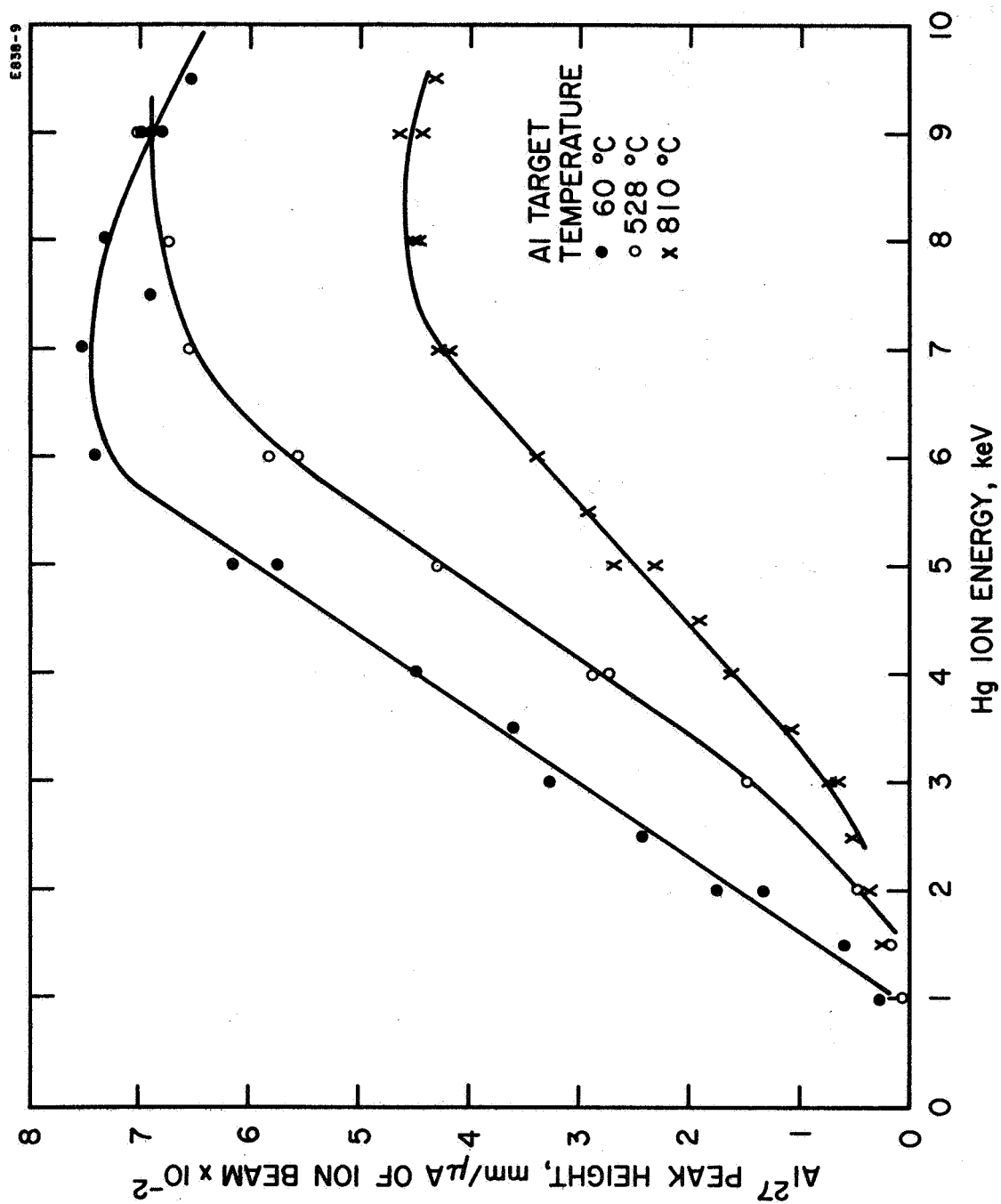


Fig. 16. Relative sputtering yield of Al²⁷ as a function of bombardment energy.

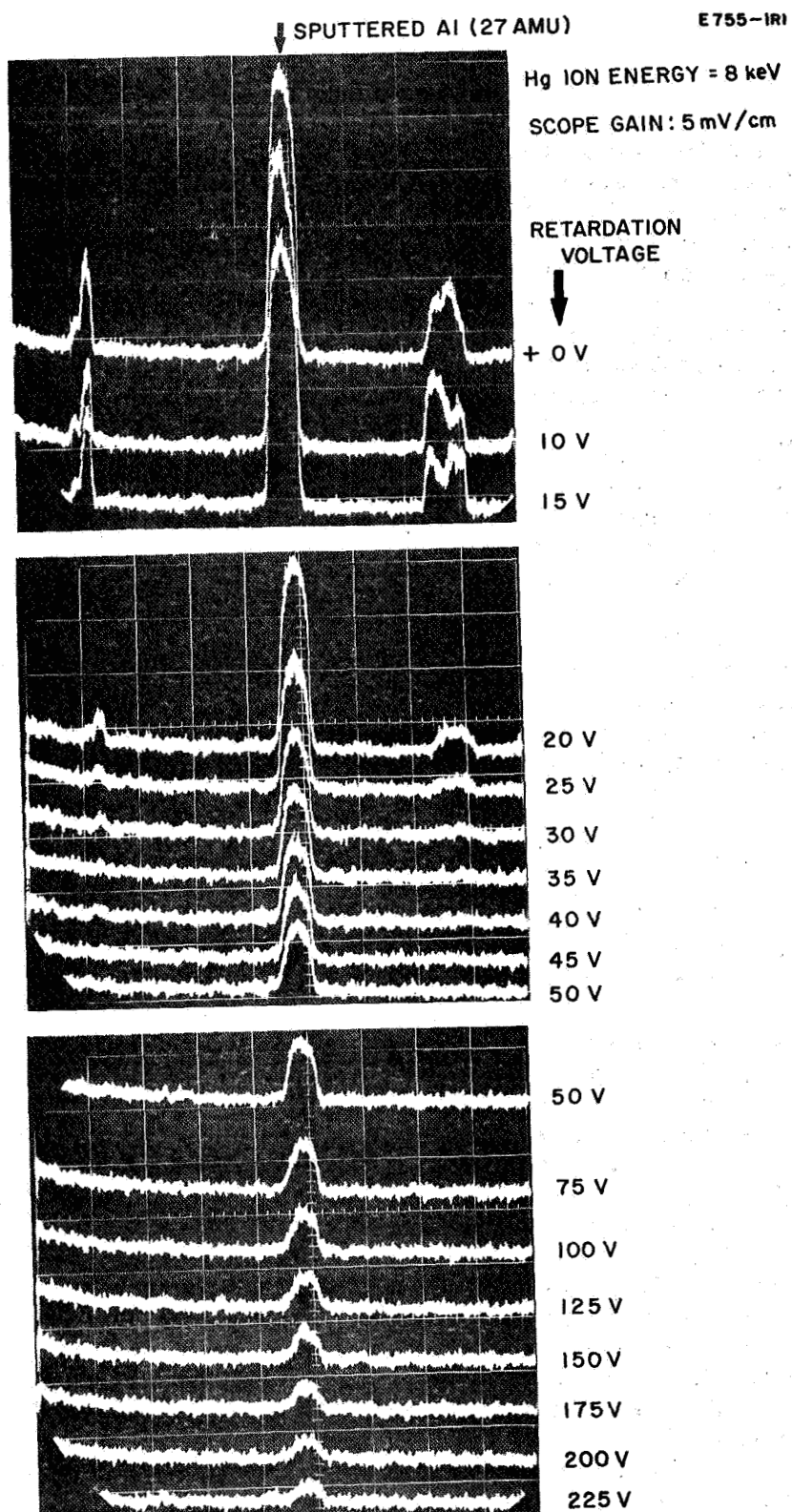


Fig. 17. Observations of the effect of the retardation potential on the peak height due to sputtered aluminum ions.

cage which was operated at ground potential. Low energy particles (such as thermally evaporating particles or residual gases) required that a small negative voltage be applied to the extraction electrode to accelerate the newly formed ions into the mass filter. Particles which were sputtered from the target at higher than thermal velocity were ionized and sufficiently well directed into the mass filter that they did not require the extraction voltage; in fact, they were able to penetrate the retardation field of the extraction electrode. Retardation studies were made for aluminum bombarded with mercury ions at energies of 2, 4, 5, 6, and 8 keV and at target temperatures of 60, 528, and 810°C. Figures 18 and 19 indicate that approximately half of the sputtered particles have energies in excess of 20 eV. In the liquid state, the half-maximum appears to increase to approximately 30 eV. A detailed analysis of these energy distribution curves is described in the following section.

The gallium target was moved under the aperture in line with the mercury ion beam for measurements similar to those made with aluminum targets. The melting point of gallium (28°C) was low enough that once melted in the system it did not refreeze. Therefore, all observations from ambient temperature (~40°C) to 900°C were made in the liquid phase.

The first observation with gallium was that the sputtered ion signal was lower than that of aluminum. However, a single peak height decrease of ~50% is expected because of the distribution of isotopes between two mass values 69 and 71 amu (aluminum is 100% 27 amu). Thus the resolution was sacrificed to obtain a measurable signal. In this case also, the ion signal was most evident and the neutral atom signal was too low for observation (less than 1% of the observed ion signal). In order to enhance the observed ion signal the target was biased positive with respect to ground; this was found to increase the number of ions which entered the QMA positioned close to the normal to the surface ($\theta = 20^\circ$). The resulting spectrum appeared as shown in Fig. 20, and observations were made of the sputtered peak height as a function of gallium target temperature (see Fig. 21). The result was alarming when the peak height increased dramatically at target temperatures above 800°C (see Fig. 22). This had not been observed in the case of the aluminum target and it was unreasonable to explain it as a sputtering phenomenon. Instead, we suspected that the effect was related to the vaporization of the gallium. This was verified by examining the QMA signal of vaporizing gallium with the ion beam off and, as shown in Fig. 22, the increase with target temperature is exactly the same. Thus, the ionization of gallium vapor by the incoming ion beam apparently is efficient enough to produce a large number of ions which are swept toward the QMA by the target bias. When the target was operated at ground potential, the temperature dependence of the signal was more easily understood and shows a slight decrease in

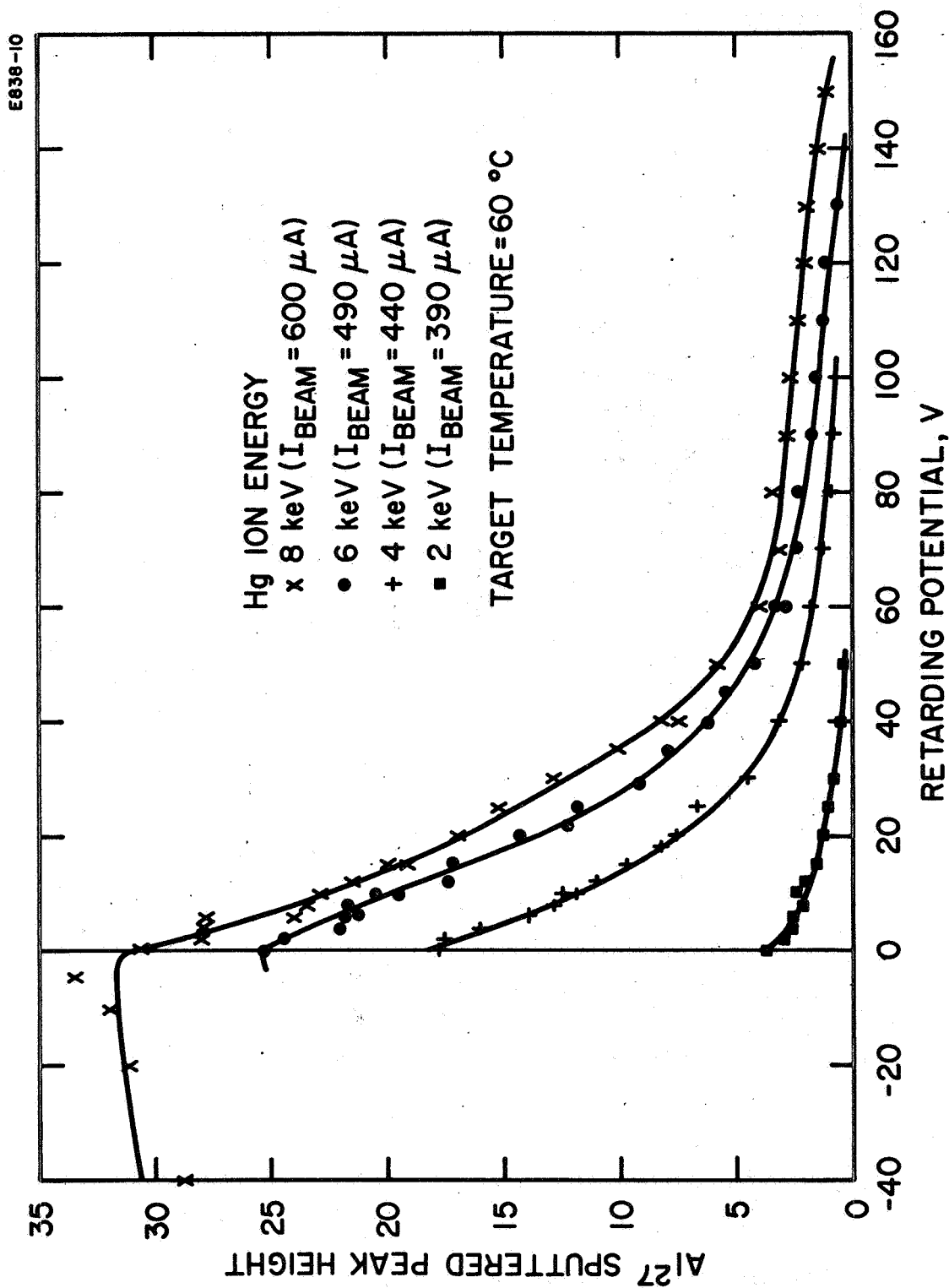


Fig. 18. Peak height of sputtered aluminum ions as a function of retardation potential for four values of ion bombardment energy.

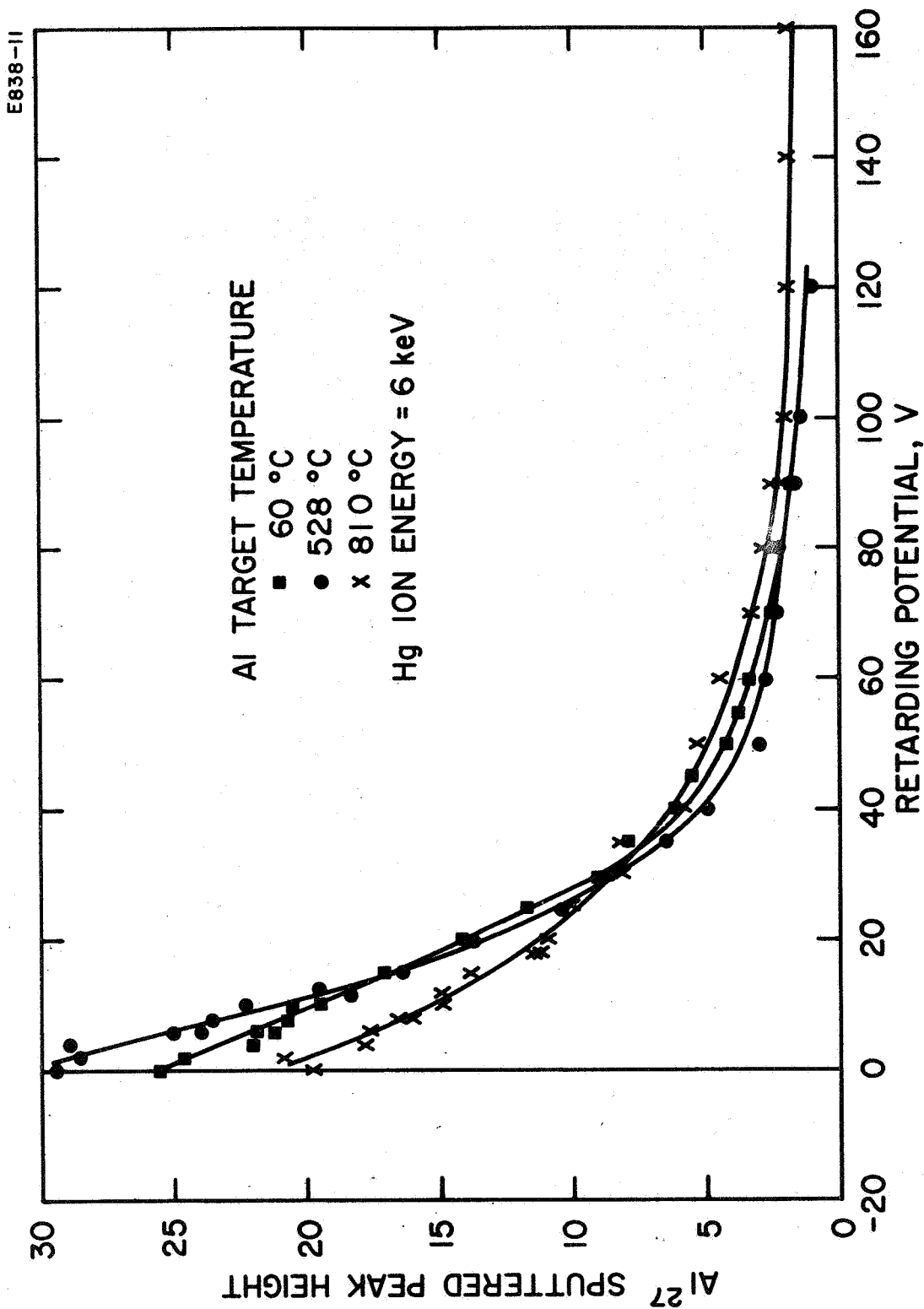


Fig. 19. Peak height of sputtered aluminum ions as a function of retardation potential.

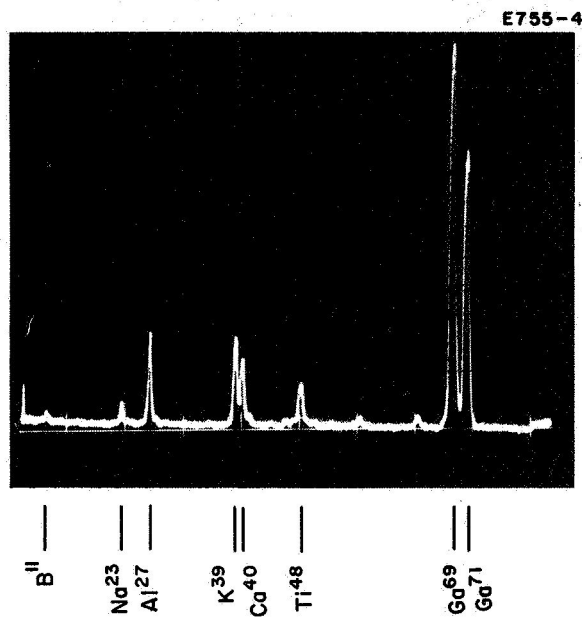


Fig. 20.
Spectrum of sputtered ions resulting from
ion bombardment of liquid gallium target.

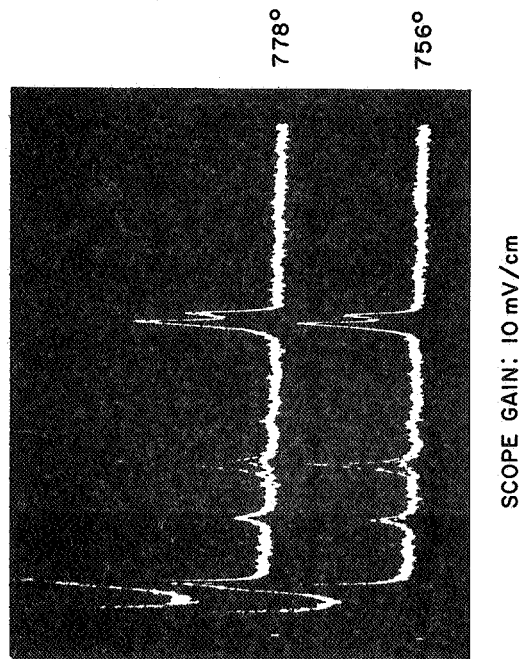
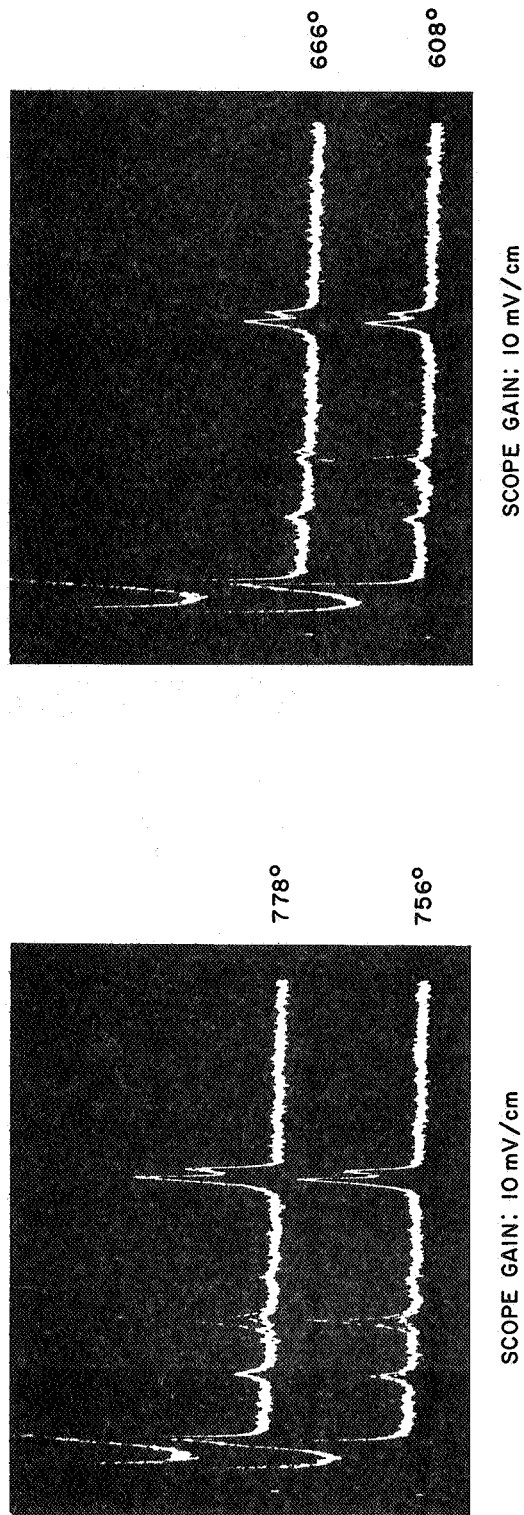
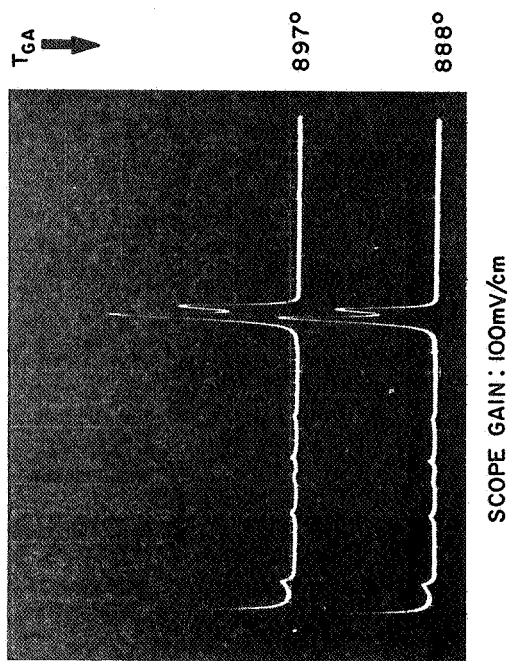
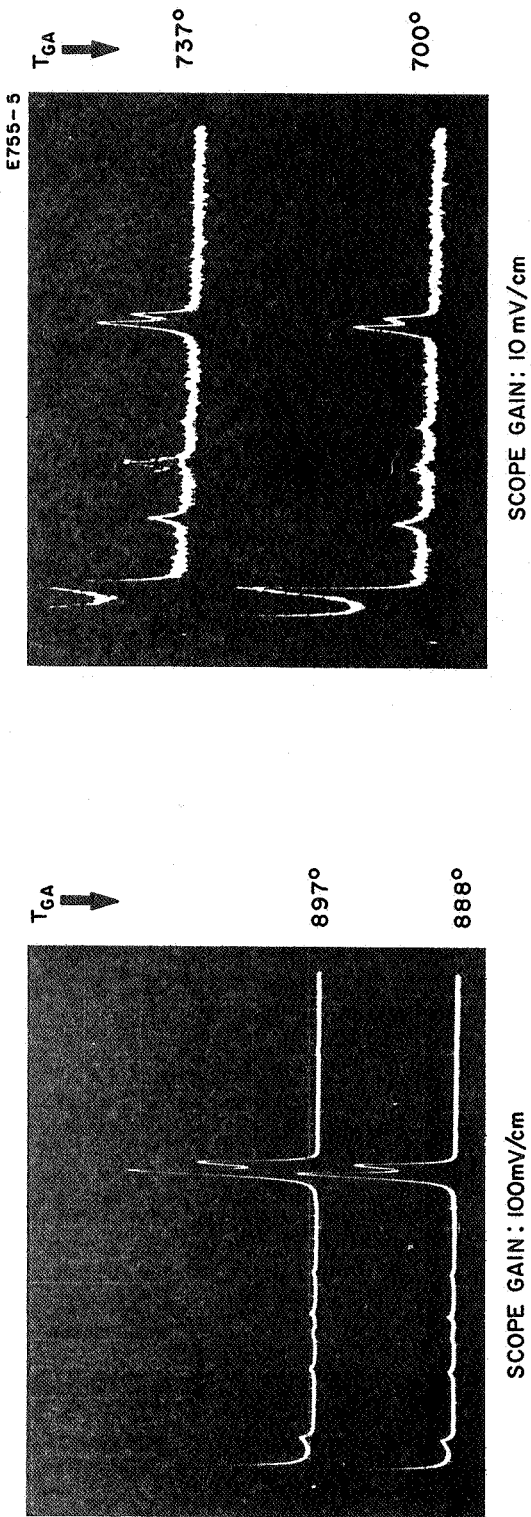


Fig. 21. Photos of output signals due to bombardment of gallium target biased to +67.5 V.

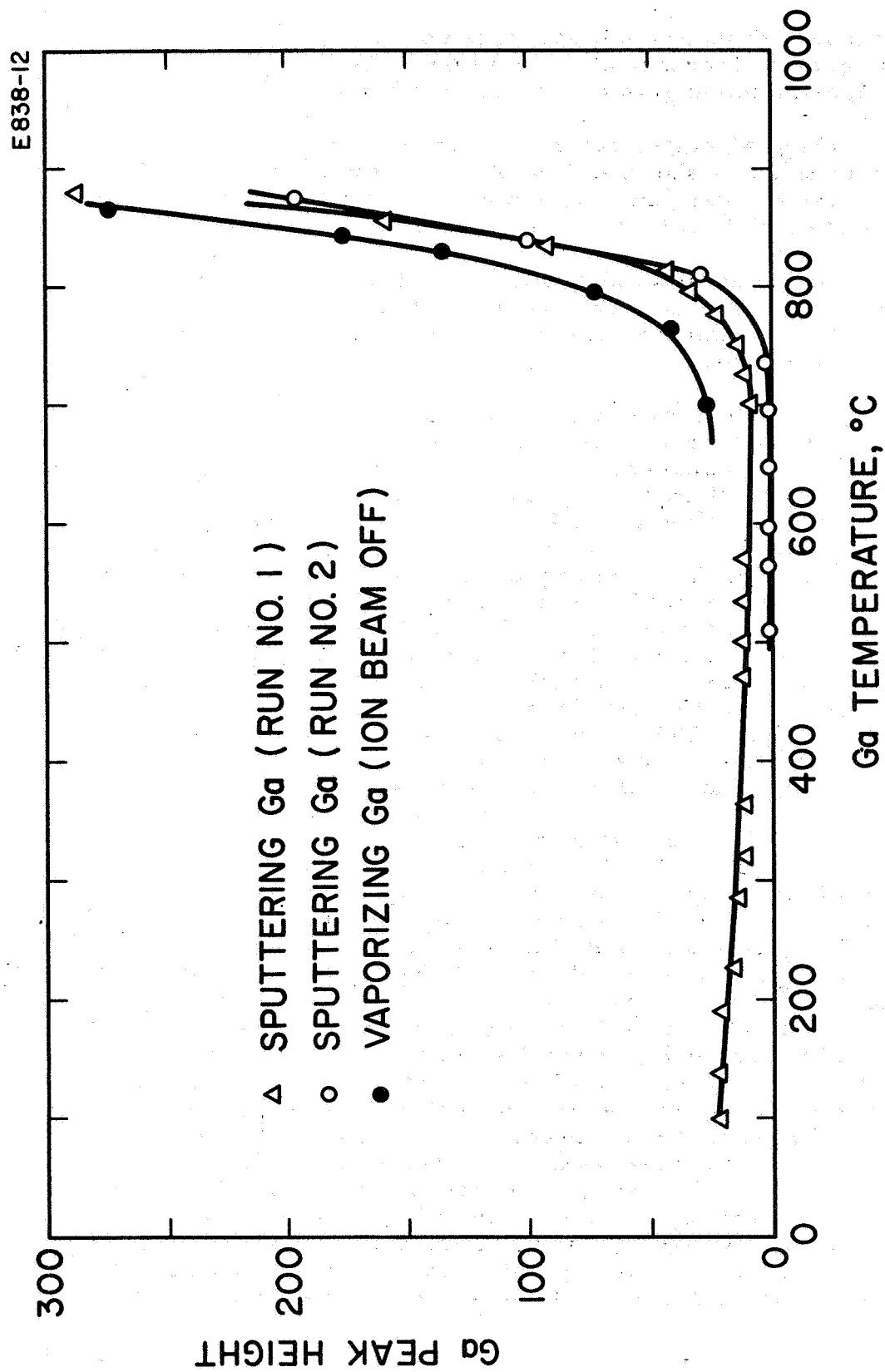


Fig. 22. Peak height due to gallium ions created by bombardment of liquid gallium target biased to +67.5 V.

magnitude with increase in target temperature (see Fig. 23). The yield shows an increase at temperatures above 850°C, indicating that vaporization effects may again be coming into play.

The peak height dependence on bombarding ion energy was observed to be as shown in Fig. 24. It approximates closely the yield curve for sputtering of liquid aluminum (Fig. 16), although the absolute yield values cannot be directly compared.

The retardation plots for the sputtered gallium ions are shown in Fig. 25. The average energies are lower than those seen for sputtered aluminum ions; they will be compared in more detail in the next section.

The gallium and aluminum target boats were replaced with indium and lead target boats, and observations were made on the sputtering characteristics of these materials. The sputtering signal was lower for indium than for gallium, but we were able to identify both the sputtered ion and the sputtered neutral atom species for the indium. These peak heights were observed separately as the target was heated through its melting point (156°C) on up to 600°C; they showed a behavior similar to that for aluminum. The sputtering yield appears to decrease as the metal goes from the solid to liquid phase (see Fig. 26). Of particular interest is the fact that the ion and atom yields do not differ significantly in their behavior. Because this comparison could not be made for aluminum, it was suspected that the decrease in sputtered ion yield on melting was accompanied by an increase in sputtered atom yield. According to the indium results, however, this does not appear to be the case.

The dependence of sputtering yield on bombarding energy is shown in Fig. 27. The characteristics are essentially the same for sputtered ions versus atoms, although higher bombarding energies (approximately 6 keV) are required for the ion signal to be distinguishable. There is a noticeable difference in energy content in the sputtered ions versus the atoms. As described above, the extractor electrode of the QMA ionizers was used to retard the incident ions, either those coming in directly from the target, or those created by electron bombardment ionization of the incident neutral atoms. In the latter case, the deflecting plates in the QMA entrance chamber were used to reject the incident ions before they entered the ionizer section. As shown in Fig. 28, the half maximum energy content of the sputtered atoms is 4 to 5 V, whereas the half maximum for the ions is approximately 15 V. Thus, sputtering deposition as a thin film technology seems attractive because the energy of the sputtered atoms is well above that of thermal vaporizing atoms but is apparently less than that of the sputtered ions. It is possible that the difference in these two energies resulted from slight acceleration of the ions by stray fields.

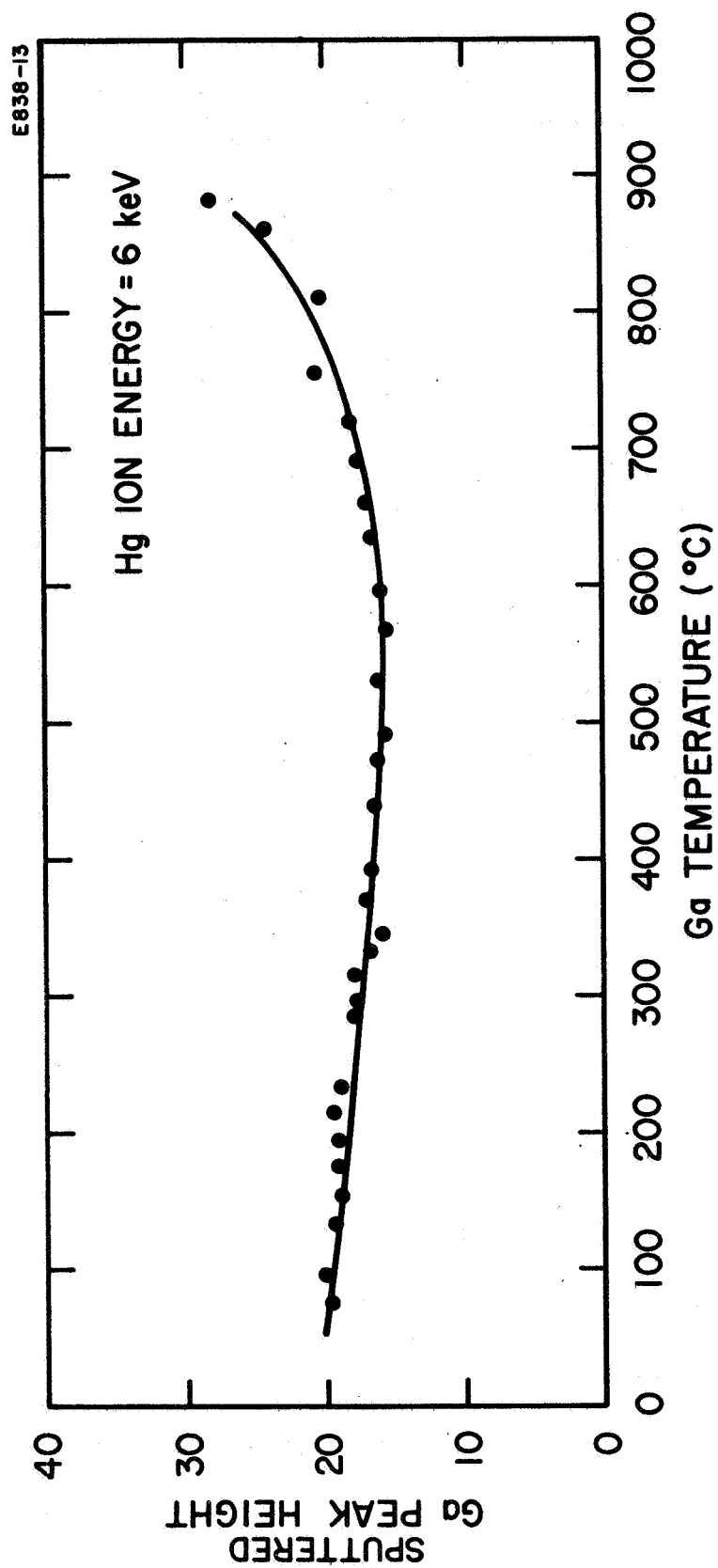


Fig. 23. Peak height of sputtered gallium ions as a function of target temperature.

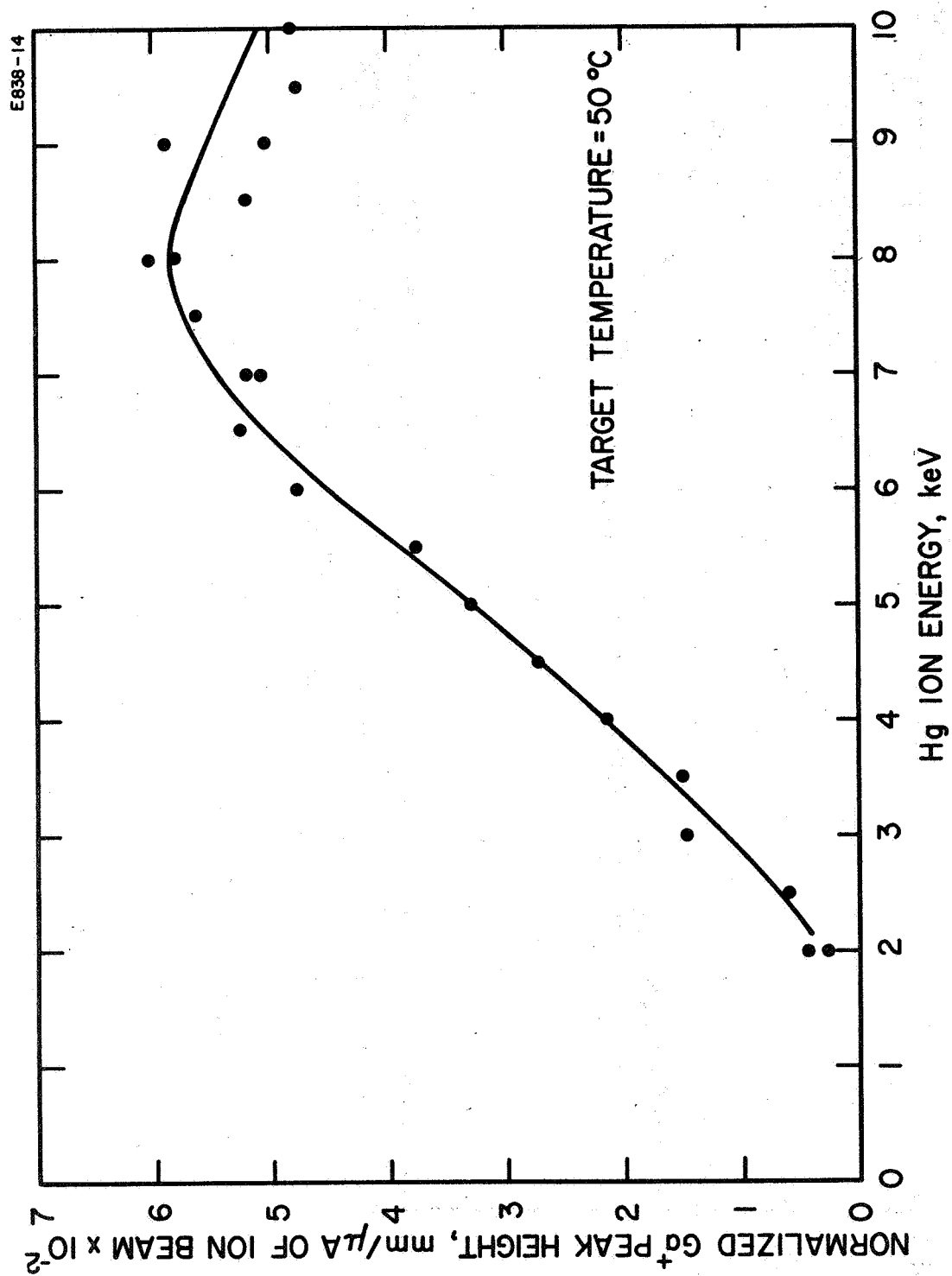


Fig. 24. Sputtering yield of gallium ions as a function of ion bombardment energy.

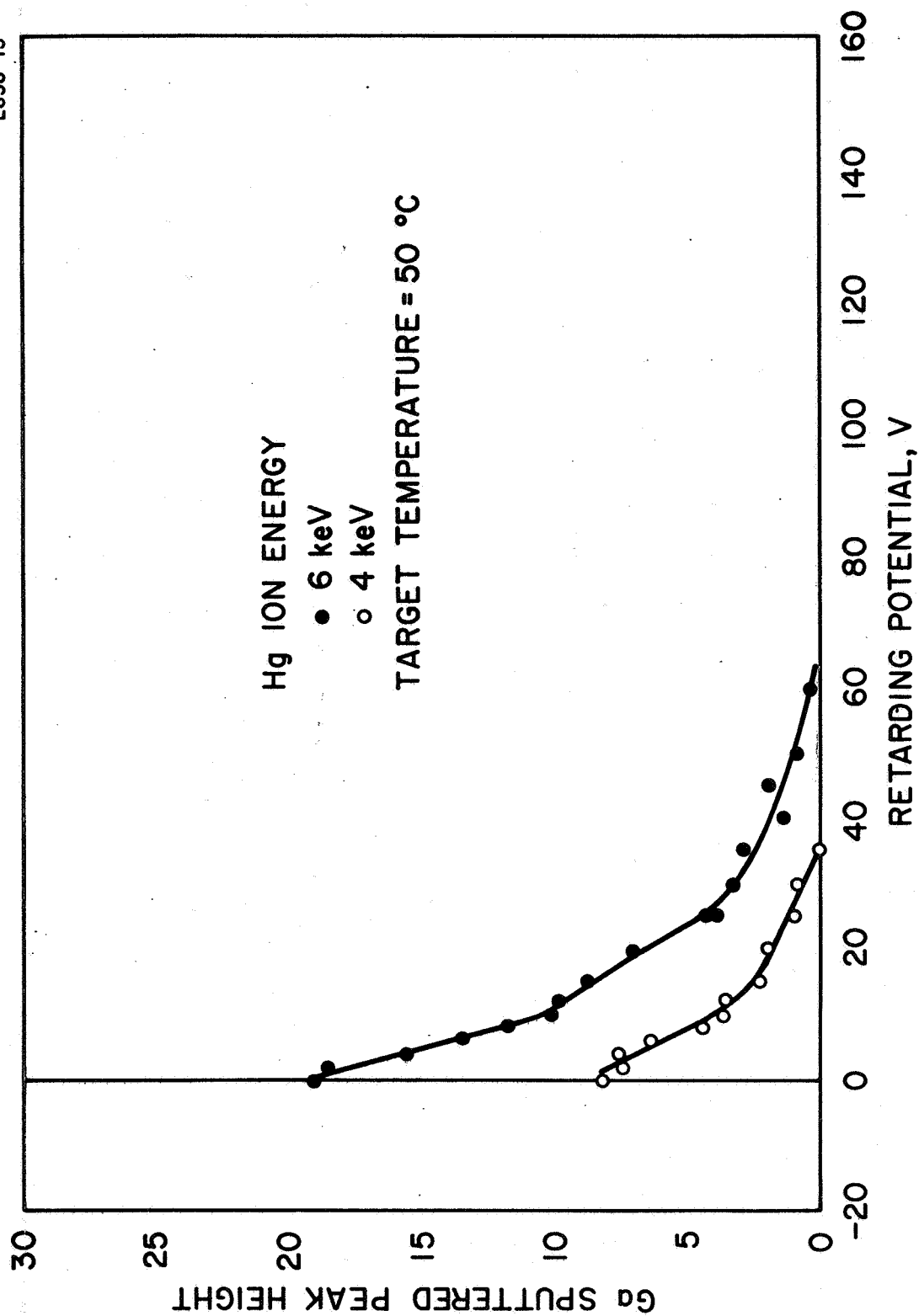


Fig. 25. Peak height of sputtered gallium ions as a function of retardation potential.

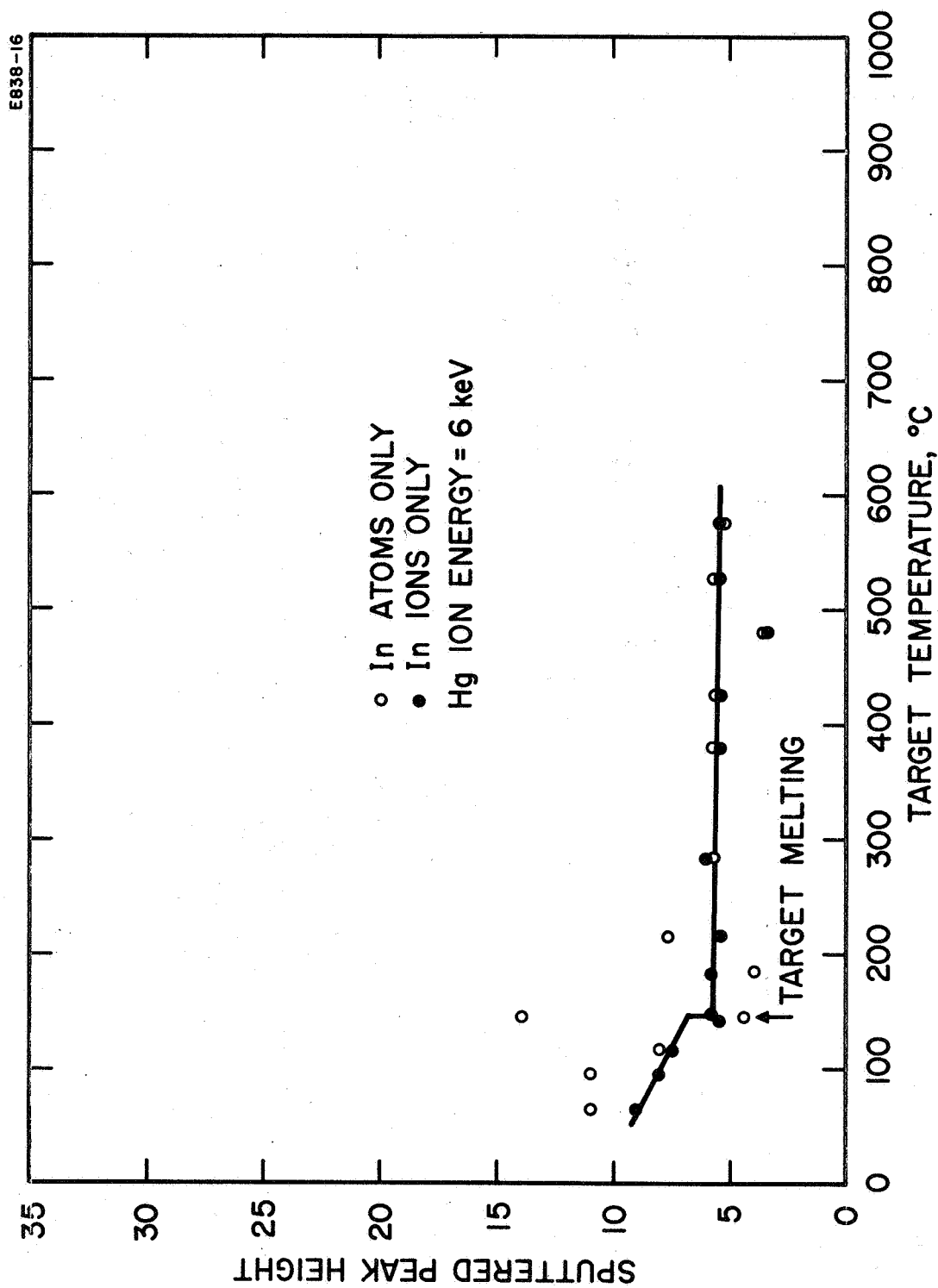


Fig. 26. Peak height of sputtered indium ions and atoms as a function of target temperature.

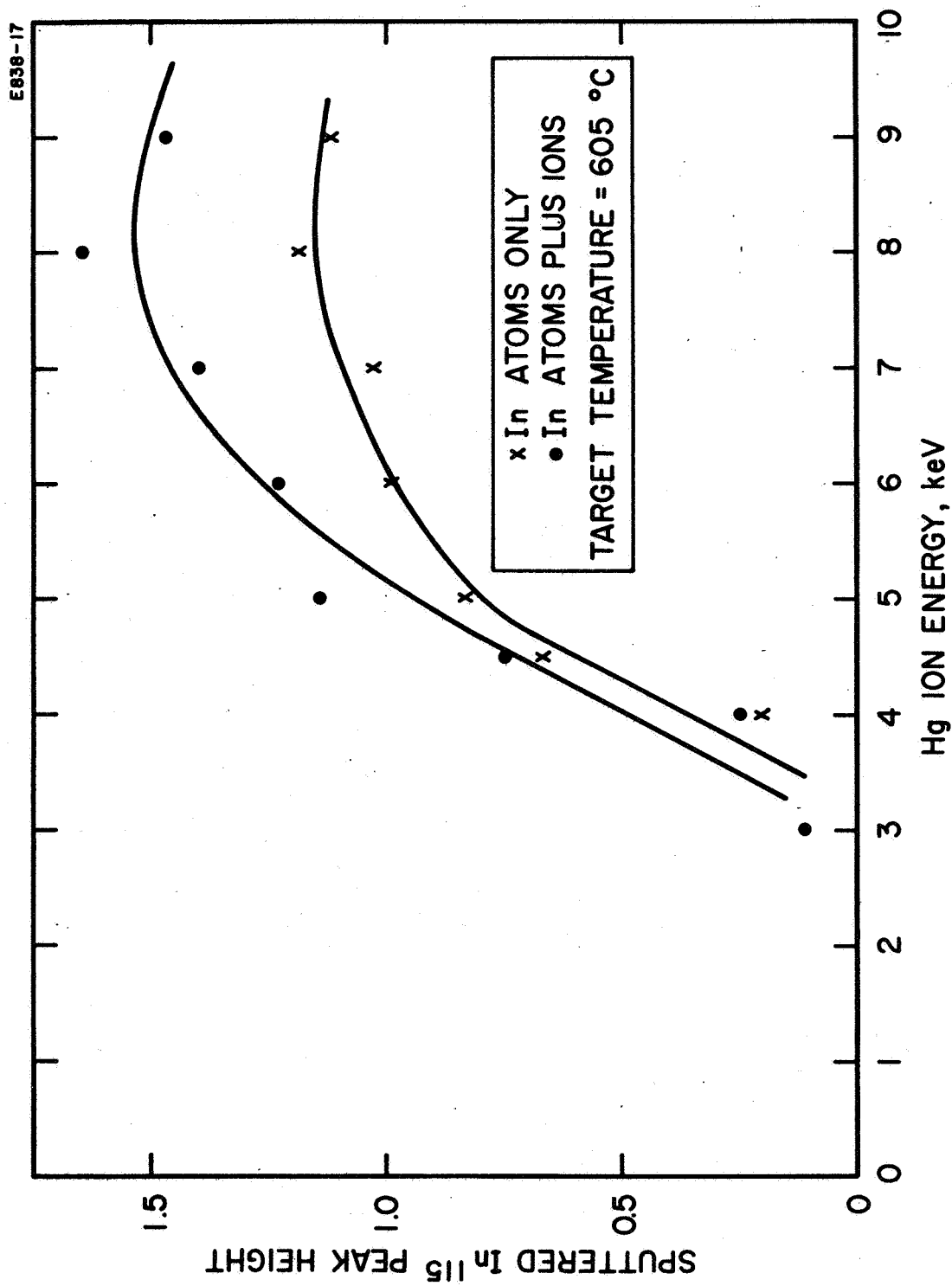


Fig. 27. Peak height of sputtered indium ions and atoms as a function of bombarding energy.

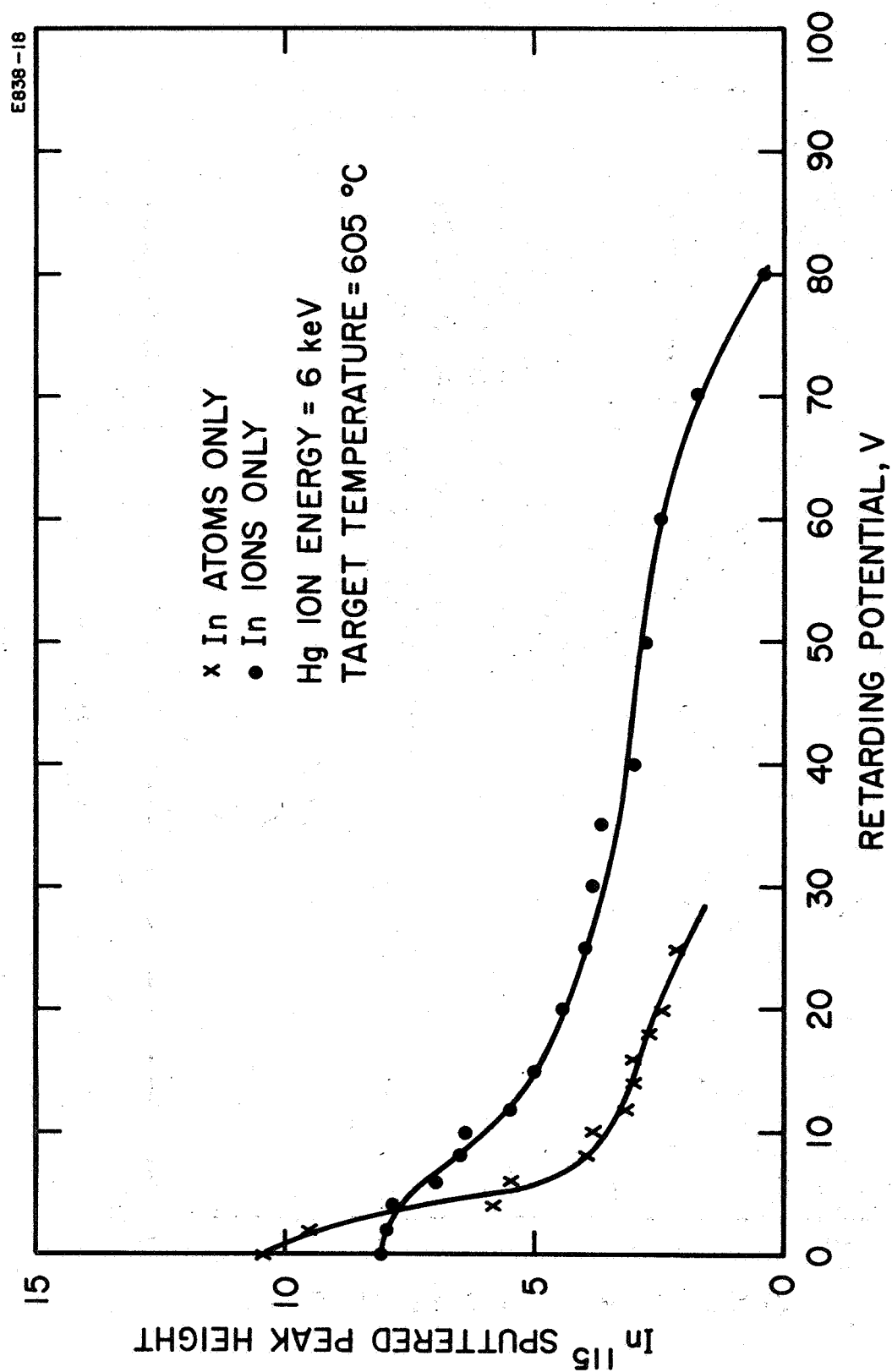


Fig. 28. Peak height of sputtered indium atoms and ions as a function of retardation potential.

However, since the ion source, target, and QMA are all well grounded, we hesitate to accept this explanation. It has been suggested by Wehner²⁵ that this apparent higher energy of the ions might be a result of the fact that the lower energy ions are more easily recaptured at the surface, thereby causing the apparent half maximum peak height to shift to a higher energy. Our system would not permit observation of this phenomenon if it were the case.

It was not possible to heat the indium target above 650°C, because the metal expanded and came in contact with the titanium shield; it then immediately drew up to form the alloy. This prevented the electrical isolation of the target so that the target current could not be measured.

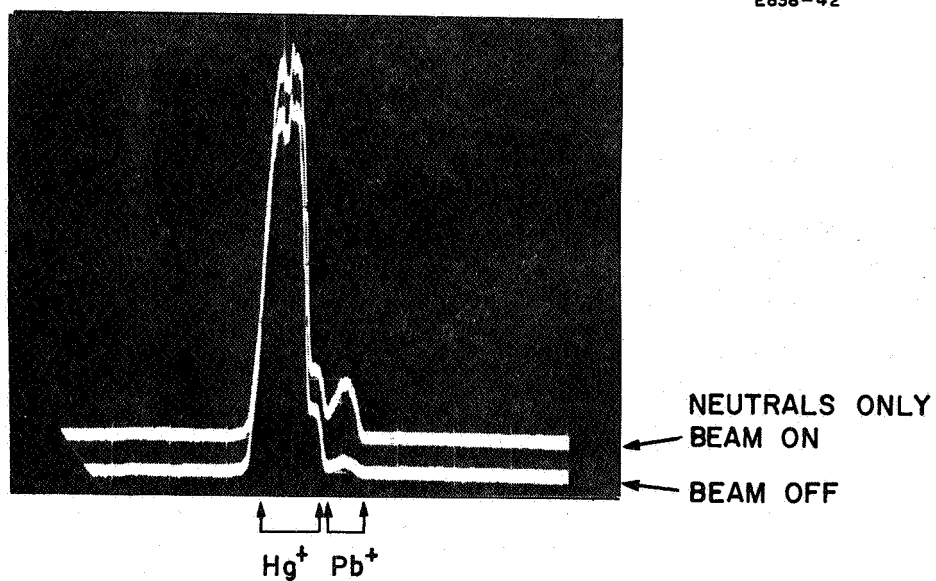
Observation of sputtering of lead proved to be very difficult. Using the QMA, as had been done with the previous targets, a beam as high as 350 μ A was used to bombard the lead target, but there was no indication of sputtered ions in the mass spectrum. The task of observing sputtered atoms is complicated by the fact that the mercury beam provides a large signal at the masses 198 to 204 amu and the primary lead peaks are at 206, 207, and 208 amu. Thus, the resolution of instrument could not be sacrificed to give greater sensitivity or the lead signal would be indistinguishable in the tail of the mercury peaks. In a compromise, the lead signal was maximized and was still distinguishable from the mercury, but the individual lead isotopes were not resolved (see Fig. 29).

When the target was bombarded, the sputtered lead was detectable but the signal was very weak (suggesting that the sputtering yield is very low or else the probability of ionizing and detecting sputtered lead atom was very low). We attempted to obtain a retardation plot (similar to the one described above for indium), but the lead signal was reduced to an unmeasurable low level when the extraction voltage was dropped to zero. The application of a small retardation voltage completely eliminated the signal. Thus, it would appear that the energy of the sputtered lead atoms is indistinguishable from thermal energies of the residual vapors, including mercury.

The lead target was heated to 600°C to determine whether the sputtering signal would increase, but there was no change. At temperatures above 470°C, the vapor pressure of lead (5×10^{-6} Torr) was sufficiently high that the lead peaks increased with vaporizing rate, and the indicated sensitivity of the QMA for detection of vaporizing lead was 10^{-3} A/Torr of lead vapor pressure. An example of the resolved spectrum is shown in Fig. 30. In terms of the detection of directed thermal neutral particles, this sensitivity would correspond to the detection of 10^{11} atoms/cm²-sec arriving at the entrance to the QMA.

The DTM crystal frequency change was monitored during the lead vaporization and a sensitivity of $\Delta f = 10^9$ cycles/gram was observed.

E838-42



(a) SCALE: 50 mV/cm

E838-43

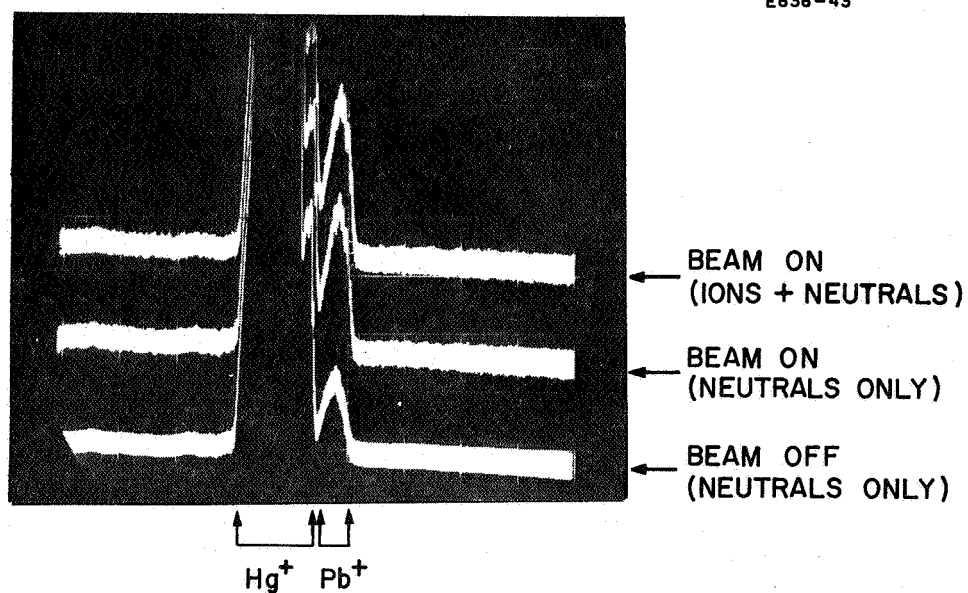
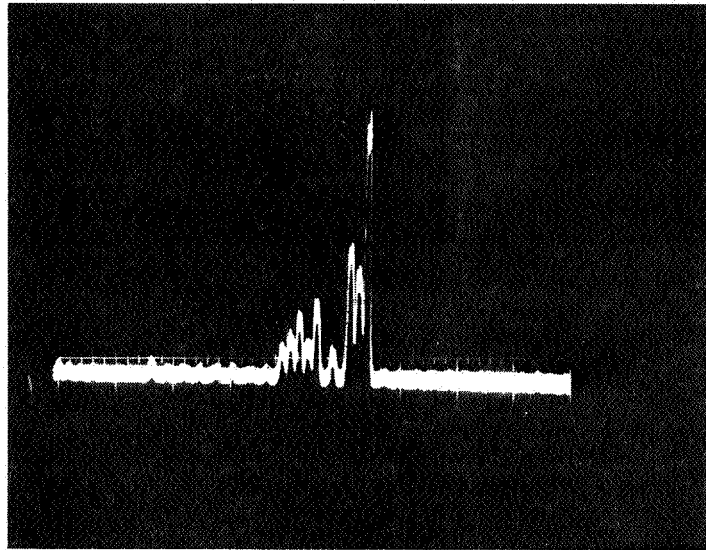


Fig. 29. Spectra showing sputtered lead atoms in the presence of residual mercury vapor.

E 838-44



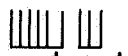

Hg⁺ Pb⁺

Fig. 30. Vaporizing spectrum of lead isotopes in the presence of mercury vapor.

The sputtered peak height for the lead was observed as a function of bombarding energy and the results are shown in Fig. 31. It can be observed that the sputtering yield for lead is slower to rise than the other materials tested and does not show a definite saturation.

The dependence of the sputtering yield of lead on the target temperature was observed up to 500°C; the results are shown in Fig. 32. It was not possible to extend the range of observation to higher temperatures because the vaporization of the lead dominated the detectable signal. We observed the same decrease in yield from the melted target for aluminum and indium.

When all of the above tests had been made with the lead, the mercury reservoir was replaced with a cesium reservoir in order to proceed with the comparative measurements required in the program. It was also hoped that the sputtered lead signal would be more easily seen if the mercury peak was reduced, if not eliminated.

B. Cesium Ion Bombardment

In converting to a cesium ion beam, the mercury reservoir was replaced with a cesium reservoir and, in addition, the ion source was disassembled, cleaned, and reassembled. The vacuum chamber was also lifted off of the ion pump and the pump disassembled and chemically cleaned. After the system was reassembled, the ion source and the QMA were heated to operating temperatures; both the lead and indium target assemblies were then heated to 400°C for three days before the cryopanel was cooled. This served to reduce the amount of residual mercury vapor in the system. Following this internal bakeout, the pressure indicated by pump current was 2×10^{-8} Torr but, as mentioned earlier, a more accurate ion gauge value would have been of the order of 10^{-9} Torr.

The cesium ion beam was found to be more difficult to control than the mercury because of the tendency toward insulation breakdown and thermionic emission enhanced leakage. However, ion bombardment currents of 10 to 300 μ A were obtained at the target.

The first observations attempted were of the sputtering of indium by cesium. The spectra shown in Fig. 33 show a marked difference from those obtained with mercury. In particular, the large sputtered ion signal was that of cesium and not that of the indium target material. This was illustrated dramatically when the beam was focused steadily through the shield aperture while the target was changed from indium to lead. The sputtered cesium ion peak remained high while the indium and lead were barely visible.

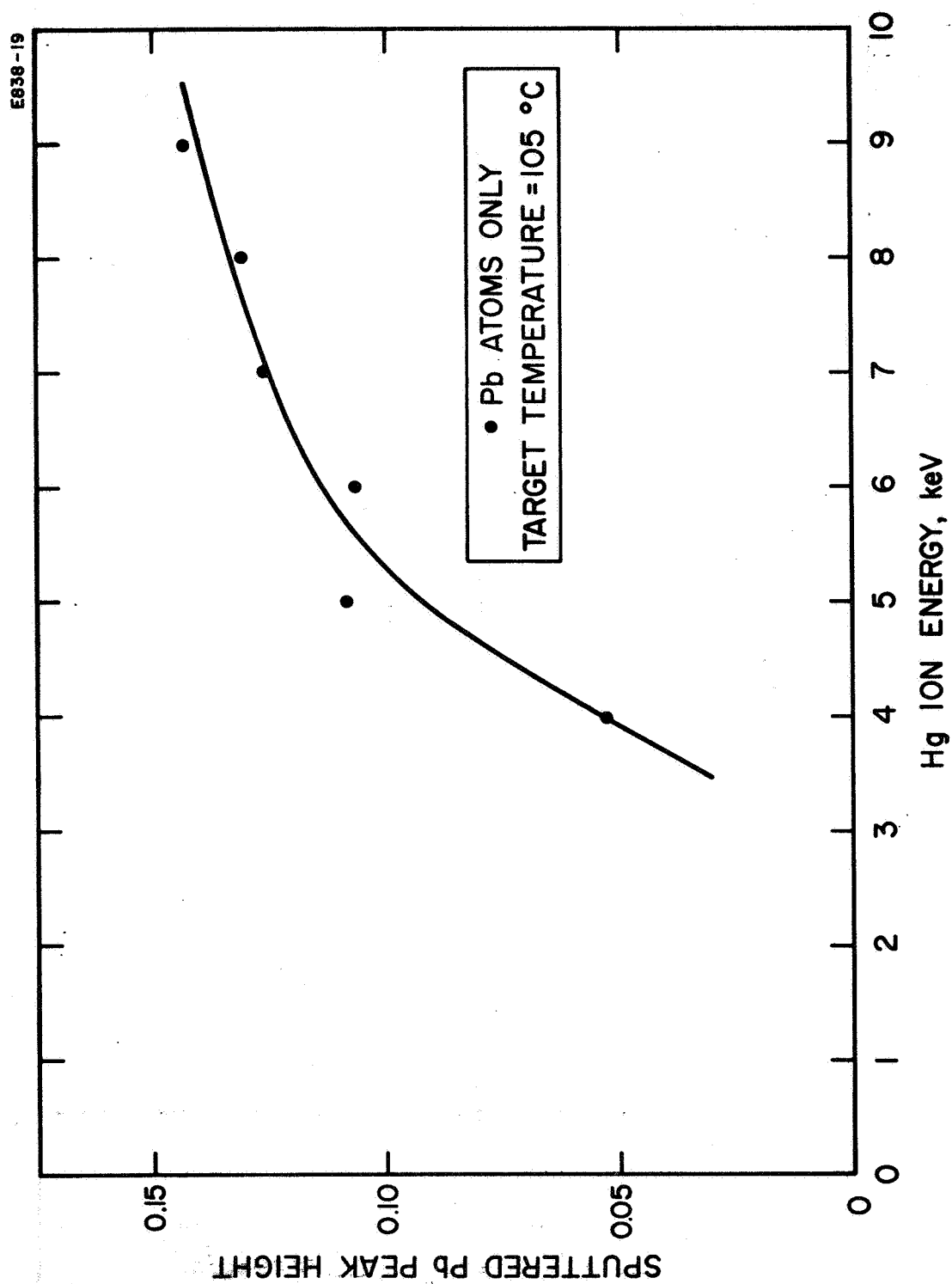


Fig. 31. Peak height of sputtered lead atoms as a function of mercury ion bombarding energy.

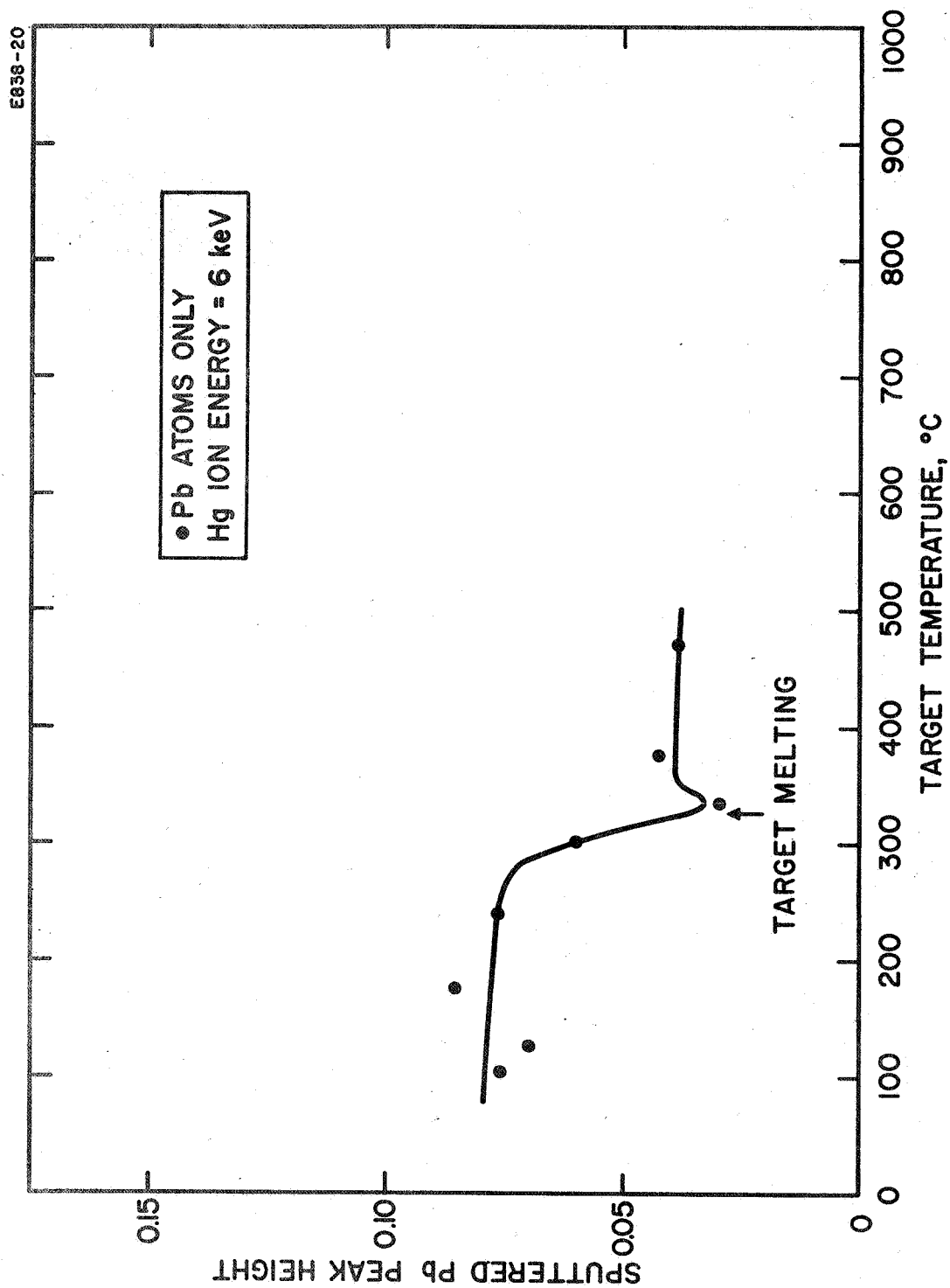
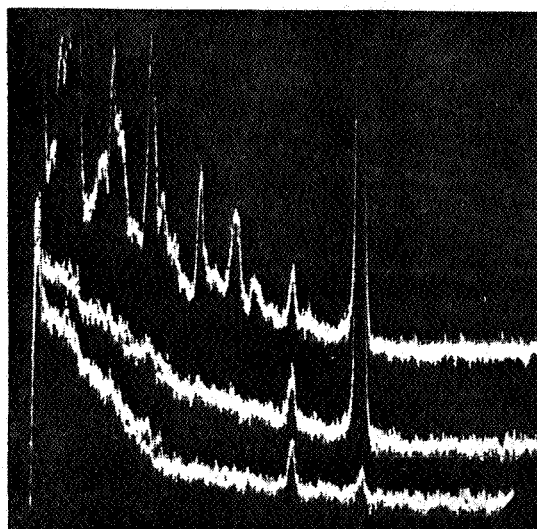


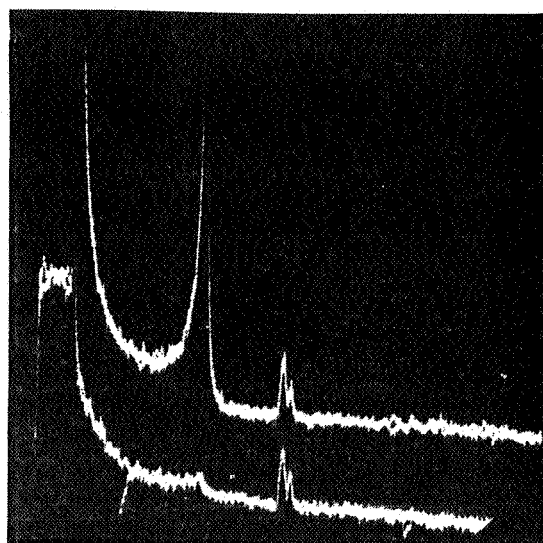
Fig. 32. Peak height of sputtered lead atoms as a function of target temperature.

E838-40



(a) MEDIUM MASS RANGE (TO 150 AMU)

E838-41



(b) HIGH MASS RANGE (TO 500 AMU)

Fig. 33. Sputtered spectra due to cesium ion bombardment of indium and lead targets.

The indium signal was so weak and (as in the case of lead sputtered by mercury) small compared with the large cesium signal that no reliable measurements could be made. When the lead target was sputtered by cesium the spectrum showed a peak near 200 amu; however, a closer examination showed that it was mainly mercury, and no sputtered ion content was detected (see Fig. 33(b)).

The energy distribution of the sputtered indium ions was measured by retardation at the QMA detector; the plot is given in Fig. 34. The average energy is seen to be approximately half the value observed when mercury ions were used for bombardment.

The sputtering signal from the indium and lead appeared so low compared with the peak of cesium ions that it was decided to test the ion source and target alignment by using an inert gas ion beam for bombardment. Without moving any component of the experiment, high purity argon gas was bled into the cesium reservoir. The feed line valve was then used to control the gaseous flow rate to the ion source. The argon ion bombardment produced cesium ions when bombarding the indium target, and the cesium signal was large compared with the indium signal. When the lead target was bombarded, both mercury atoms and cesium ions were seen, and again, the lead signal was small by comparison (see Fig. 35). The cesium signal grew larger when the target was heated to 500°C and persisted through 16 hours of heating, indicating a source of cesium vapor in the target material or in the radiation shields and mounting structure of the target. The ion source and detector were shown to be aligned properly by moving the targets back and forth under the shield aperture. Clear signals were seen from the sputtering of the insulators and target mounting materials as they came into the beam.

At this point in the experiment it was necessary to replace the filament in the ion source. We also decided to replace the lead target with the aluminum target for sputtering with cesium ions.

While outside the vacuum chamber, the indium target was melted to depress the thermocouple probe deeper into the metal. After re-evacuation of the system, the first test undertaken was sputtering by means of the argon beam. The indium sputtering signal appeared larger than in the previous measurements. After bombarding for a few hours, however, the signal seemed to decrease, suggesting a cleanup or change in the sputtering characteristics of the surface. This was confirmed qualitatively by moving the target to expose a portion of the indium surface which had been under the aperture shield. It was noted that the indium signal rose and gradually decreased in time. If a surface contamination or oxidation had occurred during the heating in air, this film may have enhanced the sputtering signal although no other peaks were observed to suggest what the material might have been. When the target was heated in the vacuum the apparent contamination did not occur and no increase in sputtering signal was seen.

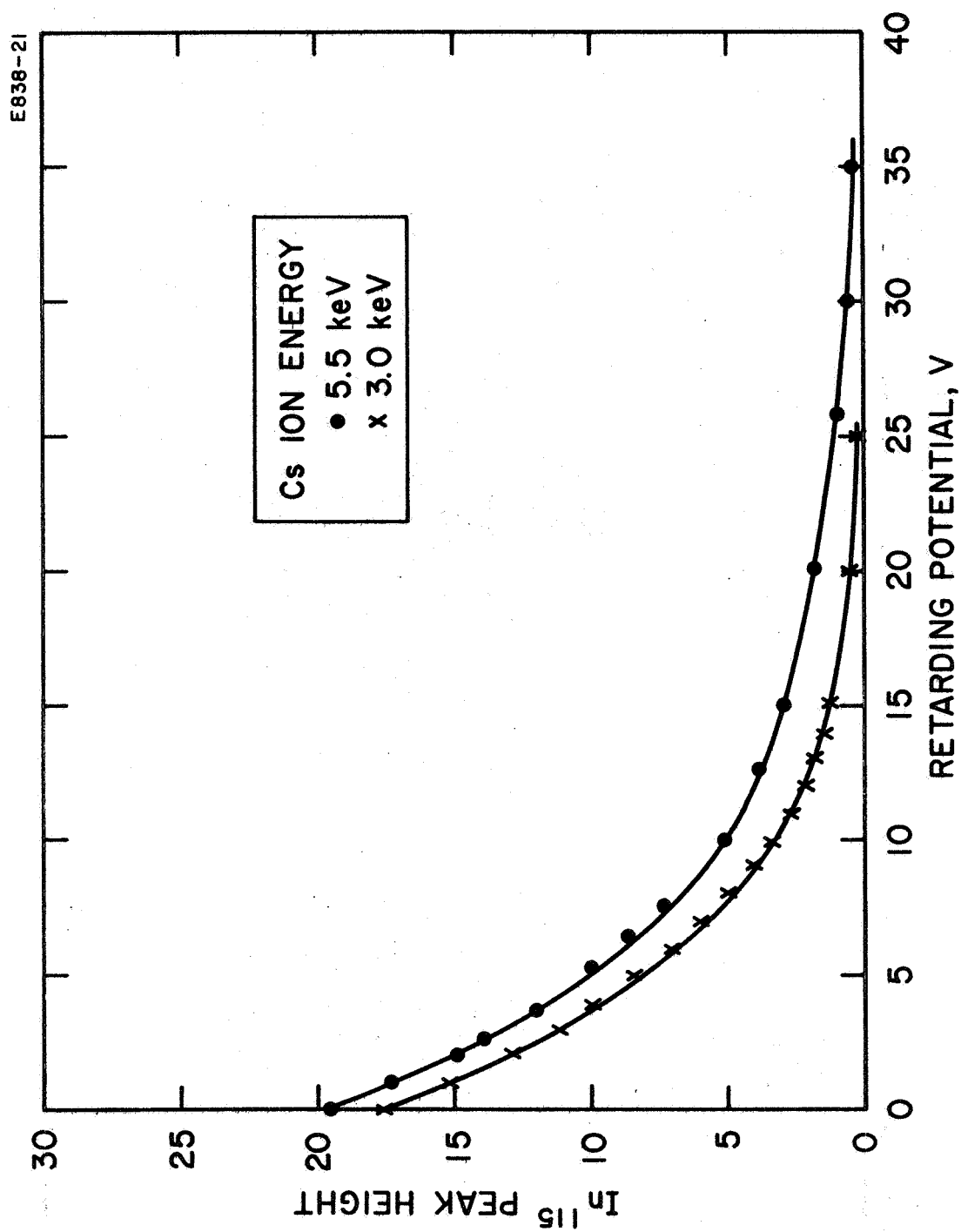
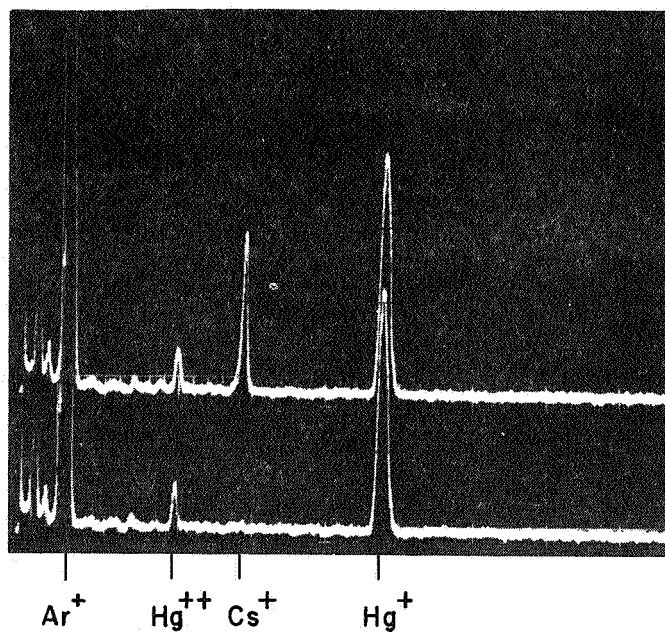


Fig. 34. Peak height of sputtered indium atoms versus retarding potential at two values of cesium ion bombardment energy.

E638-38



Ar BEAM ON

RGA WITH ION
DEFLECTOR OFF

RGA WITH ION
DEFLECTOR ON

Fig. 35. Spectra showing cesium ions sputtered from lead target under argon ion bombardment.

The argon ion beam was used to bombard the aluminum target and the mounting structures between the targets; in each case the sputtering signals were larger than that of indium.

When the argon was depleted from the reservoir, the cesium beam was used to bombard the aluminum target. The sputtering signals were similar to those seen earlier for mercury bombardment. However, as seen in Fig. 36, the aluminum signal was accompanied by a large cesium ion signal, whereas the mercury beam had not produced a mercury ion signal.

Retardation plots of the sputtered aluminum and cesium ions are shown in Figs. 37 and 38 with bombarding ion energy as a parameter. The curves are normalized at the zero retardation level and the dependence on ion bombarding energy is demonstrated. Figure 39 illustrates that the energy distribution of the sputtered cesium ions approximates that of the sputtered aluminum ions.

E839-39

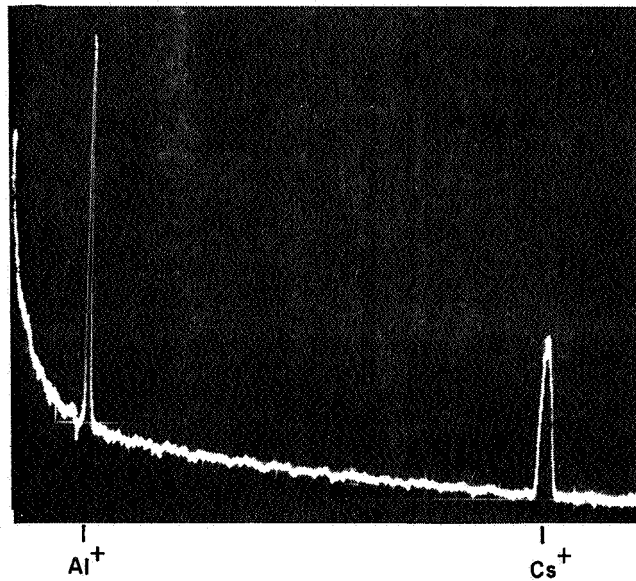


Fig. 36. Sputtered ions produced by cesium ion bombardment of aluminum at 5 keV.

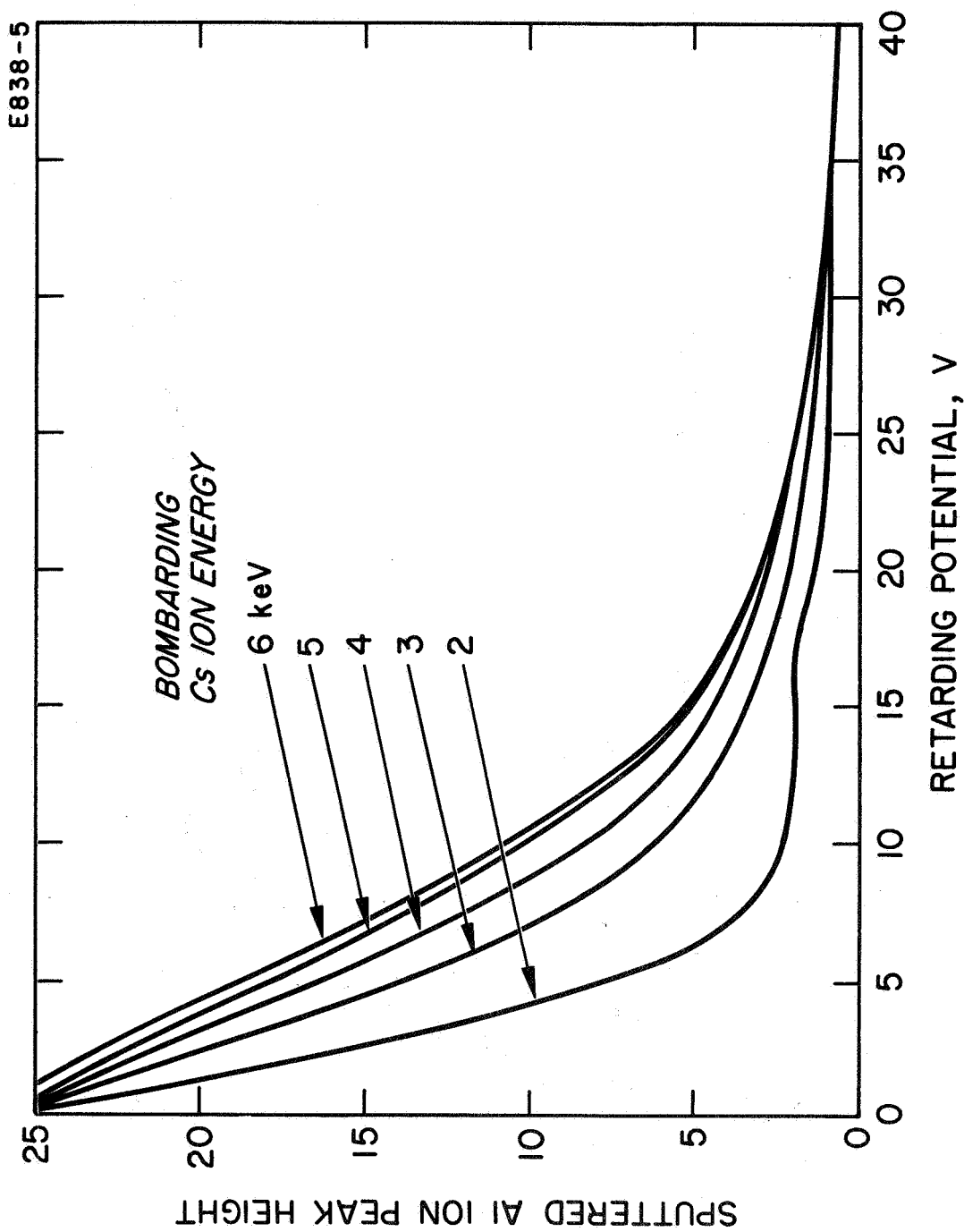


Fig. 37. Peak height of sputtered aluminum ions versus retarding potential with bombarding energy as a parameter. $T_{Al} = 60^{\circ}\text{C}$.

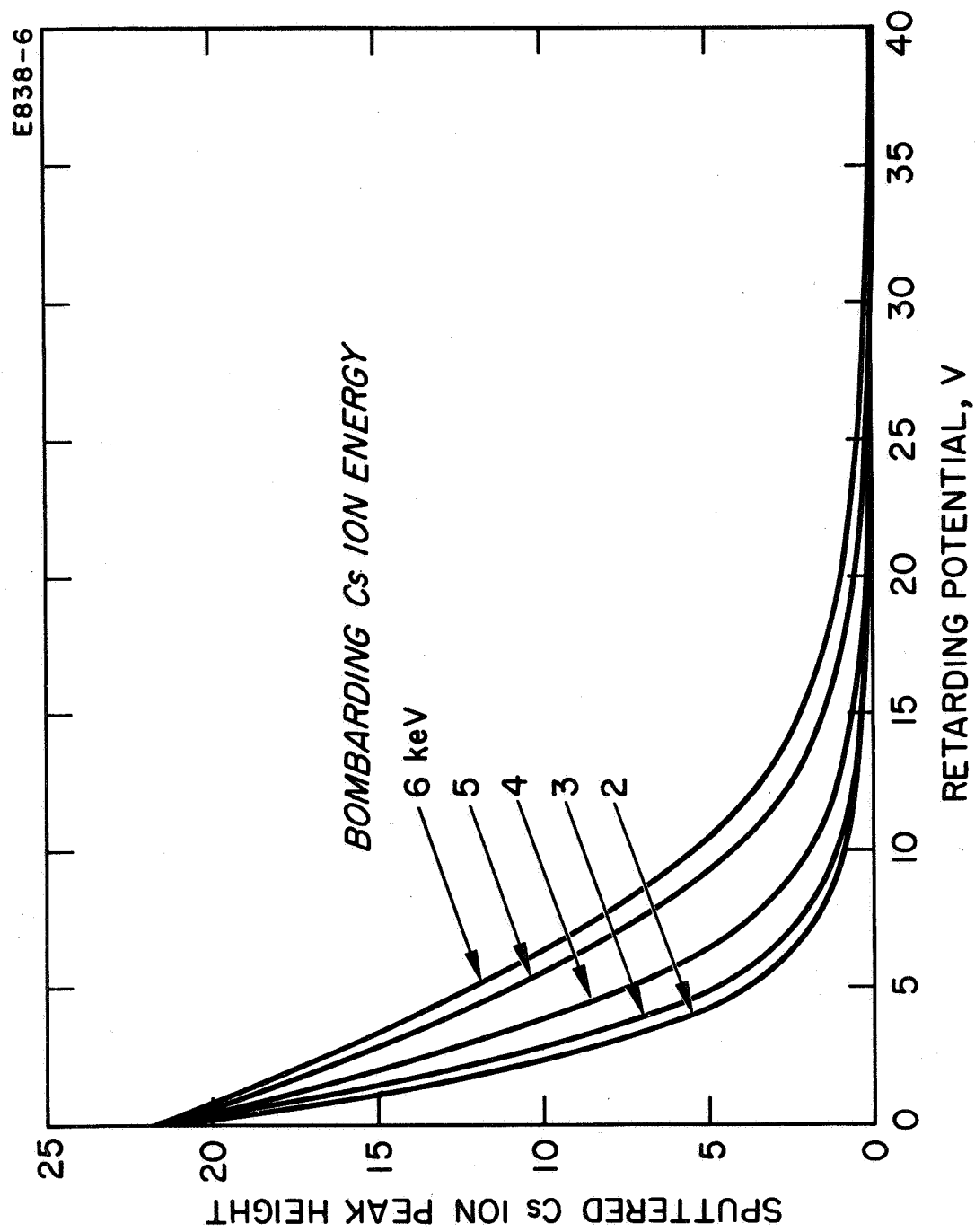


Fig: 38. Peak height of sputtered cesium ions (resulting from bombardment of aluminum target) versus retarding potential. $T_{Al} = 60^{\circ}\text{C}$.

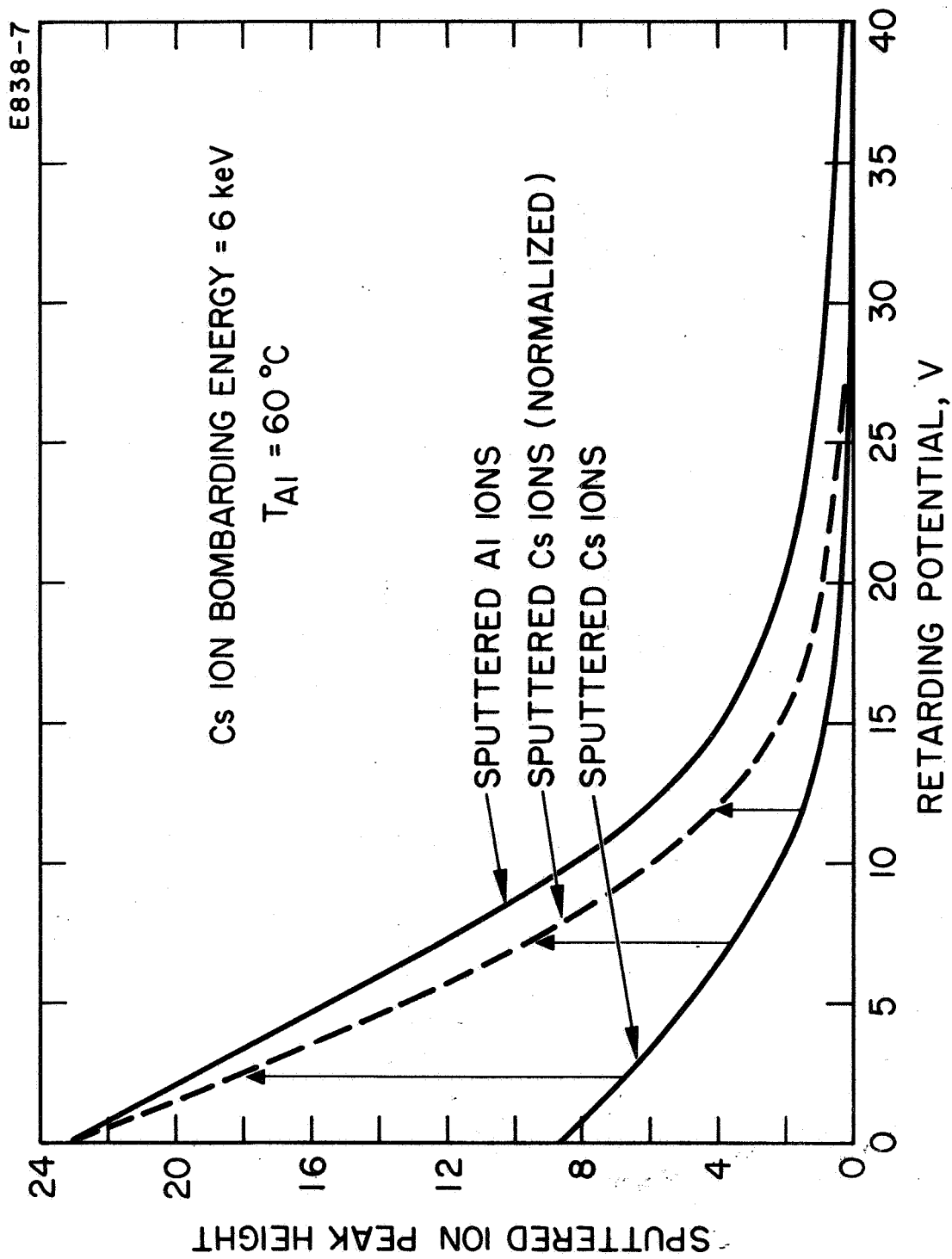


Fig. 39. Retardation plots of sputtered aluminum and cesium ions resulting from cesium ion bombardment of aluminum target. $T_{Al} = 60^{\circ}C$.

1. The first part of the document discusses the importance of maintaining accurate records of all transactions. It emphasizes that proper record-keeping is essential for the integrity of the financial system and for the ability to detect and prevent fraud.

2. The second part of the document outlines the specific requirements for record-keeping. It states that all transactions must be recorded in a timely and accurate manner, and that the records must be maintained for a minimum of five years.

3. The third part of the document discusses the role of the auditor in verifying the accuracy of the records. It states that the auditor must perform a thorough review of the records and must report any discrepancies to the appropriate authorities.

4. The fourth part of the document discusses the consequences of failing to comply with the record-keeping requirements. It states that individuals who fail to comply may be subject to fines and penalties, and that the records may be subject to seizure.

5. The fifth part of the document discusses the importance of training and education for individuals involved in record-keeping. It states that individuals must be trained in the proper methods of record-keeping and must be kept up-to-date on any changes to the requirements.

6. The sixth part of the document discusses the importance of internal controls in preventing fraud. It states that individuals must be aware of the signs of fraud and must be trained to recognize and report any suspicious activity.

7. The seventh part of the document discusses the importance of communication and cooperation between individuals involved in record-keeping. It states that individuals must be able to communicate effectively and must be able to work together to resolve any issues that may arise.

8. The eighth part of the document discusses the importance of the legal framework governing record-keeping. It states that individuals must be aware of the laws and regulations that apply to record-keeping and must ensure that they are in compliance with all applicable laws.

9. The ninth part of the document discusses the importance of the role of the government in ensuring the integrity of the financial system. It states that the government must have the authority to enforce the record-keeping requirements and must be able to take action against individuals who fail to comply.

10. The tenth part of the document discusses the importance of the role of the public in maintaining the integrity of the financial system. It states that the public must be educated about the importance of record-keeping and must be able to recognize and report any suspicious activity.

IV. INTERPRETATION OF RESULTS

In examining the results of the sputtering measurements it is evident that the experimental test apparatus which was assembled during this program constitutes a powerful tool in the observation of relative changes in sputtering yield or angular distribution. However, it is of limited value in determining the absolute yield values. This is because it is difficult to determine, in this detector system, the efficiency for ionization of fast neutral atoms. The photomultiplier amplification factor can change with incident ion mass as well as from day to day depending on the contaminating influence of the vaporizing and sputtered target material on the dynode surfaces. In addition, the QMA does not have a fixed sensitivity but will vary, depending on the resolution selected and to some degree on the velocity of the ions passing through the filter.

Absolute calibration was attempted under certain operating conditions. By detecting the signal obtained from the vaporizing of aluminum and lead targets, the QMA sensitivity was established for these materials at specific operating conditions, using the published values of vapor pressure-temperature characteristics of the materials. The DTM was cross calibrated at the same time; the cross check involves the accommodation of thermal particles on the DTM and the ionization efficiency of these thermal particles in the QMA. When sputtering takes place, the accommodation of the faster particles is expected to increase slightly (if it was not already 1.0 for thermal particles) and the ionization efficiency is expected to decrease by at least a factor of 10. It would be desirable, then, to use the DTM for calibration of the sputtered particles; unfortunately, however, fringing edges of the beam hit the target shield and the contribution of sputtered particles from those areas confuses the interpretation of the DTM results.

Thus, absolute sputtering yield values undoubtedly are determined more accurately by the use of microbalance deposition and removal measurements or by nuclear activation analysis and radioactive decay counting procedures.^{11, 25, 29}

Observations which are uniquely obtainable with the present apparatus are the sputtered ionic and atomic species for identification. In this program we have seen that ionic species of aluminum, gallium, and indium were detected but that lead produced only detectable atomic species.

The bombardment with mercury or argon ions showed no evidence of ions or of detectable fast neutral mercury or argon atoms coming from the surface, whereas the cesium produced a strong signal of fast ions and practically no evidence of fast or slow neutral atoms.

The sputtering from each of the targets produced normal isotopic distributions in the atomic and ionic particles. No neutral or positively charged molecules were detected. Even the ceramic (boron nitride) target boats and the alumina target mounts — which were bombarded when moving the target assemblies — produced sputtered ions of aluminum and boron with no complexes being seen. It is possible that negatively charged ions or complexes were sputtered (as reported by Krohn³⁰), but these would be rejected by the photomultiplier as it is presently employed.

An important observation indicated in the sputtering results is the dependence of yield on target temperature, particularly on the phase (solid or liquid) of the target metal. In the cases of aluminum, indium, and lead, the yield was observed to decrease when going from the solid to the liquid state. It might have been expected that the extra energy of fusion available in the liquid state would have facilitated the ejection of the atoms; however, we find that this must be secondary to the fact that the density of the materials tested decreases upon melting and the resulting penetration depth of the ion increases.

It was also proposed³¹ that the statistical cross section of atoms presented by a crystalline lattice of a metal would be greater than the cross section presented by randomly positioned atoms in their liquid state; thus, the direction and magnitude of change in the yield would be of the order of that observed.

The energy distribution of sputtered particles indicated by the retardation potential plots are difficult to interpret when viewed on a rectilinear plot, but when replotted in a semilog graph an exponential characteristic becomes evident. In Figs. 40 and 41, the retardation plots for the sputtered aluminum ions are shown with bombarding mercury and cesium ion energy as a parameter. Figure 42 compares the results for mercury ion bombardment with those for cesium ion bombardment. The slope of the lines suggests a characteristic energy E_s of the sputtered particles defined by the relationship of the form

$$N = N_0 e^{-(V_{\text{ret}}/E_s)}$$

where N_0 relates to the maximum sputtering yield, V_{ret} is the retarding potential, and E_s characterizes the energy of the sputtered particles — similar to the effective temperature assigned to thermionically emitted electrons. The exponential energy distribution in the ejected particles suggests that a Maxwellian distribution was attained as a consequence of the multiple collisions which took place below the surface layer. In light of the range measurements by Van Lint³² and the theoretical interpretation by Keywell,¹⁷ this is not an unexpected

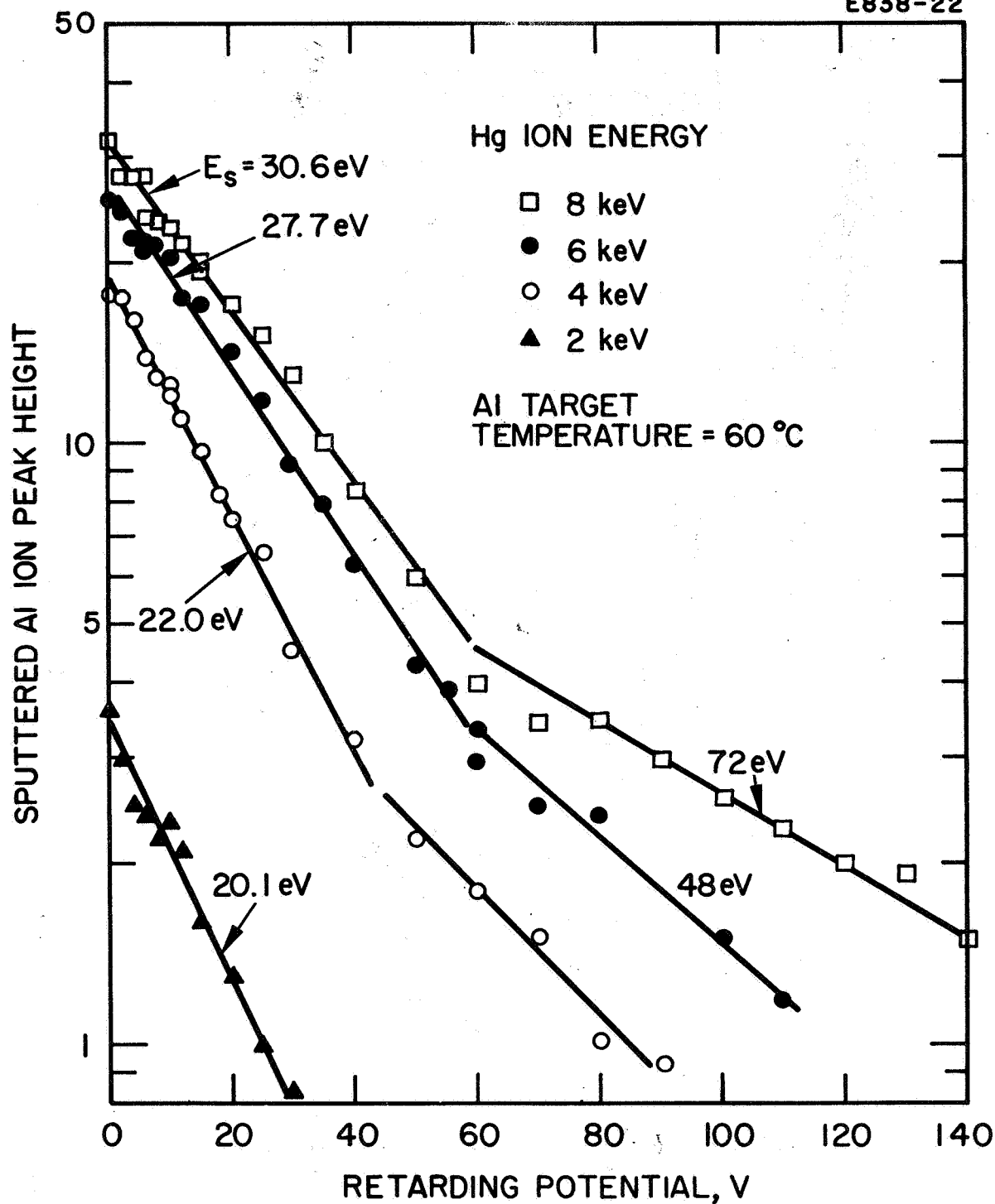


Fig. 40. Retardation plots of sputtered aluminum ions under Hg ion bombardment. E_s = characteristic energy of sputtered ions.

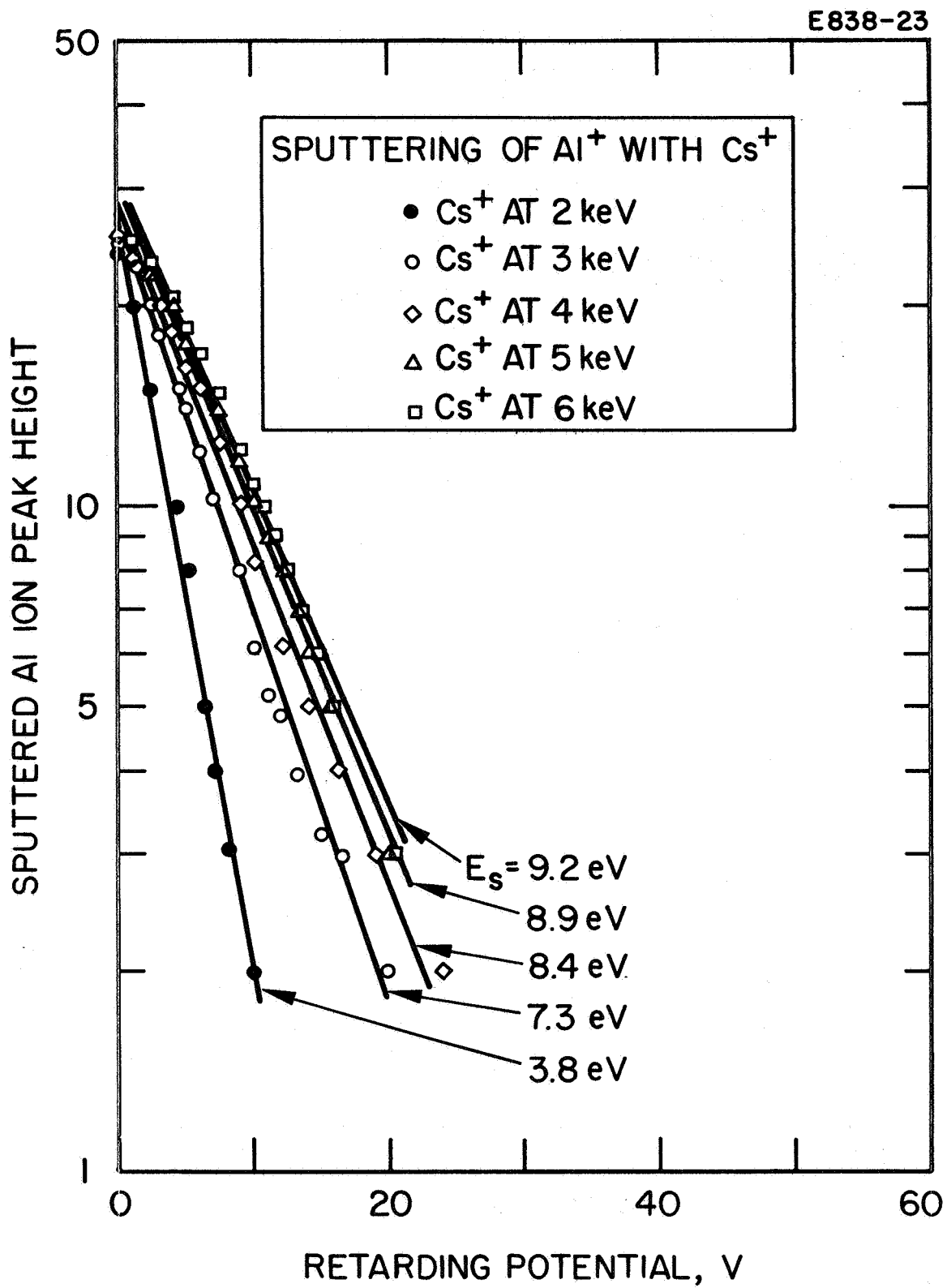


Fig. 41. Retardation plots of sputtered aluminum ions under Cs ion bombardment. E_s = characteristic energy.

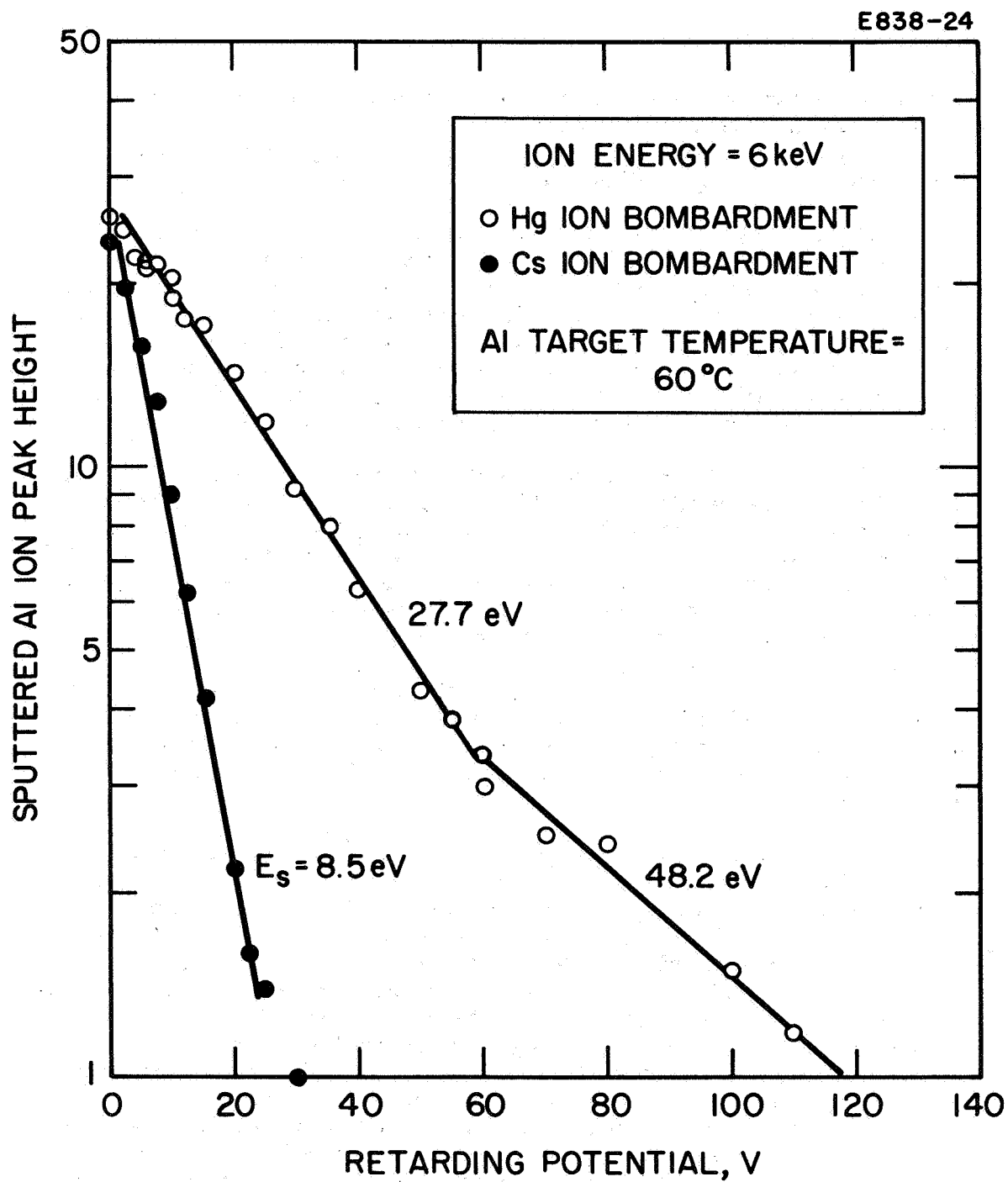


Fig. 42. Comparison of characteristics, E_s , of sputtered Al ions under Hg and Cs ion bombardment.

result. A mercury ion at 6 keV is expected to penetrate to approximately 20 atomic layers in dissipating its energy to aluminum atoms. The energy of the aluminum atoms is then quickly thermalized through secondary and tertiary collisions.

In monocrystalline material, the focusing collisions described by Silsbee¹⁸ are understood to result in angular ejection patterns which have been observed.³³ In polycrystalline material, the ejection pattern can be supposed to result from the average over many crystalline orientations; thus, no preferred direction is indicated.* The sputtering yields from metals in the liquid state are not expected to involve any focusing in orderly atomic arrangements and a resulting decrease in sputtering yield therefore could be expected.

The energy distribution of sputtered aluminum ions resulting from mercury ion bombardment (Fig. 40) also shows a high energy tail, with E_s values up to 72 eV. The appearance of a composite of Maxwell distributions was noted by Stanton³⁵ and may be attributable to the higher energy collisions occurring close to the surface. However, it should be noted that the high energy components are seen only with mercury ion bombardment, not with cesium ion bombardment.

Figure 43 depicts the energy distribution in the cesium ions ejected from the aluminum surface under cesium ion bombardment. The characteristic energies suggest that these ions are ejected by collisions from below the surface and are not reflected ions from the incident beam.

The characteristic energies of the sputtered indium atoms are shown in Fig. 44 to be lower than the values for the sputtered ions; a similar relationship could be expected to hold for aluminum and gallium. Sputtered atoms in lead were seen to be essentially thermal (less than 1 eV energy). Summaries of the characteristic energies for the sputtered aluminum, gallium, and indium ions are shown in Figs. 45 and 46. Figures 47 and 48 illustrate the dependence in sputtering of indium on the bombarding ion mass and its energy. A clear decrease in energy with increasing target mass is indicated. This result is not inconsistent with the observations that high vacuum sputter-deposited films of aluminum and molybdenum are very tenaciously held onto glass or silicon substrates, whereas high vacuum sputter-deposited lead and gold films may be easily scratched from the substrate. The results of characteristic energy observations above contradict the time-of-flight

*Note: The observations here and in other works³⁴ of the increase of sputtering yield near the normal to polycrystalline targets may result from the statistical averaging of these collisions. Further measurements — particularly of sputtering yields resulting from off-normal incidence angles — would be helpful in testing this possibility.

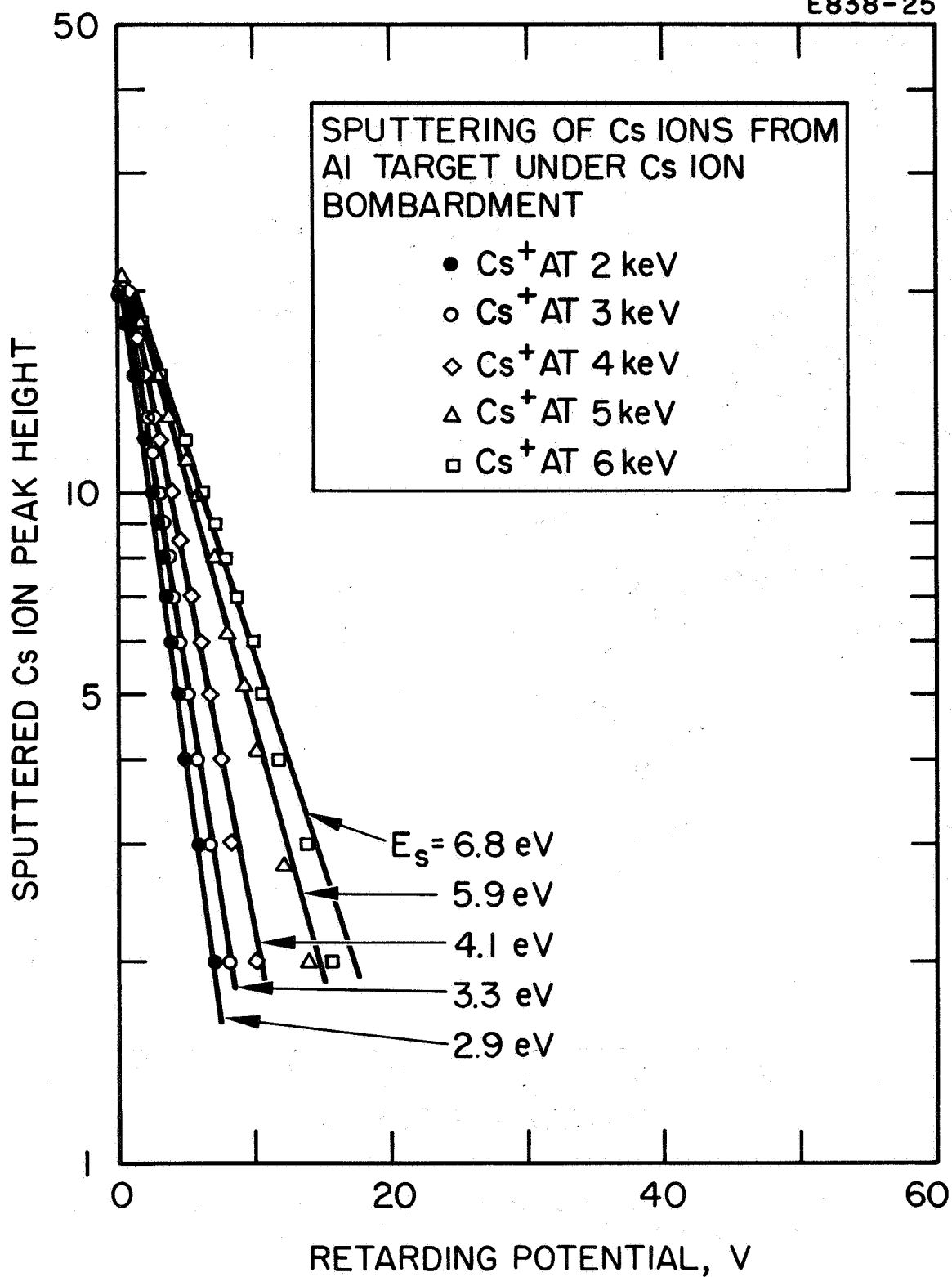


Fig. 43. Retardation plot of cesium ions sputtered from aluminum target. E_s = characteristic energy indicated by slope.

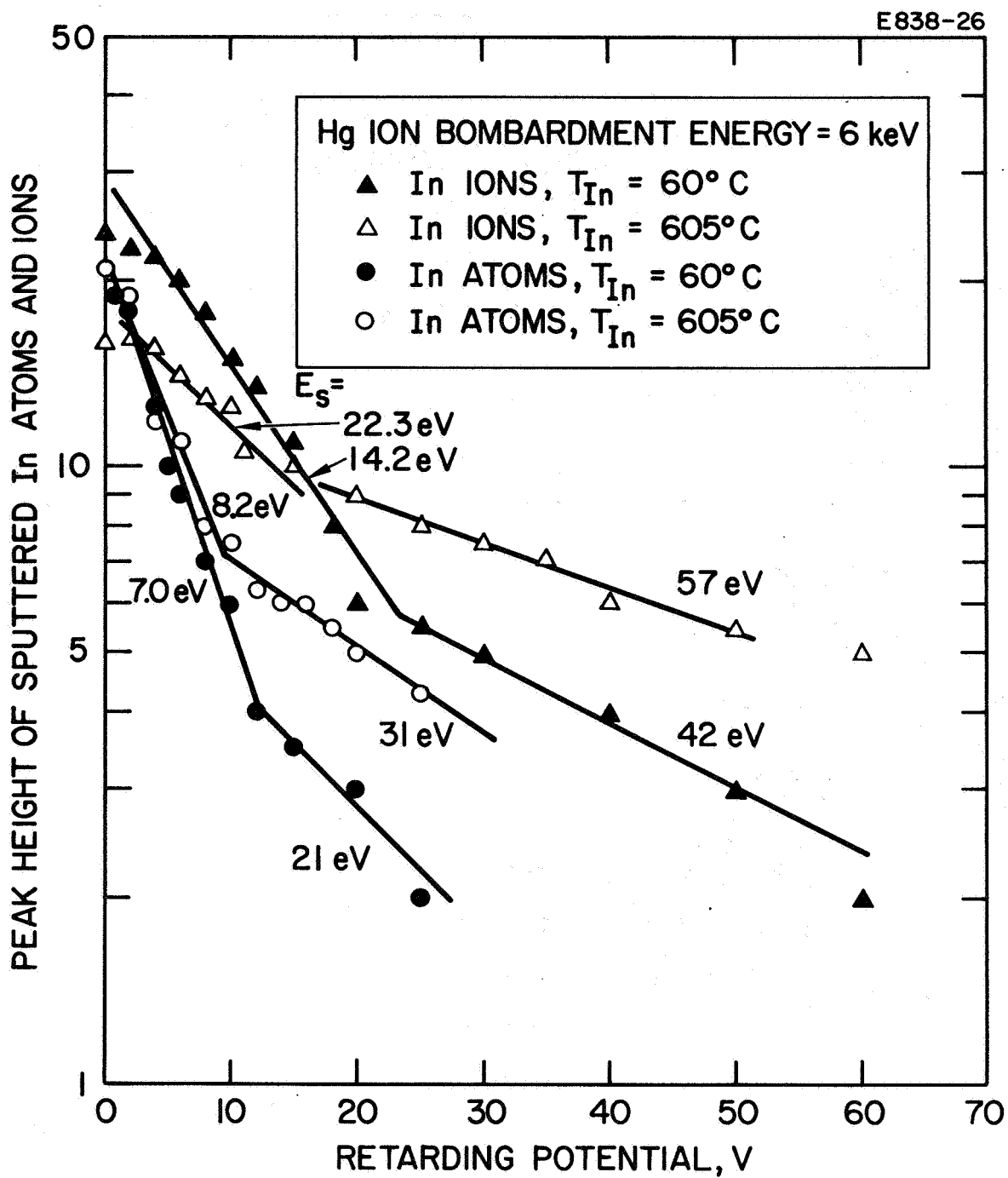


Fig. 44. Retardation plots for indium ions and atoms under Hg ion bombardment. E_s = characteristic energy.

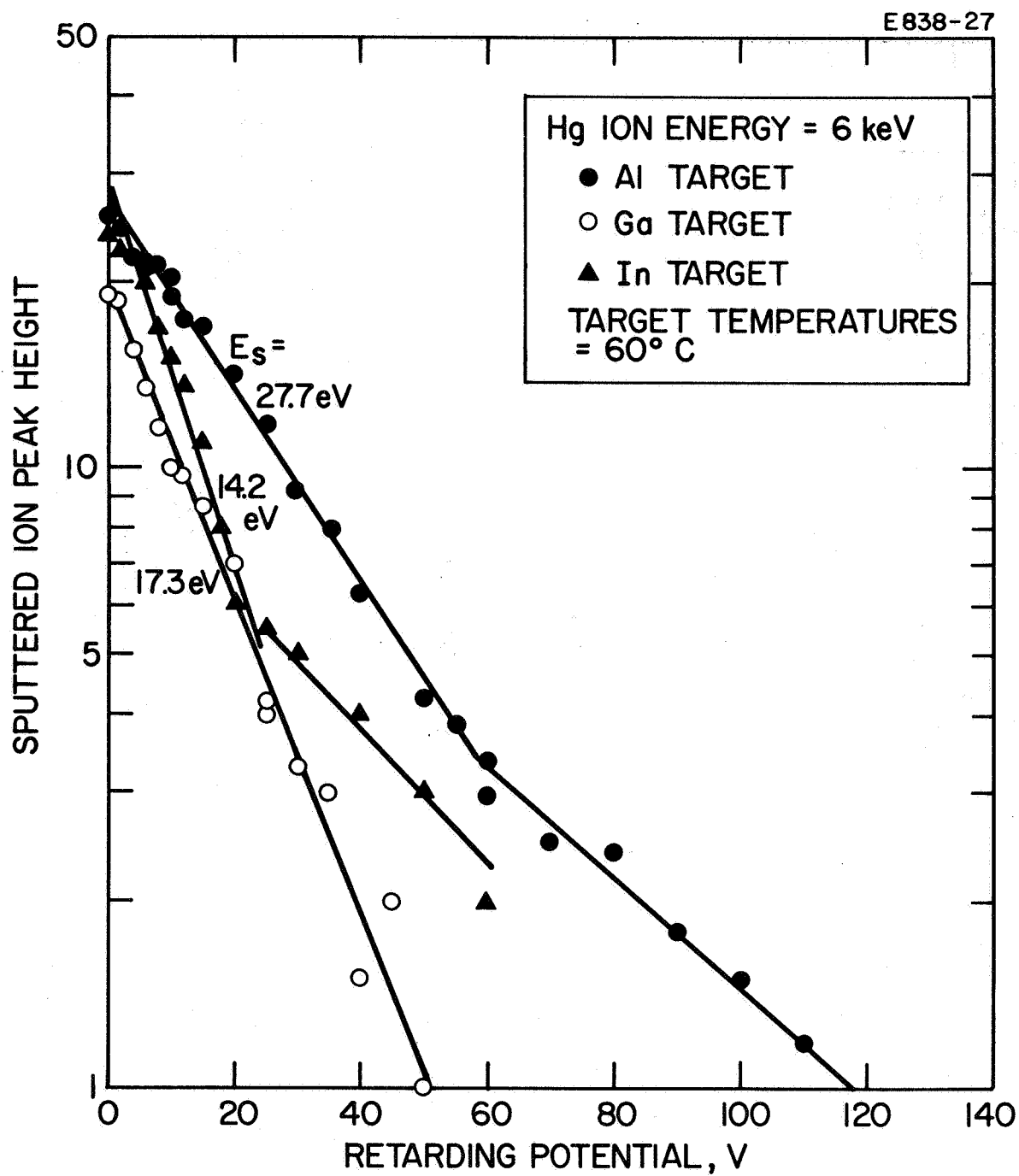


Fig. 45. Retardation plots for Al, Ga, and In ions due to Hg ion bombardment.

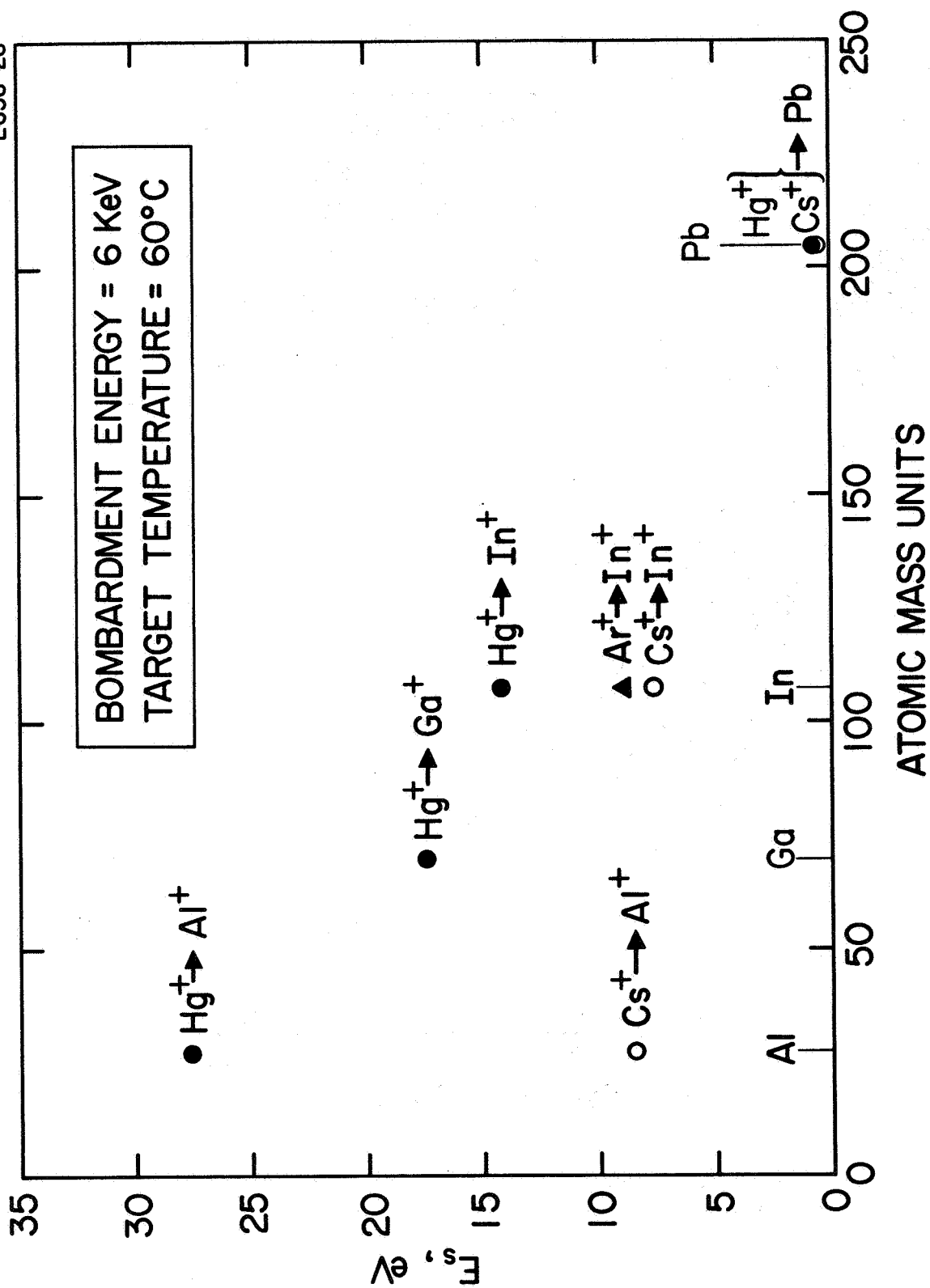


Fig. 46. Characteristic energies of ionic species as a function of target mass.

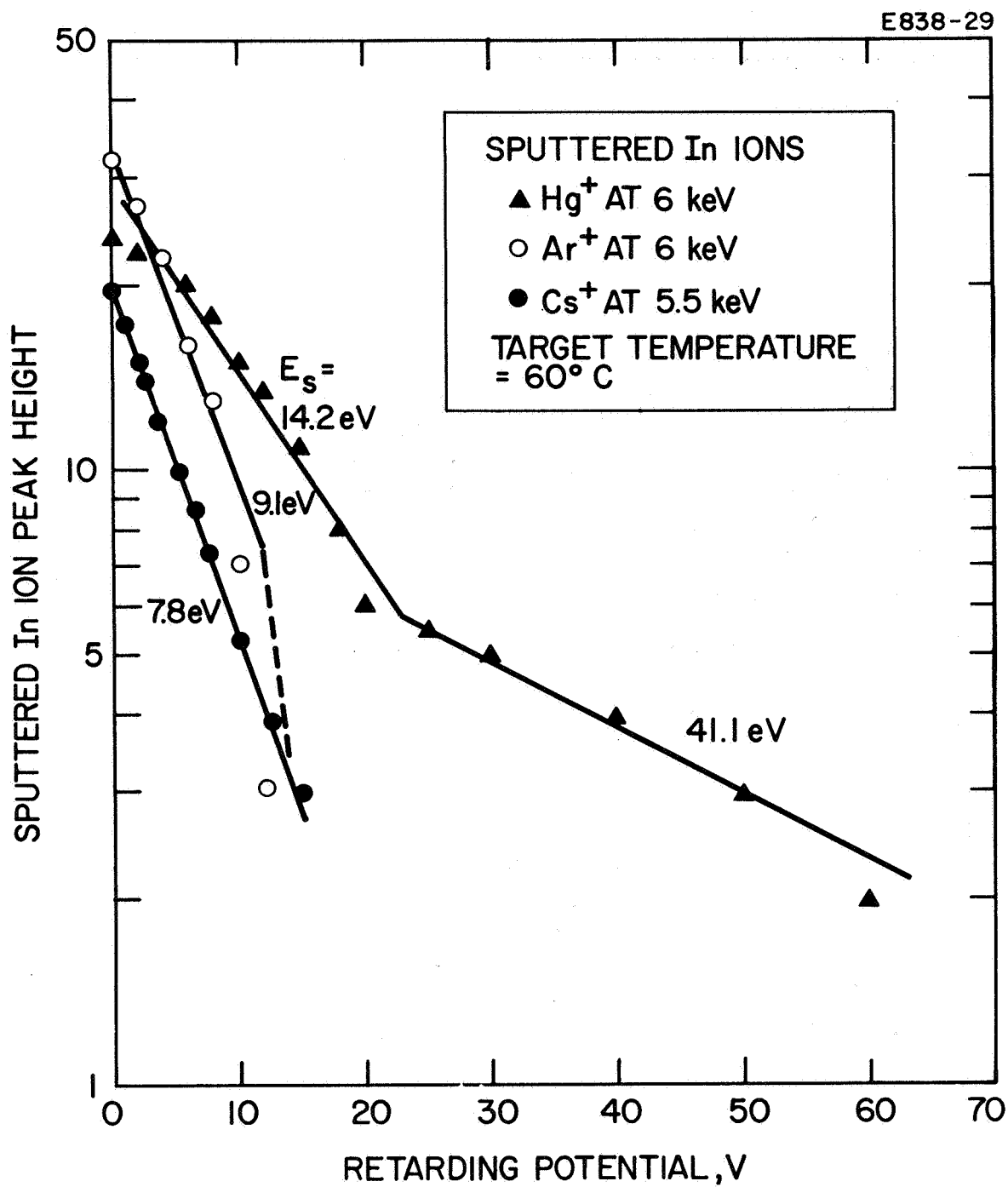


Fig. 47. Retardation plot for sputtered indium ions under Hg-, Cs-, and Ar-ion bombardment. E_s = characteristic energy indicated by slope of line.

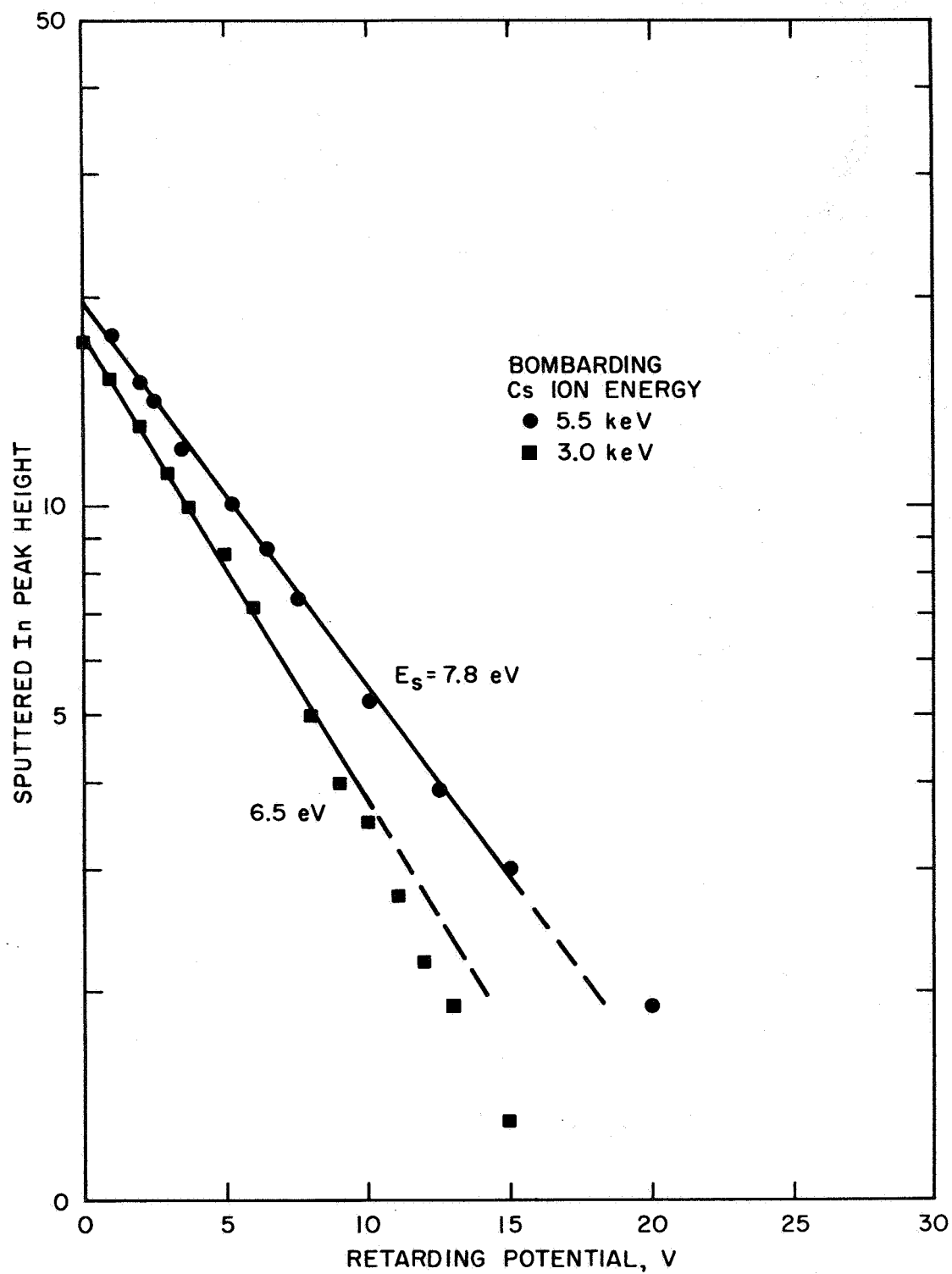


Fig. 48. Retardation plots of sputtered indium ions as a function of Cs ion bombardment energy. E_s = characteristic energy.

measurements of Wehner,³⁶ inferring a nearly constant values of velocity in the sputtered particles.

It would not be proper to generalize that sputtered energy dependence on target mass is as simple as implied by Fig. 46. The results of sputtering yield measurements show periodic sharp increases in yield as the electronic configurations approach the filled d-shell arrangement (e.g., in copper, silver, and gold).⁵⁻⁸ It happens that the gallium, indium, and lead atoms fall into the areas just above these high-yield configurations and are all expected to have relatively low-yield values. The possibility exists that the characteristic sputtered energies may also fluctuate with electronic configuration,³⁷ although, as indicated above, the relatively low tenacity of gold films deposited by high vacuum sputtering does not give a hint of a high proportion of fast sputtered particles.

Figure 49 summarizes the dependence of characteristic sputtered energy of aluminum ions on the bombarding energies of mercury and cesium ions. It also includes the observed energies in the ejected cesium ions. A monotonic increase of sputtered energy with bombardment energy is indicated, thus contradicting the conclusion by Wehner³⁶ that a saturation in energy had occurred as the bombarding energy increased from threshold to approximately 1000 eV. The relative energy transfer efficiencies seen for mercury ion bombardment are approximately 2.8 times those for cesium ion bombardment; this does not substantiate a term of the form

$$\frac{M_1 M_2}{(M_1 + M_2)^2} ,$$

where M_1 is the bombarding mass and M_2 is the target mass in a yield or transfer efficiency expression. A comparison of characteristic energies of sputtered neutral atoms would be a better test of this conclusion. The results for sputtered ions indicate that the characteristic sputtered energies may be quite strongly influenced by the penetration depth and the relative ease of emitting charged versus neutral particles from the surface.

Although the sputtering yields were observed to decrease as the targets went from the solid to the liquid phases, the characteristic sputtering energies of aluminum and indium ions were observed to increase by 33 to 50%, for the conditions of normal incident bombardment and a fixed exit angle which we employed. (See Figs. 44, 50, and 51). The energies of sputtered indium atoms remained essentially constant during the transition from solid to liquid.

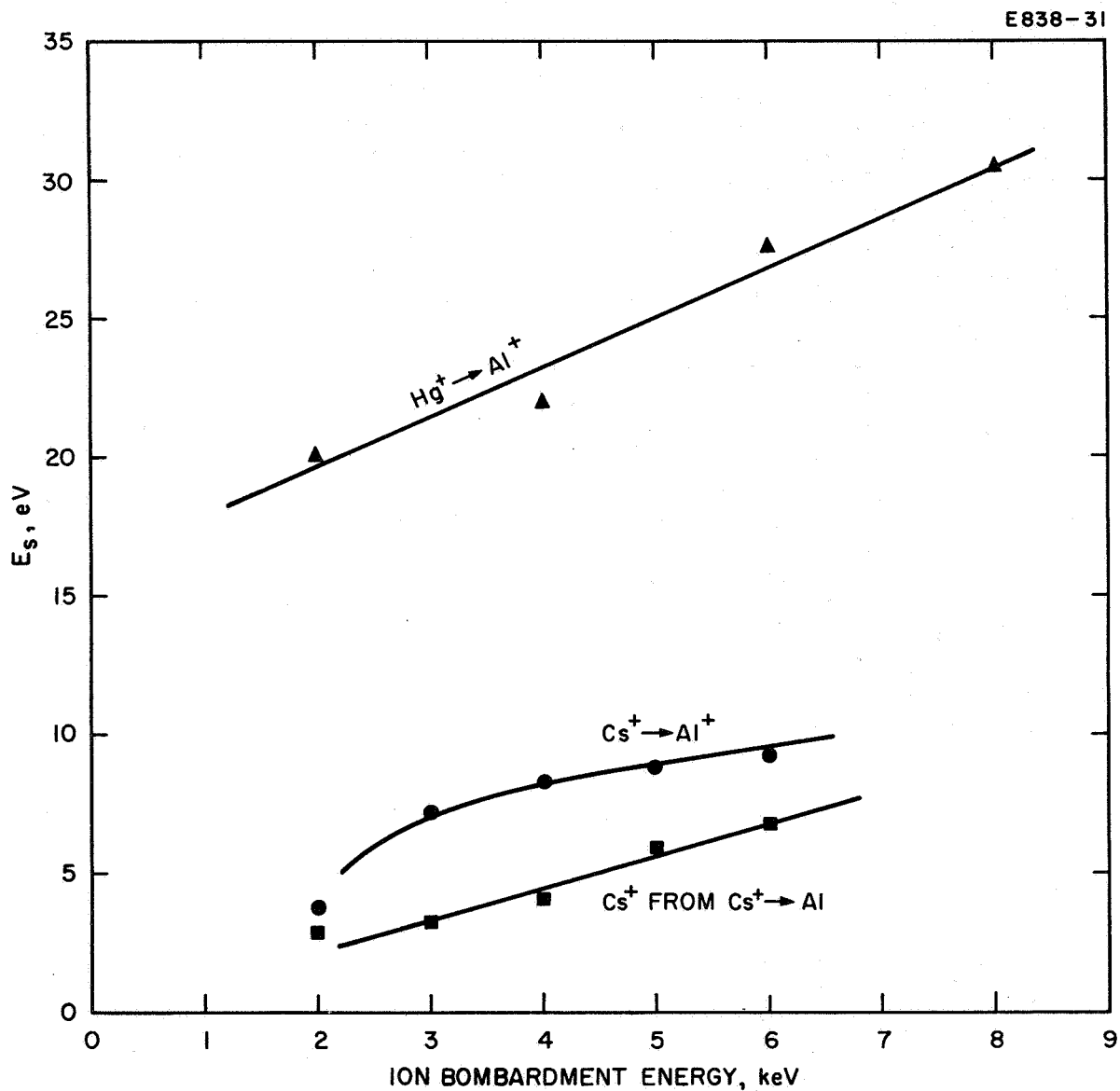


Fig. 49. Dependence of characteristic energies of sputtered Al-ions on bombarding energy. $T_{Al} = 60^\circ C$.

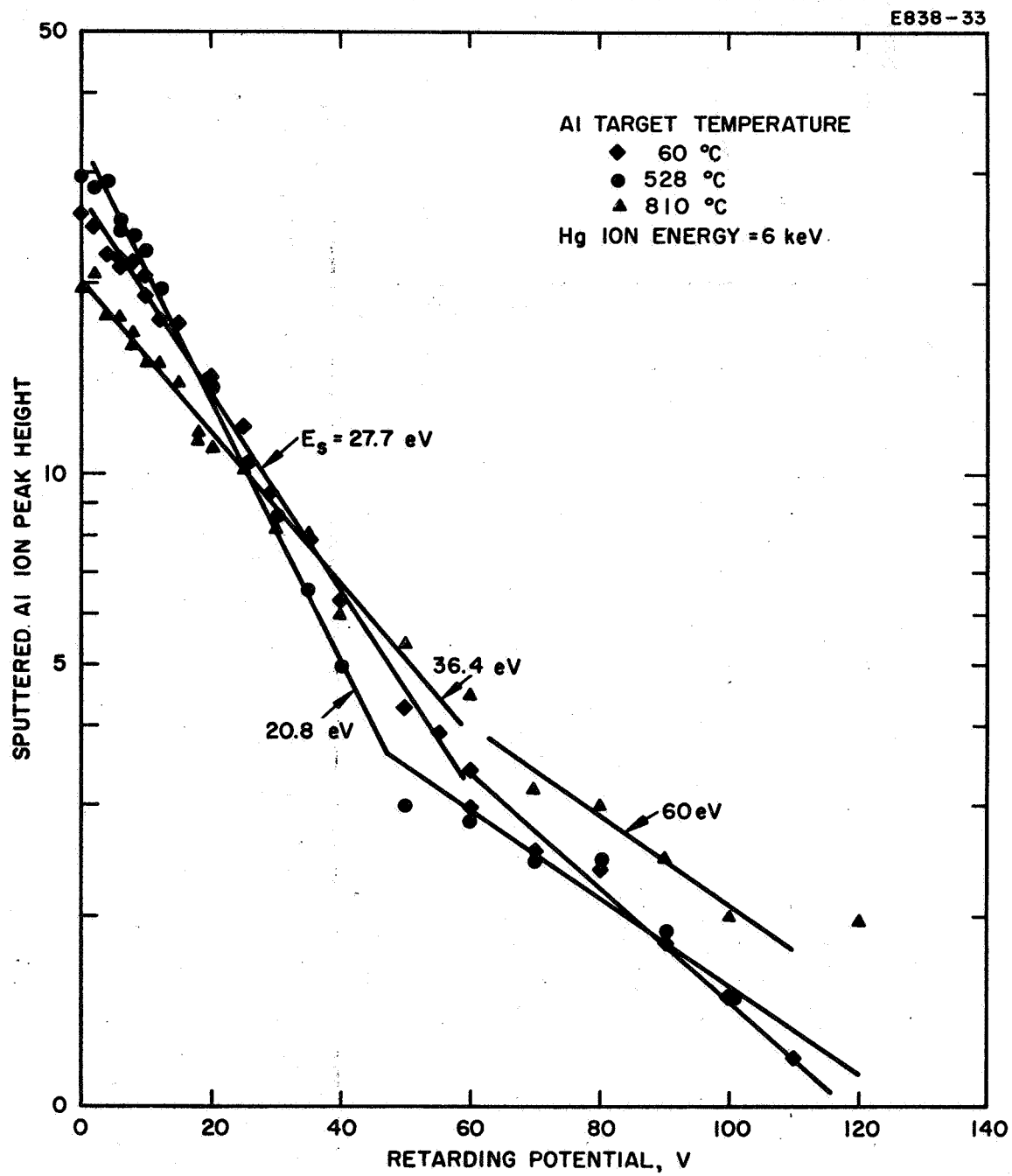


Fig. 50. Retardation plots for Al sputtered by Hg ions.

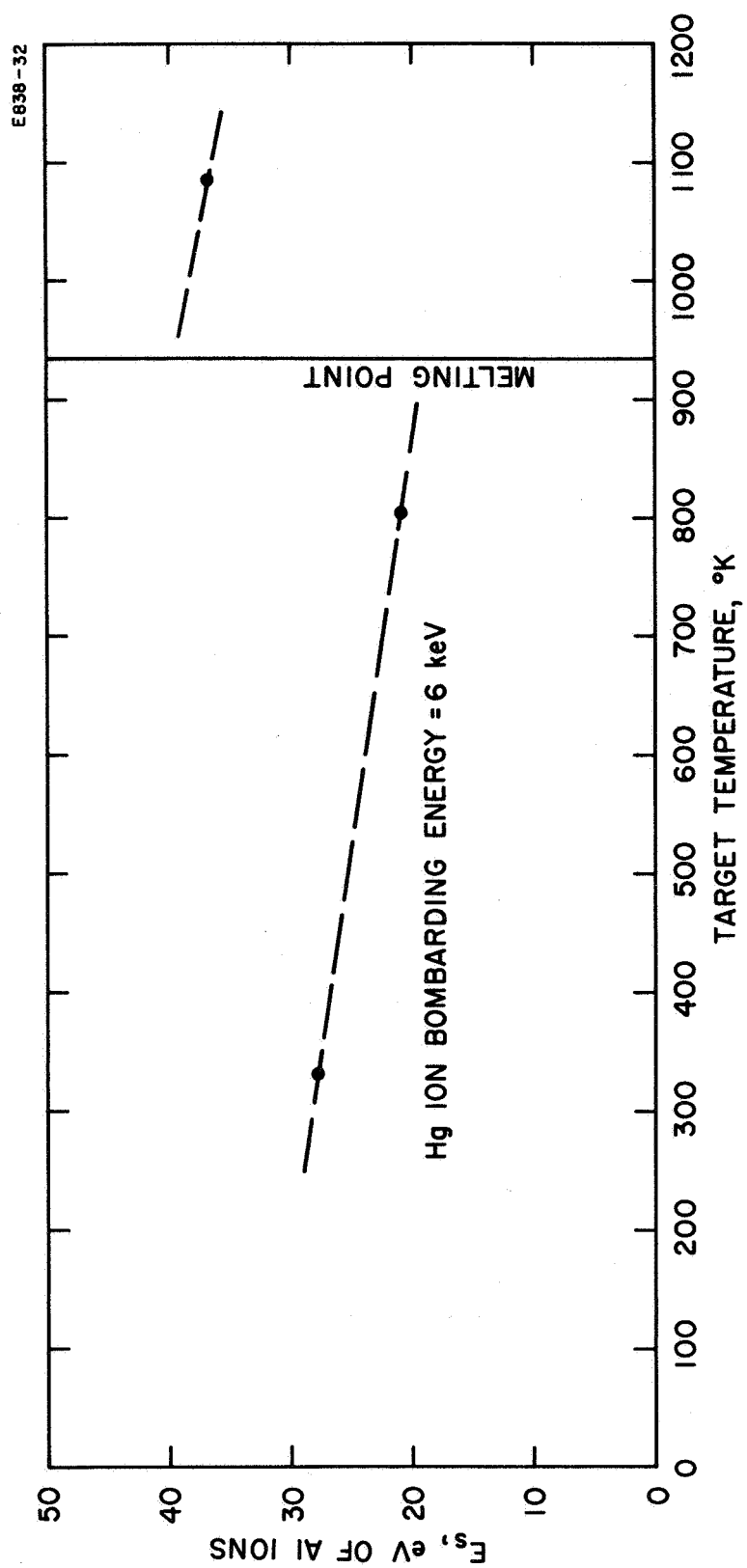


Fig. 51. Characteristic energies of sputtered aluminum ions as a function of target temperature.

An absolute measure of the transfer efficiency of sputtering would require the determination of the energy content in all sputtered particles in comparison with the energy delivered to the target by the incident beam. Thus, we would require an integration of the sputtering yield over all angles, weighted by the energy distribution of both the charged and neutral particles. Observations of the energy distribution of particles sputtered in directions at various angles to the surface normal did not indicate variations with angle. It would be possible to integrate the energies over the angular distribution indicated in Fig. 13, but without knowledge of the absolute yield of ions and atoms, the complete integration cannot be carried out at the present time. If the results of this program were to be correlated with absolute yield values from other measurements and accurate observations made of relative yields of charged versus neutral particles, the absolute values of transfer efficiency would be obtained. Before undertaking such an effort, it might be most expeditious to determine the transfer efficiency from calorimetric observations at the target. The relative transfer efficiencies reflected in the characteristic energies reported above will provide useful data to test the theoretical descriptions of the sputtering phenomena. An extension of these measurements to the observation of characteristic energies of the particles ejected in preferred directions from single-crystalline targets would be of particular value in testing the theory of focusing collisions.

V. CONCLUSIONS

The results of this experiment are of academic interest in establishing theoretical models for the sputtering of materials in their solid and liquid states. In addition, they indicate that for the conditions of normal incident ions (as would be the case on the flat surfaces of thruster electrodes), no large increase or decrease in sputtering yield results from the change in state. Thus, the employment of liquid metal electrodes in ion thrusters does not warrant the mechanical complications which would be required.

The yields observed were considerably lower for the targets with the heavier masses. Therefore, the use of mercury (frozen or liquid) for ion beam collectors for mercury electron-bombardment type ion engines is of merit if long-term laboratory operation is anticipated.

The characteristic energies observed in the sputtered ions and atoms have values in the range of 7 to 30 eV, and this energy decreases with increased target mass. The energies for the lighter elements are well above thermal values; thus, the sputtering process is attractive for the deposition of thin films which must adhere to various substrate materials.

The experimental equipment developed in the course of this program has proven of value in the identification of sputtered ionic and atomic species, the observation of the angular distribution, and the energy characteristics of the sputtered species. Because of the primary objectives in observing the sputtering effects in liquid metals, the bombarding ion beam was restricted to enter normal to the direction of the target surfaces; thus, the equipment could not be used to its fullest capacity in varying the incidence angle and then permitting observation of the resulting angular distributions and energy profile. The restriction to normal incidence would not exist for rotatable solid targets. Thus, experiments to observe the characteristic energy of particles ejected from single-crystalline and polycrystalline targets, plus observations of the sputtering species from compound target materials, might well be the subject of future investigations employing this equipment.

PRECEDING PAGE BLANK NOT FILMED.

ACKNOWLEDGMENTS

The author wishes to acknowledge the helpful efforts of Mr. David Zuccaro in designing and operating the ion source employed in the sputtering apparatus and in evaluating the results of the experiment. Thanks are also due to Mr. Klaus Robinson for his capable assistance in the fabrication and assembly of the experimental test equipment.

REFERENCES

1. G.K. Wehner, "Sputtering of metal single crystals by ion bombardment," J. Appl. Phys. 26, 1056 (1955).
2. G.K. Wehner, "Controlled sputtering of metals by low-energy Hg ions," Phys. Rev. 102, 690 (1956).
3. G.K. Wehner, "Sputtering by ion bombardment," Adv. Electron. Electron Phys. 7, 239 (1955).
4. G.K. Wehner, "Sputtering yields for normally incident Hg^+ - ion bombardment at low ion energy," Phys. Rev. 108, 35 (1957).
5. G.K. Wehner, "Low-energy sputtering yields in Hg," Phys. Rev. 112, 1120 (1958).
6. N. Laegreid and G.K. Wehner, "Sputtering yields of metals for Ar^+ and Ne^+ ions with energies from 50 to 600 eV," J. Appl. Phys. 32, 365 (1961).
7. D. Rosenberg and G.K. Wehner, "Sputtering yields for low energy He^+ , Kr^+ , and Xe^+ ion bombardment," J. Appl. Phys. 33, 1842 (1962).
8. R.V. Stuart and G.K. Wehner, "Sputtering thresholds and displacement energies," Phys. Rev. Letters 4, 409 (1960).
9. O.E. Almen and G. Bruce, "Collection and sputtering experiments with noble gas ions," Nucl.Instr. Methods 11, 257 (1961); also, "Sputtering experiments in the high energy region," Nucl. Instr. Methods 11, 279 (1961).
10. M. Kaminsky, "Atomic and Ionic Impact Phenomena on Metal Surfaces" (Academic Press, New York, 1965).
11. G.D. Magnuson, C.E. Carlston, D. McKeown, and A.Y. Cabezas, "Sputtering Mechanisms Under Ion Propulsion Conditions," Final Report prepared for NASA on Contract NAS 3-2591, October 1964 "Sputtering yields of single crystals bombarded by 1- to 10- keV Ar^+ ions," J. Appl. Phys. 34, 3267 (1963).
12. S.Y. Lebedev, Y.Y. Stavisskii, and Y.V. Shut'ko, "Cathode sputtering under the action of cesium ions," Soviet Phys. - Tech. Phys. 9, 854 (1964).

13. A.L. Southern, W.R. Willis, and M.T. Robinson, "Sputtering experiments with 1 to 5 keV Ar⁺ ions," J. Appl. Phys. 34, 153 (1963).
14. N.V. Pleshivtsev, "The Technology of Cathode Sputtering," (Eng. Trans.) Pribery i Tekhn. Eksperim. 5, (1964).
15. V.A. Molchonov, V.G. Tel'Kovskii, and V.M. Chickerov, "Variation of the cathode sputtering coefficient as a function of the angle of incidence of ions on a target," Soviet Phys. — Doklady 6, 137 (1961), and "Angular distribution of sputtered particles on irradiation of a single crystal by an ion beam," Soviet Phys. — Doklady 6, 486 (1961).
16. E.B. Hensichke, "New collision theory of cathode sputtering of metals at low ion energies," Phys. Rev. 106, 737-753 (1957).
17. F. Keywell, "Measurements and collision-radiation damage theory of high-vacuum sputtering," Phys. Rev. 97, 1611-1619 (1955).
18. R.H. Silsbee, "Focusing in collision problems in solids," J. Appl. Phys. 28, 1246-1250 (1957).
19. J. Lindhard and M. Scharff, "Energy dissipation by ions in the keV range," Phys. Rev. 124, 128-130 (1961).
20. D. Moore, "Liquid-Protected Electrodes," AIAA Paper 65-378 presented at the AIAA Second Annual Meeting, San Francisco, July 1965; R. K. Parker, "A Study of the Protective Effect of a Thin Film on a Surface Exposed to Sputtering," Thesis for the Master of Science Degree, Air Force Institute of Technology, GSP/Phys/66-15, March 1966.
21. R. Seeliger and K. Sommermeyer, "Bemerkung zur theorie der kathodenzerstanburg," Z. Phys. 93, 692-695 (1935).
22. W. Paul and W. Raether, "Das elektrische massenfilter," Z. Physik 140, 262 (1955).
23. H.J. King and I. Kohlberg, "Low-current-density ion engine development — Final Technical Report No. 38 TR-102," prepared for NASA-Lewis Research Center under Contract NAS 8-1684, January 1963, pp. 103-110.
24. V.I. Veksler, "Energy distribution of sputtered and scattered ions in the bombardment of tantalum and molybdenum by positive cesium ions," Soviet Phys. — JETP 11, 235 (1960).

25. G.K. Wehner, private communication.
26. T.W. Snouse, "Sputtering at Oblique Angles of Ion Incidence," NASA TN D-2235, April 1964.
27. D.E. Harrison and G.D. Magnuson, "Sputtering thresholds," Phys. Rev. 122, 1421-1430 (1961).
28. N.T. Olson and H.P. Smith, "Yield and angular distribution of cesium sputtered copper using a radioactive tracer technique," AIAA J. 4, 916 (1966).
29. A.E. Andrews, E.H. Hasseltine, N.T. Olson, and H.P. Smith, "Cesium ion sputtering of aluminum," J. Appl. Phys. 37, 3344-3347 (1966).
30. V.E. Krohn, "Emission of negative ions from metal surfaces bombarded by positive cesium ions," J. Appl. Phys. 33, 3523 (1962).
31. H.P. Smith, private communication.
32. V.A.J. VanLint, R.A. Schmitt, and C.S. Suffredini, "Range of 2- to 60-KeV recoil atoms in Cu, Ag, and Au," Phys. Rev. 121, 1457-1463 (1961).
33. J.M. Flint, P.K. Rol, and J. Kistemaker, "Angular-dependent sputtering of copper single crystals," J. Appl. Phys. 34, 690 (1963).
34. N.V. Pleshivtsev, "Sputtering of copper by hydrogen ions with energies up to 50 KeV," Soviet Phys. - JETP 37, 878 (1960).
35. H.E. Stanton, "On the yield and energy distribution of secondary positive ions from metal surfaces," J. Appl. Phys. 31, 678 (1960).
36. R.V. Stuart and G.K. Wehner, "Energy Distributions of Sputtered Atoms," Annual Report on the Office of Naval Research Contract No. Nonr 1589 (15), November 1964.
37. K. Kopitzki and H.E. Stier, "Mittleri kinetische energie der bei der kathodenzerstndbung von metallen ausgesandten partikel," Z. Naturforsch. 17a, 346 (1962).



DISTRIBUTION LIST

<u>Recipient</u>	<u>Address</u>
NASA Headquarters (1)	NASA Headquarters FOB - 10B 600 Independence Ave., S.W. Washington, D.C. 20546 Attn: RNT/James Lazar
NASA-Lewis Research Center (22)	NASA-Lewis Research Center 21000 Brookpark Road Cleveland, Ohio 44135 Attn: Spacecraft Technology Procurement Section (M.S. 54-2) (1) Attn: Technology Utilization Office (M.S. 3-19) (1) Attn: Technical Information Division (M.S. 5-5) (1) Attn: Library (M.S. 3-7) (2) Attn: Spacecraft Technology Division (M.S. 54-1) a. J.H. Childs (1) b. J.A. Wolters (12) Attn: Electric Propulsion Laboratory (M.S. 301-1) a. W. Moeckel (1) b. H.R. Kaufman (1) c. W.R. Kerslake (1) Attn: Reports Control Office (M.S. 5-5) (1)
NASA Scientific and Technical Information Facility	NASA Scientific and Technical Information Facility Box 33 College Park, Maryland 20740 Attn: NASA Representative RQT-2448 (6)
NASA-Marshall Space Flight Center	NASA-Marshall Space Flight Center Huntsville, Alabama 35812 Attn: Ernest Stuhlinger (M-RP-DIR) (1)

<u>Recipient</u>	<u>Address</u>
Research and Technology Division	Research and Technology Division Wright-Patterson AFB, Ohio 45433 Attn: AFAPL (APIE-2)/ R. F. Cooper (1)
AFWL	AFWL Kirtland AFB, New Mexico Attn: WLPC/Cap. C. F. Ellis (1)
Aerospace Corporation	Aerospace Corporation P.O. Box 95085 Los Angeles, California 90045 Attn: Library/Technical Documents Group (1)
Jet Propulsion Laboratory	Jet Propulsion Laboratory 4800 Oak Grove Drive Pasadena, California 91103 Attn: J.W. Stearns (1)
Electro-Optical Systems, Inc. (2)	Electro-Optical Systems, Inc. 300 North Halstead Street Pasadena, California 91107 Attn: J. Perel (1) Attn: D.B. Medved (1)
Ion Physics Corporation	Ion Physics Corporation South Bedford Street Burlington, Massachusetts Attn: Sam Nablo (1)
TRW Space Technology Laboratories	TRW Space Technology Laboratories Thompson Ramo Wooldrige, Inc. One Space Park Redondo Beach, California Attn: D.B. Langmuir (1)
Westinghouse Astronuclear Laboratories	Westinghouse Astronuclear Laboratories Electric Propulsion Laboratory Pittsburgh, Pennsylvania 15234 Attn: H.W. Szymanowski (1)

<u>Recipient</u>	<u>Address</u>
TAPCO	TAPCO, A Division of Thompson Ramo Wooldridge, Inc. New Product Research 23555 Euclid Avenue Cleveland, Ohio Attn: R. T. Craig (1)
General Electric	General Electric Space Flight Propulsion Laboratory Cincinnati, Ohio 45215 Attn: M. L. Bromberg (1)
General Dynamics	General Dynamics/Astronautics P.O. Box 1128 San Diego, California 92101 Attn: G.D. Magnuson (1)
Field Emission Corporation	Field Emission Corporation 611 Third Street McMinnville, Oregon 97128 Attn: L. W. Swanson (1)
NASA-Ames Research Center	NASA-Ames Research Center Moffett Field, California 94035 Attn: T. W. Snouse (1)
University of California	University of California Space Science Laboratory Berkeley 4, California Attn: H.P. Smith (2)
Aerospace Power Division	Aerospace Power Division Wright-Patterson AFB, Ohio 45433 Attn: Jack W. Geis-AFAPL/APIT (1)